

ALMA MATER STUDIORUM · UNIVERSITÀ DI BOLOGNA

Scuola di Scienze
Dipartimento di Fisica e Astronomia
Corso di Laurea Magistrale in Fisica

**MOLECULAR DYNAMICS
SIMULATIONS OF CONDUCTING
POLYMER NANOCOMPOSITES**

Relatore:

Prof. Tobias Cramer

Presentata da:

Armando Consiglio

Correlatore:

Prof. Andrei V. Komolkin

Anno Accademico 2018/2019

Abstract

Among the conducting polymers, poly(3,4-ethylenedioxythiophene):poly(styrene sulfonate) (PEDOT:PSS) is one of the most used materials in the field of bioelectronics due to its biocompatibility, chemical stability and high electronic as well as ionic charge transport mobilities.

Despite many experimental findings, a microscopic understanding of the materials electronic properties is currently elusive; the main reason is the lack of structural atomistic data of the polymer blend, that is, difficult to obtain because of the disordered and nano-crystalline morphology.

In this thesis work we develop and use Molecular Dynamics based methods to simulate the structure of PEDOT:PSS in presence of an interface, investigating how a surface and some physical quantities (temperature, water content and electric charge on PEDOT oligomers) would introduce order to the evolving structure, and pointing out the differences between interfacial and bulk behaviour.

The results obtained by computer simulations are used to estimate experimentally accessible parameters and to compare them with already existing experimental data.

Sommario

Il poli(3,4-etilenediossitiolfene):poli(stirene sulfonato) (PEDOT:PSS) è uno dei polimeri conduttori maggiormente impiegati nel settore della bioelettronica data la sua biocompatibilità, stabilità chimica e grande mobilità dei portatori di carica (sia ionici che elettronici).

Sebbene in letteratura vi siano numerosi risultati sperimentali in proposito, al momento la comprensione delle proprietà microscopiche di questo materiale è sfuggente; in particolare questo è dovuto alla mancanza di dati strutturali della miscela polimerica, difficili da ottenere a causa della morfologia disordinata e nano-cristallina.

Questo lavoro di tesi si basa sull'utilizzo di tecniche di dinamica molecolare col fine di simulare la struttura del PEDOT:PSS in presenza di un'interfaccia, analizzando come una superficie e alcune grandezze fisiche (temperatura, contenuto d'acqua e carica elettrica posseduta dagli oligomeri di PEDOT) possano concorrere all'evoluzione del sistema, sottolineando le differenze col caso in cui tale superficie sia assente.

I risultati ottenuti dalle simulazioni al computer sono stati adoperati sia per stimare i valori di parametri sperimentalmente accessibili e sia per confrontarli con i dati esistenti.

Introduction

Since some decades computer simulations are becoming an indispensable tool in almost every field of science, being a valid complement for both theory and conventional experiments; this is also due to the remarkable increase in computer power, following the well known Moore's law.

With a computer simulation we want to describe and predict reality, and in order to do this it is necessary to specify the initial state of the system and the parameters that can influence its evolution. Moreover the simulations should be as much as possible efficient and accurate so it must be clear from the beginning what is the range of spatial and temporal lengths in which we want to work: it is not possible to use the Schrödinger equation or the rules of relativistic quantum mechanics to simulate the behavior of hundreds of thousands of atoms as well as, in general, chemical reactions cannot be studied by using continuum mechanics.

Molecular Dynamics Simulation turns out to be a powerful computational method to study and describe the atomic and molecular motion of fluids, solutions, liquid crystals etc. by means of Classical Mechanics (Newton's equations) and the use of Statistical Mechanics to link the information of the microscopic (nanoscopic) world with the macroscopic one. Molecular Dynamics based methods offer the opportunity to provide structural atomic models for disordered polymeric materials that cannot be accessed by experimental scattering methods. This is a challenging problem to deal with.

Several experimental studies already elucidate that the morphology and the electronic properties of conducting polymers, also in contact with a surface,

are relevant for bioelectronic devices and applications. This is because they support the transport of both ions and electrons, turning out to be useful as neural probes to record neuronal activities, as implantable drug delivery devices, as biosensors etc.

However a consistent theoretical description of the structure-properties relationship in this material class has not been presented, and this lack of knowledge hinders further optimization of polymeric nanocomposites with mixed ionic and electronic properties.

For this thesis work, computer simulations based on Molecular Dynamics methods have been carried out to obtain a qualitative and quantitative description of the conducting polymer blend PEDOT:PSS in different physical conditions, so that the relationship between the structure of the system and its properties can be analyzed.

These goals have been achieved by developing a suitable Force Field to simulate PEDOT:PSS in bulk phase and in presence of a surface (amorphous glass) and generating the starting geometries.

After the equilibration stage, the output file have been analyzed to calculate some parameters that link to experimental data.

In particular, attention has focused on:

- Calculation of Diffusion Coefficients for the different components of the system;
- Study of bending of poly(styrene sulfonate) through the analysis of Probability Density Function (pdf);
- Analysis of the equilibrium positions of Na^+ counterions;
- Visualization of the local structures, to analyze how the components of the system interact among each others. Specifically, interaction among PEDOT oligomers in the formation of ordered structures and interactions among PEDOT and PSS;

- Distribution of components of the system, in the case of simulations in presence of a surface.

Comparisons of results are made between:

- Bulk PEDOT:PSS system at $T = 25$ °C, with neutral PEDOT;
- Bulk PEDOT:PSS system at $T = 25$ °C, with every PEDOT oligomers being charged 2+.

and

- PEDOT:PSS system in presence of a glass surface, at $T = 90$ °C, with neutral PEDOT;
- PEDOT:PSS system in presence of a glass surface, at $T = 90$ °C, with every PEDOT oligomers being charged 2+.

Some of the results contained in this thesis have been already presented in the *International Student Conference "Science and Progress 2018"* at Faculty of Physics of Saint-Petersburg State University and in the *16th International School-Conference Spinus 2019 <<Magnetic resonance and its applications>>*, held in Saint-Petersburg.

Contents

1	Conducting Polymers	1
1.1	Organic Polymers	7
1.1.1	Poly(3,4-ethylenedioxythiophene) - PEDOT	10
1.1.2	Poly(Styrene Sulfonate) - PSS	11
1.1.3	PEDOT:PSS	12
1.1.4	Applications of PEDOT:PSS	17
2	Molecular Dynamics Simulation	23
2.1	Structure of the Simulations	26
2.1.1	The Initial Configuration	26
2.1.2	Equilibration Stage	29
2.1.3	Output File	30
2.2	Periodic Boundary Conditions	32
2.3	Force Field Descriptions	36
2.3.1	Bonded Interactions	37
2.3.2	Non Bonded Interactions	40
2.3.3	Classical Force Fields	41
2.4	The Importance of Water	43
2.5	Equations of Motion and Algorithms	44
2.6	Thermodynamic ensembles	50
2.6.1	Thermostat and Barostat Algorithms	51
2.7	Long-Range Interactions Calculation	52
2.7.1	Ewald Summation	53

2.8	Properties of the System from the Trajectories	57
2.8.1	Ergodic Hypothesis	62
2.9	Limits of Molecular Dynamics Simulations	64
2.10	Molecular Dynamics Simulations for Polymer Composites . . .	65
2.10.1	Molecular Dynamics Simulations for Polymer Compos- ites/Interface	68
2.10.2	Molecular Dynamics Simulations for PEDOT:PSS . . .	69
3	Problem Statement	73
4	Discussion and Results	75
4.1	Computational Details	75
4.1.1	Visualization of the 3D structures	87
4.2	Analysis of PEDOT:PSS in Bulk Phase	88
4.2.1	System at $T = 25$ °C with neutral PEDOT	102
4.2.2	System at $T = 25$ °C with PEDOT 2+	109
4.3	PEDOT:PSS/SiO ₂ interface	116
4.3.1	System at $T = 90$ °C with neutral PEDOT	119
4.3.2	System at $T = 90$ °C with PEDOT 2+	129
5	Conclusions	137

List of Figures

1.1	Schematics of an inorganic semiconductor, silicon, and an organic semiconductor, PEDOT, at the interface with an electrolyte. The hydrated ion is meant to be the same in both schematics, defining the relative scale. The insets show the action of <i>p-type</i> dopants, boron in silicon, and PSS in PEDOT, respectively.	4
1.2	Chemical structures of conductive polymers	8
1.3	Chemical structure of thiophene, 3,4-ethylenediothiophene (EDOT) and PEDOT.	10
1.4	Monomer of Poly(Styrene Sulfonate).	12
1.5	Schematic view of the chemical structure of charged PEDOT and PSS polymer.	12
1.6	(a) Weight loss of a sample of PEDOT:PSS with a weight ratio of PEDOT to PSS as 1:20 monitored while heating at a constant rate of 5 K/min. (b) Weight increase of a PEDOT:PSS sample owing to the absorption of water as a function of time. [63]	15
1.7	(a) Sheet resistance of films of PEDOT:PSS including 5% ethylene glycol as a function of time. (b) Sheet resistance of PEDOT:PSS films exposed to a Xe lamp as a function of time, compared to a non-exposed sample [63].	16

1.8	(a) Absorbance of a thin film of PEDOT:PSS (110 nm). In the inset, absorbance of PEDOT:PSS and PSS in the spectral range from 185 to 500 nm. (b) Optical absorption spectra of a PEDOT:PSS electrode in an electrochemical cell for different applied voltages. [63]	16
1.9	Thermopower for (a) highly doped PAc, (b) PAni, (c) PPy. [48]	20
1.10	a) Micrograph of the electrodes. b) Micrograph of an array conforming to the midrib of a small leaf. [46]	21
1.11	Examples of wearable sensors.[13]	21
1.12	Architecture of an OECT integrated with barrier tissue layer; tissue is supported on a permeable membrane. On the right is showed a tightly packed epithelial cells with junctional proteins that regulate transport. [46]	22
2.1	Time and length scales for computer simulations.	25
2.2	Ethanol molecule created with Jmol software.	27
2.3	Spatial coordinates of the above ethanol molecule.	27
2.4	Some of the parameters needed in the initial stage of a simulation.	28
2.5	Initial atomic spatial configuration for the simulation of water/ethanol mixture (5 molecules of water for every ethanol molecule).	28
2.6	Diffusion coefficients of water molecules (green line) and ethanol molecules (purple line) in water/ethanol mixture, at $T = 25$ °C.	30
2.7	2-dimensional periodic boundary conditions.	33
2.8	Minimum image convention interactions.	34
2.9	2-body harmonic interaction between two particles.	37
2.10	3-body harmonic angle bending.	38
2.11	4-body torsional interaction.	39
2.12	Dihedral angle distribution of ethanol molecules in water/ethanol mixture, $T = 25$ °C.	39
2.13	Example of three particles water model.	44

2.14	Example of four particles water model. The particle M is very near to the Oxygen atom (few Å), so the distances of the image are not representative.	44
2.15	Snapshot of a .PDB file of water/ethanol mixture simulation model at $T = 25$ °C, after ~ 3 ns.	45
2.16	Zoom of the snapshot of a .PDB file of water/ethanol mixture simulation model at $T = 25$ °C, after ~ 3 ns. Details on the hydrogen bonding are showed.	46
2.17	Zoom of the snapshot of a .PDB file of water/ethanol mixture simulation model at $T = 25$ °C, after ~ 3 ns. Details on the hydrogen bonding are showed.	46
2.18	Twin range cut-off method.	53
2.19	Schematic representation of a 2-D system with Periodic Boundary Conditions and electric charges.	54
2.20	Schematic view of the Ewald method.	56
2.21	Diffusion Coefficients of PEDOT oligomers, PSS polymers, water molecules and Na ⁺ counterions in PEDOT:PSS bulk system ($T = 25$ °C), at the very beginning of a simulation (equilibration stage, $t_{simulation} < 1$ ns). Values obtained from the analysis of the trajectories.	61
2.22	Mean Squared Displacements of PEDOT oligomers, PSS polymers, water molecules and Na ⁺ counterions in PEDOT:PSS bulk system ($T = 25$ °C), at the very beginning of a simulation (equilibration stage, $t_{simulation} < 1$ ns). Values obtained from the analysis of the trajectories.	61
2.23	Calculation of the Radial Distribution Function.	62
2.24	Rouse model for polymers.	67

2.25	(a) Molecular structure of PEDOT and TOS. (b-e) Snapshots of the PEDOT:TOS structures. PEDOT is shown in blue, TOS in green, and water in light blue; water is not shown in parts c-f. (b) Random initial position of PEDOT chains, TOS and water in $12 \times 12 \times 12$ nm ³ computational box; PEDOT chain length $N = 12$, carrier concentration $c_h = 33\%$. (c) Aqueous PEDOT:TOS solution after equilibration time of 20 ns; water content is 82% w/w (only thiophene rings and sulfur atoms from TOS are showed). (d) PEDOT:TOS in a dry phase after five steps of water evaporation (H and O atoms and methyl groups from TOS are not shown). (e) Zoom of a representative crystallite from part d with the indicated distances r_{SO_3-S} (in Å) between Sulfur atoms of PEDOT and TOS. α and β mark TOS molecules. (f) Previous crystal rotated 90° (left) and a neighboring crystallite (right).	70
4.1	Dimer of PEDOT. Yellow spheres are Sulfur atoms, red spheres are Oxygen atoms, gray spheres are Carbon atoms and white spheres are Hydrogen atoms.	76
4.2	Oligomer of PEDOT, used during the simulations. Yellow spheres are Sulfur atoms, red spheres are Oxygen atoms, gray spheres are Carbon atoms and white spheres are Hydrogen atoms.	77
4.3	Monomer of Styrene Sulfonate.	77
4.4	Side view of a PSS polymers. Note the structure obtained from polystyrene by the addition of sulfonate functional groups. Yellow spheres are Sulfur atoms, red spheres are Oxygen atoms, gray spheres are Carbon atoms and white spheres are Hydrogen atoms.	78

4.5	Top view of a syndiotactic PSS polymers. Note the structure obtained from polystyrene by the addition of sulfonate functional groups. Yellow spheres are Sulfur atoms, red spheres are Oxygen atoms, gray spheres are Carbon atoms and white spheres are Hydrogen atoms.	78
4.6	Top view of atactic PSS polymers. Note the structure obtained from polystyrene by the addition of sulfonate functional groups. Yellow spheres are Sulfur atoms, red spheres are Oxygen atoms, gray spheres are Carbon atoms and white spheres are Hydrogen atoms.	79
4.7	Top view of another atactic PSS polymers. Note the structure obtained from polystyrene by the addition of sulfonate functional groups and the differences with the above PSS polymer. Yellow spheres are Sulfur atoms, red spheres are Oxygen atoms, gray spheres are Carbon atoms and white spheres are Hydrogen atoms.	79
4.8	Initial atomic spatial configuration for the simulation of PEDOT:PSS in bulk phase from a top view. Water molecules are not shown.	80
4.9	Initial atomic spatial configuration for the simulation of PEDOT:PSS in bulk phase from a side view. Water molecules are not shown.	81
4.10	Amorphous glass surface used for the simulations.	81
4.11	Evaporation of water for PEDOT:PSS in contact with the glass surface. Note the non-cubic simulation box.	82
4.12	Lamellar structure of PEDOT oligomers in PEDOT:PSS. The typical distance between the plane is of $\sim 3.5 \text{ \AA}$	84
4.13	Interaction among a charged PEDOT oligomer (2+) and a charged PSS polymer (12-). The PEDOT oligomer is green, PSS polymer is red and its backbone is white.	85

4.14	Example of PSS bending during the simulation run. PEDOT oligomers, water molecules and Na^+ counterions are not shown in this image.	86
4.15	Average motion of PEDOT and PSS for bulk system at $T = 25^\circ\text{C}$, with uncharged PEDOT.	89
4.16	Average motion of PEDOT and PSS for bulk system at $T = 25^\circ\text{C}$, with charged PEDOT.	90
4.17	Radial distribution function of the distance between Oxygen atoms of the SO_3 group of PSS, and the Na^+ counterions, for the bulk phase system at $T = 25^\circ\text{C}$ and neutral/charged PEDOT.	94
4.18	Radial distribution function of the distance between Sulfur atoms of the SO_3 group of PSS, and the Na^+ counterions, for the bulk phase system at $T = 25^\circ\text{C}$ and neutral/charged PEDOT.	95
4.19	Graphical comparison among the Diffusion Coefficients of the PEDOT oligomers in bulk system at $T = 25^\circ\text{C}$ (uncharged and charged PEDOT).	95
4.20	Graphical comparison among the Diffusion Coefficients of the PSS polymers in bulk system at $T = 25^\circ\text{C}$ (uncharged and charged PEDOT).	96
4.21	a) Computational tomography of uncharged PEDOT, in the $x - y$ plane ($z = 25.2 \text{ \AA}$) b) Computational tomography of uncharged PEDOT, in the $x - y$ plane ($z = 29.0 \text{ \AA}$) c) Computational tomography of charged PEDOT, in the $x - y$ plane ($z = 25.2 \text{ \AA}$) d) Computational tomography of charged PEDOT, in the $x - y$ plane ($z = 29.2 \text{ \AA}$).	97
4.22	a) Computational tomography of uncharged PEDOT, along y direction ($x - z$ plane, $y = 25.2 \text{ \AA}$) b) Computational tomography of charged PEDOT, along y direction ($x - z$ plane, $y = 25.2 \text{ \AA}$).	98

4.23	a) 3-D densities of Carbon atoms around uncharged PEDOT b) 3-D densities of Carbon atoms around uncharged PEDOT, at a distance of 4.4 Å from the molecule plane c) 3-D densities of Carbon atoms around charged PEDOT d) 3-D densities of Carbon atoms around charged PEDOT, at a distance of 4.4 Å from the molecule plane.	99
4.24	a) 3-D densities of Oxygen atoms around uncharged PEDOT b) 3-D densities of Oxygen atoms around uncharged PEDOT, at a distance of 4.4 Å from the molecule plane c) 3-D densities of Oxygen atoms around charged PEDOT d) 3-D densities of Oxygen atoms around charged PEDOT, at a distance of 4.4 Å from the molecule plane.	100
4.25	a) Distributions of Carbon atoms of phenyl rings of PSS around neutral PEDOT in the $x - y$ plane, at $z = 25.2$ Å b) Distributions of Carbon atoms of phenyl rings of PSS around charged PEDOT in the $x - y$ plane, at $z = 25.2$ Å c) Distributions of Carbon atoms of phenyl rings of PSS around neutral PEDOT in the $x - y$ plane, at $z = 29.4$ Å d) Distributions of Carbon atoms of phenyl rings of PSS around charged PEDOT in the $x - y$ plane, at $z = 29.2$ Å e) Distributions of Carbon atoms of phenyl rings of PSS around neutral PEDOT in the $x - z$ plane, f) Distributions of Carbon atoms of phenyl rings of PSS around charged PEDOT in the $x - z$ plane	101
4.26	a) Average motion of PEDOT and PSS b) Diffusion Coefficients for the different components of the system c) Radial Distribution Function for the distances of Na^+ counterions from the SO_3 group of PSS d) Probability Density Function concerning the bending of PSS (distance among the extremal Carbon atoms).	102

4.27	Computational tomography of uncharged PEDOT in the $x-y$ plane, with height in z direction of 25.2 Å, for neutral PEDOT and $T = 25$ °C.	103
4.28	Computational tomography of uncharged PEDOT in the $x-y$ plane, with height in z direction of 29.0 Å, for neutral PEDOT and $T = 25$ °C.	103
4.29	Computational tomography of uncharged PEDOT in the $x-y$ plane, with height in z direction of $x=33.0$ Å, for neutral PEDOT and $T = 25$ °C.	104
4.30	Computational tomography of uncharged PEDOT in the $x-z$ plane, with position along the y direction in $y = 25.2$ Å, for neutral PEDOT and $T = 25$ °C.	104
4.31	3-D densities of Carbon atoms of PSS backbone around uncharged PEDOT, seen in $x-y$ plane.	105
4.32	3-D densities of Carbon atoms of PSS backbone around uncharged PEDOT, out of the $x-y$ plane (4.4 Å under the plane of PEDOT).	105
4.33	3-D densities of Oxygen atoms of PSS around uncharged PEDOT, seen in $x-y$ plane.	106
4.34	3-D densities of Oxygen atoms of PSS around uncharged PEDOT, out of the $x-y$ plane (4.4 Å under the plane of PEDOT).	106
4.35	Probability density function of the distance between the Carbon atoms at the extremes of PSS for a system in the bulk phase at $T = 25$ °C and neutral PEDOT.	107
4.36	Radial distribution function of the distance between Oxygen and Sulfur atoms of the SO ₃ group of PSS, and the Na ⁺ counterions, for the bulk phase system at $T = 25$ °C and neutral PEDOT.	107
4.37	Diffusion Coefficients of the components of bulk system at $T = 25$ °C, with uncharged PEDOT.	108

4.38	a) Average motion of PEDOT and PSS b) Diffusion Coefficients for the different components of the system c) Radial Distribution Function for the distances of Na^+ counterions from the SO_3 group of PSS d) Probability Density Function concerning the bending of PSS (distance among the extremal Carbon atoms).	109
4.39	Computational tomography of PEDOT:PSS in the $x-y$ plane, with height in z direction of 25.2 \AA , for charged PEDOT (2+) and $T = 25 \text{ }^\circ\text{C}$	110
4.40	Computational tomography of PEDOT:PSS in the $x-y$ plane, with height in z direction of 29.2 \AA , for charged PEDOT (2+) and $T = 25 \text{ }^\circ\text{C}$	110
4.41	Computational tomography of PEDOT:PSS in the $x-y$ plane, with height in z direction of 32.6 \AA , for charged PEDOT (2+) and $T = 25 \text{ }^\circ\text{C}$	111
4.42	Computational tomography of PEDOT:PSS in the $x-z$ plane, with position along the y direction in $y = 25.2 \text{ \AA}$, for charged PEDOT (2+) and $T = 25 \text{ }^\circ\text{C}$	111
4.43	Computational tomography of PEDOT:PSS in the $y-z$ plane, for charged PEDOT (2+) and $T = 25 \text{ }^\circ\text{C}$	112
4.44	3-D densities of Carbon atoms of PSS backbone around charged PEDOT, seen in $x-y$ plane.	112
4.45	3-D densities of Carbon atoms of PSS backbone around charged PEDOT, out of the $x-y$ plane (4.4 \AA under the plane of PEDOT).	113
4.46	3-D densities of Oxygen atoms of PSS around charged PEDOT, seen in $x-y$ plane.	113
4.47	3-D densities of Oxygen atoms of PSS around charged PEDOT, out of the $x-y$ plane (4.4 \AA under the plane of PEDOT).	114

4.48	Probability density function of the distance between the Carbon atoms at the extremes of PSS for a system in the bulk phase at $T = 25$ °C and charged PEDOT (2+).	114
4.49	Radial distribution function of the distance between Oxygen and Sulfur atoms of the SO ₃ group of PSS, and the Na ⁺ counterions, for the bulk phase system at $T = 25$ °C and charged PEDOT (2+).	115
4.50	Diffusion Coefficients of the components of bulk system at $T = 25$ °C, with charged PEDOT.	115
4.51	Time dependence of water molecules in both system at $T = 90$ °C.	117
4.52	Evaporation process at $t = 42.433348$ ns (a) and $t = 42.433350$ ns (b). Note the disappearance of water molecules at the top of the simulation cell in Fig. b.	118
4.53	Front view of the PEDOT:PSS system in presence of a glass surface at $T = 90$ °C, with neutral PEDOT, at the end of the water evaporation process. Yellows are PEDOT oligomers and blue are PSS polymers.	120
4.54	Top of view of the PEDOT:PSS system in presence of a glass surface at $T = 90$ °C, with neutral PEDOT, at the end of the water evaporation process. Yellow molecules are PEDOT oligomers and blue molecules are PSS polymers. Note also the stacking ordering of PEDOT.	121
4.55	Distribution of components of the system, as a function of the z -coordinate. Data are obtained by considering the average values for the simulation time among 20.00 ns and 29.99 ns.	122
4.56	Distribution of components of the system, as a function of the z -coordinate. Data are obtained by considering the average values for the simulation time among 30.00 ns and 39.99 ns.	122

4.57	Distribution of components of the system, as a function of the z -coordinate. Data are obtained by considering the average values for the simulation time among 40.00 ns and 49.99 ns.	123
4.58	Distribution of components of the system, as a function of the z -coordinate. Data are obtained by considering the average values for the simulation time among 50.00 ns and 59.99 ns.	123
4.59	Distribution of components of the system, as a function of the z -coordinate. Data are obtained by considering the average values for the simulation time among 60.00 ns and 69.99 ns.	124
4.60	Distribution of components of the system, as a function of the z -coordinate. Data are obtained by considering the average values for the simulation time among 70.00 ns and 79.99 ns.	124
4.61	Distribution of components of the system, as a function of the z -coordinate. Data are obtained by considering the average values for the simulation time among 80.00 ns and 89.99 ns.	125
4.62	Distribution of components of the system, as a function of the z -coordinate. Data are obtained by considering the average values for the simulation time among 90.00 ns and 99.99 ns.	125
4.63	Distribution of components of the system, as a function of the z -coordinate. Data are obtained by considering the average values for the simulation time among 100.00 ns and 109.99 ns.	126
4.64	Distribution of components of the system, as a function of the z -coordinate. Data are obtained by considering the average values for the simulation time among 110.00 ns and 119.99 ns.	126
4.65	Distribution of components of the system, as a function of the z -coordinate. Data are obtained by considering the average values for the simulation time among 120.00 ns and 129.99 ns.	127
4.66	Distribution of components of the system, as a function of the z -coordinate. Data are obtained by considering the average values for the simulation time among 130.00 ns and 139.99 ns.	127

4.67	Distribution of components of the system, as a function of the z -coordinate. Data are obtained by considering the average values for the simulation time among 140.00 ns and 149.99 ns.	128
4.68	Water Density Probability during evaporation process, among 20.00 ns and 149.99 ns.	128
4.69	Evaporation of water in system with charged PEDOT 2+ at a) 53.4 ns b) 63.4 ns c) 73.4 ns d) 83.4 ns.	129
4.70	Evaporation of water in system with charged PEDOT 2+ at a) 93.4 ns b) 103.4 ns c) 113.4 ns d) 123.4 ns.	130
4.71	Distribution of components of the system, as a function of the z -coordinate. Data are obtained by considering the average values for the simulation time among 40.00 ns and 49.99 ns. .	131
4.72	Distribution of components of the system, as a function of the z -coordinate. Data are obtained by considering the average values for the simulation time among 50.00 ns and 59.99 ns. .	132
4.73	Distribution of components of the system, as a function of the z -coordinate. Data are obtained by considering the average values for the simulation time among 60.00 ns and 69.99 ns. .	132
4.74	Distribution of components of the system, as a function of the z -coordinate. Data are obtained by considering the average values for the simulation time among 70.00 ns and 79.99 ns. .	133
4.75	Distribution of components of the system, as a function of the z -coordinate. Data are obtained by considering the average values for the simulation time among 80.00 ns and 89.99 ns. .	133
4.76	Distribution of components of the system, as a function of the z -coordinate. Data are obtained by considering the average values for the simulation time among 90.00 ns and 99.99 ns. .	134
4.77	Distribution of components of the system, as a function of the z -coordinate. Data are obtained by considering the average values for the simulation time among 100.00 ns and 109.99 ns.	134

4.78	Distribution of components of the system, as a function of the z -coordinate. Data are obtained by considering the average values for the simulation time among 110.00 ns and 199.99 ns.	135
4.79	Distribution of components of the system, as a function of the z -coordinate. Data are obtained by considering the average values for the simulation time among 120.00 ns and 123.413 ns.	135
4.80	Water Density Probability during evaporation process, among 40.00 ns and 123.413 ns.	136
4.81	Comparison of Density Probability among PEDOT and PEDOT 2+ after ~ 80 ns of simulation.	136

List of Tables

2.1	Contributions to the total temperature T of the system.	58
2.2	Contributions to the total pressure P of the system.	58
2.3	Contributions to the total energy of the system.	59
2.4	Contributions to the kinetic energy of the system.	59
2.5	Contributions to the energy of the system.	59
4.1	Values of Diffusion Coefficient for bulk systems at $T = 25$ °C, for charged and neutral PEDOT oligomers.	96

Chapter 1

Conducting Polymers

With the advancement of technology, electronic devices are becoming more integrated in our everyday life, with key components being LEDs, transistors and solar cells [89].

Besides traditional electronic devices, mainly based on Silicon (Si) or other inorganic materials (Ge, GaAs, etc.), there is an alternative and complementary class of materials in view of some specific applications.

The quick progresses in conductive polymer technologies has induced to use these materials as alternatives to conventional conductors and semiconductors. The coupling of organic electronic devices (electrodes and transistors) with biological systems has led to a great development of Bioelectronics field.

The field of Organic Bioelectronics arises from the development of conductive polymers and their consequent application to biological studies, having opened up completely new possibilities.

The starting point of Bioelectronics is commonly considered due to the experiments of Luigi Galvani on bioelectricity in the 18th century. It is “the discipline resulting from the convergence of biology and electronics”, citing the U.S. National Institute of Standards and Technology (NIST). This field of research indeed studies the interactions between electrical charges (or, from

a more engineering-oriented point of view, electronic devices) and biological entities, revolutionizing science both in view of research and applications.

So, organic devices have attracted great interest for their innovative properties, and their characterization and optimization is nowadays an intense research field; it is important to understand the relations between material structures and their key characteristics in order to develop innovative materials.

Organic electronics has emerged as a rich field of research and development that involves chemistry, physics, biology, materials science, engineering and technology, being versatile enough to be used in a wide range of new applications in fields ranging from healthcare to welfare, especially when flexibility, transparency, large area and/or low cost are paramount.

Recent advances in organic materials have permitted a great evolution in nearly all electronic products - which are already incorporated into commercial ones - such as displays, lighting, power sources, sensors and integrated smart systems-in-foil [98].

Among other physical parameters, the carrier mobility is commonly used as a figure of merit to characterize the performance of materials, devices or fabrication methods [98] and up to now different theoretical models have been proposed [59]: many of them have been supported by evidence in different experiments and computer simulations. Garnier et al., in 1990, reported a carrier mobility of $4.3 \times 10^{-1} \text{ cm}^2/\text{Vs}$ for thin film transistors that used evaporated hexathiophene as an active material; carrier mobilities in conventional a-Si:H TFTs are in the range of 10^{-1} to $1 \text{ cm}^2/\text{Vs}$.

In recent years has been seen that the proper growth of organic crystals can lead up to very high mobilities, up to $100 \text{ cm}^2/\text{Vs}$.

Organic semiconductors (OSCs), in particular, are solids mainly composed by low-molecular weight materials and polymers made up by carbon and hydrogen atoms, and sometimes by hetero-atoms (e.g. oxygen, phosphorus, sulfur and bromine). Both have a conjugated p -electron system formed by

the p_z orbitals of sp^2 -hybridized C atoms in the molecules; those π bonds are usually weaker than σ bonds and the performance of the devices based on organic semiconductors strongly depends on the efficiency with which charge carriers move within the π -conjugated materials [12].

The semiconductor behavior of these materials arises from the presence of conjugated molecules, with the term conjugated that refers to the existence of alternating single and double carbon-carbon bonds.

Although polymer chains may be quite long, the π -conjugation is interrupted by defects, hence the conjugated polymers can be considered as an assembly of conjugated segments [80]. The length of the segments varies randomly and that is a major reason for energetic disorder implying inhomogeneous properties, with the width of the DOS that determines the charge transport characteristics of the material [11].

The major difference between organic semiconductors based on small-molecules and conjugated-polymers is the method of preparation, indeed while small molecules are deposited from the gas phase by sublimation or evaporation, polymers are generally processed by wet chemical techniques.

In the ground state of the molecule, all bonding orbitals up to the highest occupied molecular orbital, the HOMO, are filled with two electrons of anti-parallel spin while the anti-bonding orbitals, from the lowest unoccupied molecular orbital (LUMO) onwards, are empty.

Neutral excited states can be formed for example by light absorption in a molecule, when an electron is promoted from the HOMO to the LUMO.

In general, any configuration with an additional electron in an anti-bonding orbital and a missing electron in a bonding orbital corresponds to a neutral excited state.

It's interesting to consider why organic materials receive so much attention by the scientific community, being a valid complement to the classic inorganic materials: we need then a comparison with silicon, that is one of the

most used materials for technological applications (Fig. 1.1).

About the structures, Silicon is held together by a network of covalent bonds

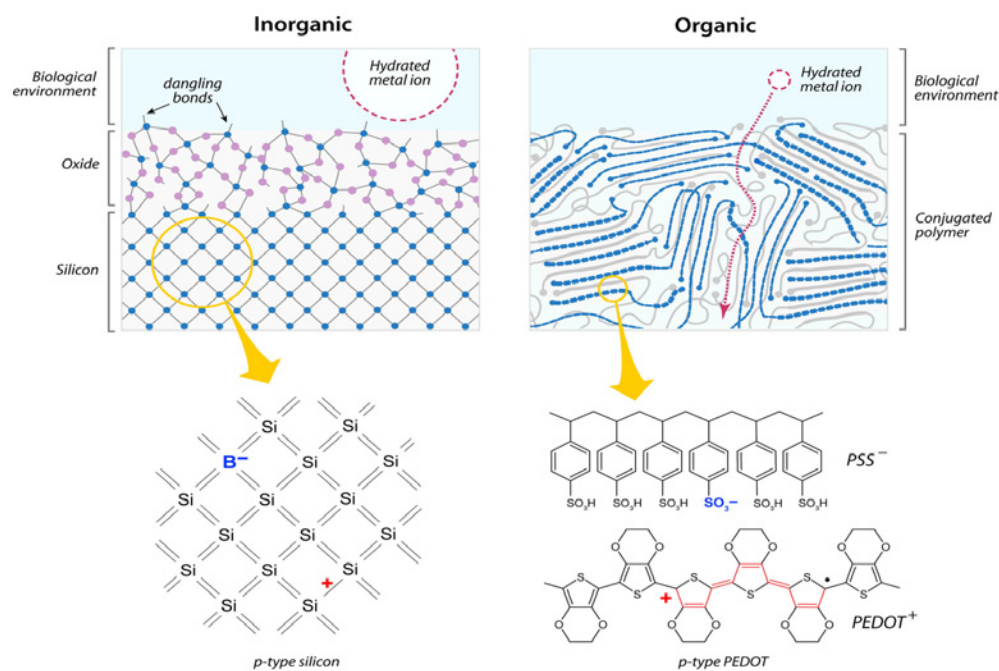


Figure 1.1: Schematics of an inorganic semiconductor, silicon, and an organic semiconductor, PEDOT, at the interface with an electrolyte. The hydrated ion is meant to be the same in both schematics, defining the relative scale. The insets show the action of *p-type* dopants, boron in silicon, and PSS in PEDOT, respectively.

where each atom shares valence electrons with four neighbors [74] while the organic materials consists of (macro-)molecular blocks within which atoms are covalently bonded to each other; these blocks are held together by means of weak van der Waals interactions and, in the case of doped materials, electrostatic interactions as well [74].

The prevalence of van der Waals interactions in the soft organic material is one of the main reasons for the difference with the hard silicon [74].

The identifying characteristics of organics arise from this bonding arrangement.

First, organics offer facile chemical modification so that the toolbox of organic chemistry can be used to modify the structure of the molecular blocks. The functionality can be engineered by altering the π -conjugated backbone or the side groups, thus changing (opto-)electronic, mechanical or biologically relevant properties. Moreover the structures can range from single crystals to exotic forms such as disordered composites and hydrogels.

Second, organics offer the possibility of low temperature processing [74]. Indeed the weak interactions that hold the molecular blocks together can be easily overcome by mild heating (mostly in small molecules) or a solvent (mostly in polymers), and a film can be deposited from vapor or solution on a wide variety of substrates.

Third, organics allow for oxide-free interfaces with aqueous electrolytes and this means that it can be in direct contact with the biological milieu [74].

Fourth, organics can support efficient ion transport at room temperature: indeed the relatively large space between molecules due to the weak van der Waals interactions allows ions to move efficiently in the film.

Finally, in organics, excitations couple strongly to the structure of the molecule. The presence of electronic charges in silicon does not modify the lattice appreciably because atoms are bonded with covalent bonds; consequently, electronic interactions between the atomic orbitals are strong, and wide bands with bandwidths on the order of a few eV are formed.

In contrast, molecular crystals are kept together by weak van der Waals bonds and electronic interactions between the molecular orbitals of adjacent lattice sites are weak: the resulting bands are narrow, with bandwidth below 500 meV.

The charge transport in organic materials is then different in nature respect to the inorganic ones for two main reasons.

First because an excited electron and its respective hole remain bounded together in an hydrogenoid system commonly called (Frenkel) exciton [91]. This is consequence of the poor screening of charges in organic materials due to low dielectric constants (typically $\epsilon_r \simeq 3.5$).

Second, organic materials are soft: a single charge carrier, hopping in an organic material, strongly interact with the vibrations on its nearby molecules, creating quantum quasi-particles called polarons [91]. In the case of the traditional, covalently bound inorganic semiconductors, the electron-phonon interactions are usually much smaller than the electronic interactions and simply account for the scattering of delocalized carriers.

In contrast in organic semiconductors the extensive experimental and theoretical investigations of the last decades have shown that the electron-phonon interactions are comparable to, or even larger than the electronic interactions, and this means that electronic and geometric properties are strongly coupled.

Charges must be able to move between different molecules without being scattered or trapped [95], for an efficient charge transport, and so their mobility is influenced by structural factors including molecular packing, disorder, presence of impurities, temperature, electric field, charge-carrier density, size/molecular weight, and pressure [95].

To conclude, the doping efficiency in organic semiconductors is much smaller than in inorganic semiconductors and the doping concentrations that one need are much higher [96].

1.1 Organic Polymers

The word ‘polymer’ comes from Greek and is composed of two parts: *poly* that means many and *mer* that means part. Indeed a polymer is a macromolecule composed of a chain of repeated units (called monomers) bounded to each other by means of covalent bonds and we refer to the degree of polymerization as the number of repeating units per macro-molecule.

The structure is obtained through the chemical process of polymerization:



or also by the process of condensation based on the elimination of a small molecule, usually water or HCl, when two monomers join.

In everyday life polymers are everywhere, e.g. in rubber and in plastics, because they are extremely versatile and they can give rise to different behaviors.

Their classification can be based on the structure (linear polymers, cross-linked polymers, branched chain polymers), on their mode of polymerization (addition polymers, condensation polymers), on their way of production (synthetic polymers, bio-polymers) and so on.

In the last decades conducting polymers (CPs), i.e. organics polymers that conduct electricity, have gained a lot of attention because of their characteristic and properties.

Many known polymers really are insulating, but they can become also be semi-conductive in presence of a π -conjugated system and in particular in presence of alternating double and single bonding.

Of the four electrons in the outer shell of each carbon atom, three of these electrons are used to form sp^2 hybridized orbitals, and when two of these orbitals belonging respectively to two adjacent carbon atoms combines in-plane, a σ bond is formed. The fourth electron forms a p_z orbital perpendicular to

the σ bond, and from the overlap of two p_z orbitals, a π bond is formed.

The electrons in the double bonds so can move along the carbon chain because of the continuous overlapping of the p_z orbitals.

This means that electrons are de-localized over the polymer backbone because of the extended orbitals in π -conjugated system, with the π -electron de-localization that is reduced by structural disorder: the value of the band gap is then similar to the difference between the $\pi - \pi^*$ levels, where π^* is the anti-bonding orbital.

This is a fundamental aspect because the electronic structure determines the electrical conductivity.

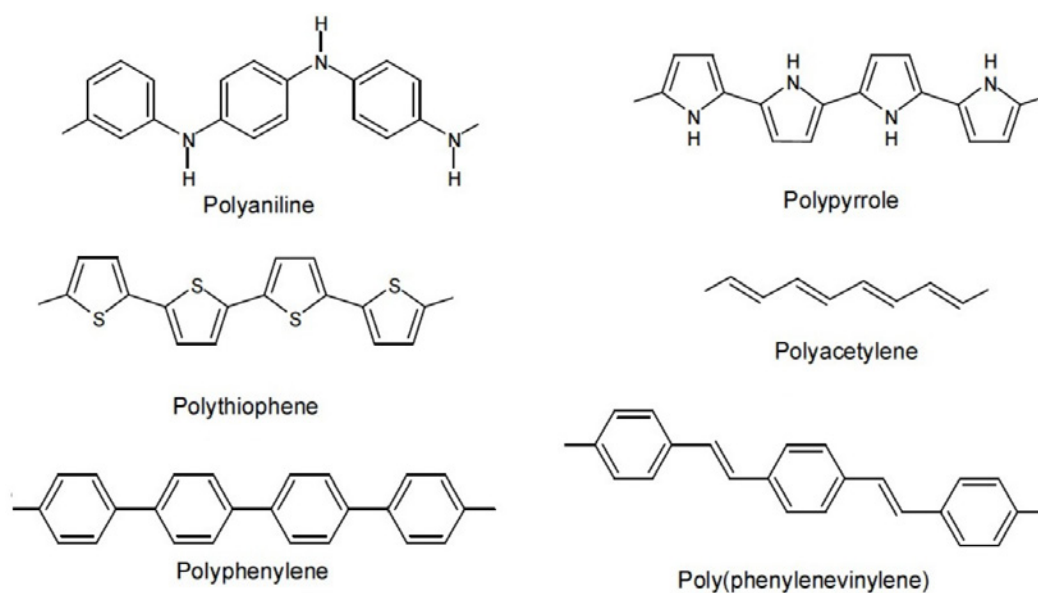


Figure 1.2: Chemical structures of conductive polymers

Conductive polymers can achieve a conductive state through a process of doping that is different in nature compared with the doping of inorganic materials, and indeed is based on the chemical or electrochemical p-doping (oxidation) or n-doping (reduction); this also leads to a reversible process of doping based on the ease of oxidation or reduction (less frequently) of the

polymer.

In this way some electrons are added or removed from the polymers and the charge carriers can move along the chain (intra-chain transport), but also through the inter-chain hopping between different chains.

Indeed, in conjugated polymers, the charge transfer reaction is the key point in the doping process.

The process of doping can be very effective depending on the couple polymer-dopant and the electrical conductivity of the uncharged polymer can be increased up to 10-12 orders of magnitude, reaching and going beyond values of 1000 S/cm [100]. Otherwise the uncharged polymer would be almost an insulator. The process of electrochemical doping, that also result in a change of the doping state, can be obtained when ions from an electrolyte enter an organic film, or vice versa: the compensating electronic charge is supplied by a metal contact.

One can then evaluate if a polymer can be a potentially conducting polymer or not by studying the ease of oxidation or reduction, having in mind that that the electrical conductivity also results from the ability of charge carriers to move along the π -system (carrier delocalization).

π -bonded unsaturated polymers represents a choice because of their small ionization potentials and/or large electron affinities. The σ -bonds that hold the polymer together are at most only slightly influenced by the π electrons that are removed or added (easily).

Solitons, polarons and bipolarons are the way in which exist charges that are generated in doping processes [101]. These states are characterized not only by a charge, but also by a lattice distortion. This is due to energetic reasons and in particular because the localization of a charge, with the consequent local distortion (relaxation) of the lattice around it in energetically favorable in organic polymers.

Literature focused on the calculation based on the Hückel theory report that

in conjugated polymers polaron formation coupled with lattice deformation is always energetically favorable respect to ionization.

Solitons instead only occurs in degenerate polymers, i.e. polymers that possess two different geometrical structures in the ground state with exactly the same energy; e.g. trans-polyacetylene (PAC) is one of the most common example.

1.1.1 Poly(3,4-ethylenedioxythiophene) - PEDOT

PEDOT, or Poly(3,4-ethylenedioxythiophene), is an organic conducting polymer that results from the polymerization of EDOT (ethylenedioxythiophene) monomers, derived in turn from the polymerization of thiophene heterocyclic compound. The process of polymerization of PEDOT molecules, starting

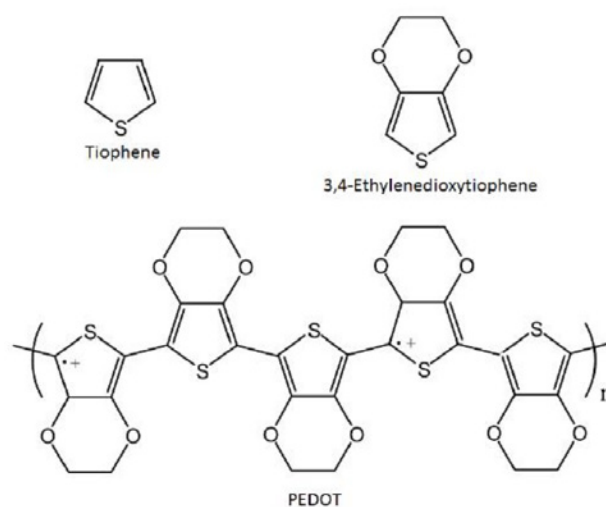


Figure 1.3: Chemical structure of thiophene, 3,4-ethylenedioxythiophene (EDOT) and PEDOT.

from the monomers, can be based for example on a chemical oxidative polymerization process.

PEDOT is one of the most studied conducting polymers: it was first synthesized in 1988 by Bayer's laboratories AG in Germany [32] in order to synthesize a new conductive polymer that does not decrease its conductivity over long periods of time, as instead happens with the polythiophene, and has given rise to a growing interest because of the showed values of conductivity [103] and excellent thermal and air stability [102], also in the oxidized state.

Synthesis methods for a large-scale manufacturing are also relatively simple, at this made it a material of choice for many applications (organic electronics, electrodes, electro-chemical transistor etc.).

High conductivity of PEDOT is achieved in a doped state where the positive charges in the polymer backbone are compensated by negative counterions (usually polymeric counterions such as Poly(Styrene Sulfonate) PSS or molecular counterions such as tosylate).

However it is totally insoluble in any solvent. For this reason a doping counterion (again the PSS) is used during the polymerization process, giving rise to the PEDOT:PSS.

The PSS then does not contribute directly to the charge transport, instead it allows to the PEDOT oligomers to disperse in aqueous solution, moreover balancing the charges of PEDOT.

1.1.2 Poly(Styrene Sulfonate) - PSS

Poly(Styrene Sulfonate) is a polymer derived from Polystyrene and, limited to our purposes, it is used together with PEDOT for some main reasons:

- it keep the PEDOT oligomers dispersed in an aqueous medium, forming a micro-dispersion whose color ranges from dark blue to transparent
- it acts as a counterion, balancing the positive charges of the polymer chain of the PEDOT oligomers.

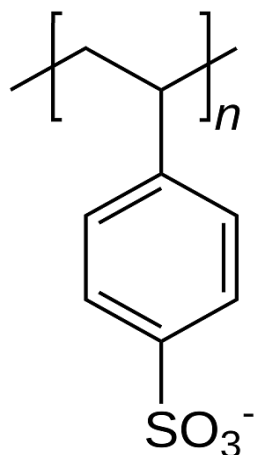


Figure 1.4: Monomer of Poly(styrene Sulfonate).

1.1.3 PEDOT:PSS

PEDOT:PSS results from the union of poly-cations (PEDOT) and poly-anions (PSS) in aqueous solution: the molecular masses of their monomers are respectively 140 g/cm^3 and 182 g/cm^3 .

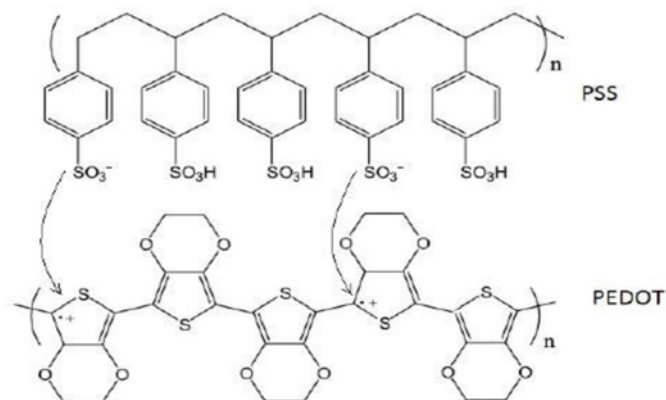


Figure 1.5: Schematic view of the chemical structure of charged PEDOT and PSS polymer.

The physical parameters of the polymeric film are influenced by the ratio between PEDOT and PSS, in particular for what it concerns the conduc-

tivity: higher PSS concentrations give less conductivity but more flat films. Anyway in view of the applications different values of the conductivity can be more or less suitable.

The PEDOT oligomers are connected to the PSS polymers via electrostatic and van der Waals interactions, and the conductivity of the complex arises from the arrangement of the PEDOT oligomers in lamellar structures: the transport of charge then is not given by the PSS polymers, because they simply allows the oligomers of PEDOT to disperse in aqueous solutions.

Experimental results tell us that approximately the oxidation level of the PEDOT oligomer is of 1 charge for 3 monomers of EDOT (because of the oxidative polymerization process), so that the holes density in a PEDOT:PSS thin film is of $n_h = 3 \times 10^{20} \text{ cm}^{-3}$.

Other experimental findings concern the phase separation of the PEDOT:PSS. Indeed PEDOT:PSS separates into PEDOT-rich regions with a size of tens of nanometers with a surrounding PSS-rich phase.

Moreover this composite is permeable to ions and shows high ionic mobilities.

About deposition of PEDOT:PSS dispersed in water, all common techniques employed for the deposition of waterborne coatings can be used.

Deposition techniques through which uniform coatings can be obtained are spraying, electrospinning, slit coating, drop casting, bar coating and spin coating.

Other employed techniques are inkjet, screen printing, nozzle printing and contact printing (gravure, flexographic and offset printing), mainly when is required a structured deposition.

Structured deposition of PEDOT:PSS have been realized by modifying the wetting properties of the surface, that is by depositing water repellants or by introducing photolithographical techniques.

Uniform films and specific deposition technique need that the pristine PEDOT:PSS dispersion in water has to be adjusted. The film quality is determined by important properties such as the surface tension, the adhesion to the substrate and the viscosity.

Different grades of PEDOT:PSS hence can be used, which differ in the ratio of PEDOT to PSS and the gel particle distribution, or by the addition of water soluble or dispersible additives.

There exist many commercially available ready-to-use formulations optimized for specific applications and deposition techniques, for example by Heraeus GmbH (under the commercial name Clevios™) and Sigma-Aldrich.

An easily accessible technique to obtain uniform films in a thickness range that span from 10 to 1000 nm is given by the spin coating.

The electrochemical polymerization represents another technique for the deposition of PEDOT:PSS thin films.

PEDOT:PSS films gained much attention because of their thermal stability.

This property has been studied by thermogravimetric analysis (TGA) of thick layers at Bayer Laboratories and gives us information about the weight loss over time while the sample is heated at a constant rate.

The results is that, between 100 °C and 200 °C, the weight loss is only determined by evaporation of remaining water. Things are different at about 250 °C, as the sample weight decreases significantly.

Interesting is also the behavior of PEDOT:PSS films when are exposed to light, as the wavelength of radiation affects the kinetic of degradation significantly; conductivity of PEDOT:PSS films especially decreases for absorbed UV photons with $\lambda < 320$ nm, resulting in a degradation of the material over time when exposed to UV light (like most polymers).

Proper protections are hence needed for the use of conducting polymers in

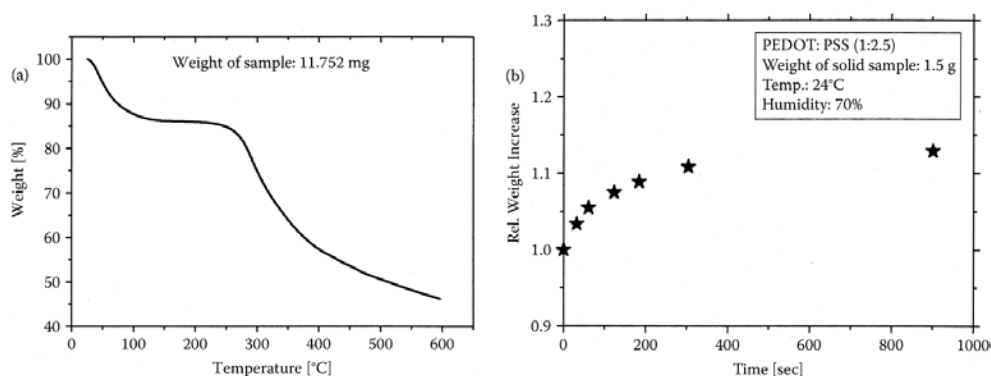


Figure 1.6: (a) Weight loss of a sample of PEDOT:PSS with a weight ratio of PEDOT to PSS as 1:20 monitored while heating at a constant rate of 5 K/min. (b) Weight increase of a PEDOT:PSS sample owing to the absorption of water as a function of time. [63]

outdoor applications.

Also mechanical properties have been investigated through tensile strength tests on PEDOT:PSS films. Relative humidity (rH) level turns out to be a parameter that strongly influence the mechanical characteristic.

X-ray diffraction (XRD) analysis and morphology observations performed with scanning probe microscopy techniques indicate that PEDOT:PSS films are amorphous; chemically in situ polymerized PEDOT films, which do not contain PSS, instead exhibit crystalline ordering and fibril-like structures.

The light absorption spectrum of PEDOT:PSS is almost identical to the absorption of in situ chemically polymerized PEDOT without PSS.

PEDOT:PSS thin films are highly transparent in the visible spectral range and the light-blue appearance is related to an higher absorption in the red.

The absorbance spectrum for a 100 nm thin film of PEDOT:PSS, see 1.8, consists of a broad feature above 400 nm increasing all the way up to 3200 nm

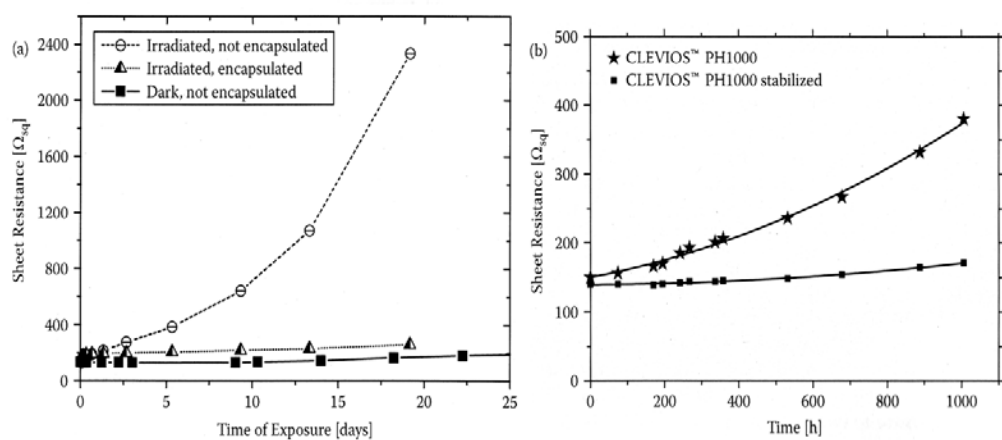


Figure 1.7: (a) Sheet resistance of films of PEDOT:PSS including 5% ethylene glycol as a function of time. (b) Sheet resistance of PEDOT:PSS films exposed to a Xe lamp as a function of time, compared to a non-exposed sample [63].

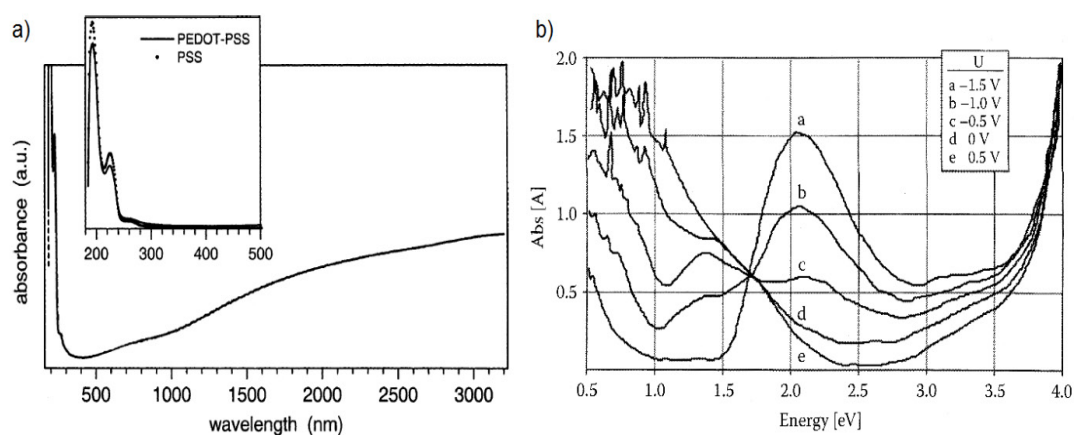


Figure 1.8: (a) Absorbance of a thin film of PEDOT:PSS (110 nm). In the inset, absorbance of PEDOT:PSS and PSS in the spectral range from 185 to 500 nm. (b) Optical absorption spectra of a PEDOT:PSS electrode in an electrochemical cell for different applied voltages. [63]

and this can be interpreted as the free charge contribution to the absorption. Shorter wavelengths results in two pronounced absorbance peaks at 193 and

225 nm.

We also stress that the absorption spectrum of PEDOT and PEDOT:PSS strongly depends on the PEDOT oxidation state: this is a consequence of the generation of charged states (polarons and bipolarons) along the polymer backbone, that is coupled to the formation of energy levels within the energy gap. Uptake of water and significant swelling characterize the behavior of PEDOT:PSS thin films: indeed the greater is the amount of water in the environment and the greater is the amount of PSS polymers compared to PEDOT oligomers in the composition of the film, the more is the water absorption, that results in a weight gain. The presence of water residues can adversely affect the performance of PEDOT:PSS films.

Regarding the dependency of the conductivity on the temperature, this can be understood in the framework of the Variable Range Hopping (VRH) model, by which we have this kind of behavior:

$$\sigma(T) = \sigma_0 \exp \left[- \left(\frac{T}{T_0} \right)^\alpha \right] \quad (1.1)$$

The conductivity can be defined by the elementary charge e , together with the charge mobility and the charge density, by the relation:

$$\sigma = e\mu_e n_e + e\mu_h n_h \quad (1.2)$$

Only the holes give a contribution to the charge transport in PEDOT: this is because the injection of electrons leads to a recombination in oxidised PEDOT sites.

The conductivity in PEDOT:PSS film reaches values also of $\sigma = 1000$ S/cm by which we can obtain a value for the hole's mobility of $\mu_h = 20$ cm²/V·s.

1.1.4 Applications of PEDOT:PSS

PEDOT and its derivatives are by far the most used conducting polymers and they represent the material of choice for many applications.

The ratio between PEDOT and PSS have an influence on the physical parameters of the polymer film because of the different electrical and chemical properties. This results in different bulk conductivity, sheet resistance, solids content, and surface roughness, and hence also results in different applications.

PEDOT:PSS or PEDOT without PSS doping, for example, have found wide applications in energy conversion and storage fields (organic solar cells, supercapacitors, fuel cells etc.). This polymeric blend indeed is a good candidate as transparent electrode for organic solar cells, i.e. for the 3rd generation of photovoltaic technology, that can replace the more rigid and expensive Indium Tin Oxide (ITO).

This material is a popular hole transport layer in organic solar cells (OSC), having also been traditionally employed as a hole injection layer in organic light emitting diodes; the reason is due to good film forming property via solution processes, excellent optical transparency in visible light range and because of intrinsically high work function.

Conductive polymers, among other properties, possess high capacity, high conductivity, flexibility, large voltage window, good reversibility, low environmental impact and low cost and they become an optimal material for electrochemical capacitors, also known as supercapacitors.

Their interest is due to the increasing demand for portable electronic systems and electric vehicles.

Examples of conducting polymers able to deliver specific capacity at a high current rate are PANI (polyaniline), PPy (polypyrrol), PEDOT and PTh (polythiophene). PEDOT in particular is a derivative of thiophene and can be easily p-doped or n-doped and exhibits low oxidation potential with a wide voltage window of 1.2-1.5 V, high thermal and chemical stability and high charge mobility for fast electrochemical kinetics.

PEDOT moreover can be repeatedly doped and undoped, and its almost transparent and light blue color in the oxidized state can be easily changed into opaque and dark blue in the neutral state. A change in its doped state hence results in a color change and this is useful for optical applications, such as electrochromic displays.

The intrinsic low thermal conductivity of organic conductive polymers (0.028-0.6 Wm⁻¹K⁻¹) which is orders of magnitude lower than those of the inorganic thermoelectric materials (TMs), makes them more suitable also in thermoelectric applications.

We recall that thermoelectric materials are materials able to turn waste heat into electricity or provide refrigeration without any liquid coolants, turning out to be a great resource for applications in both power generation and solid-state cooling or heating.

The dimensionless figure of merit ZT determines the performance of TMs, and is defined as:

$$ZT = \frac{S^2 \sigma T}{k} \quad (1.3)$$

where S is the Seebeck coefficient, σ is the electrical conductivity, T absolute temperature and k the thermal conductivity.

High ZT values so can be obtained with a high power factor σS^2 and/or with low thermal conductivity.

Early studies on organic TMs focused mainly on polyaniline, polypyrrole, and polythiophene, but these materials suffered from relatively low electrical conductivities.

PEDOT:PSS then is a promising material in this field because of high electrical conductivity.

Among the applications of PEDOT:PSS, it is worth mentioning those in the field of bioelectronics.

PEDOT:PSS-based devices can so be schematized into other two classes of

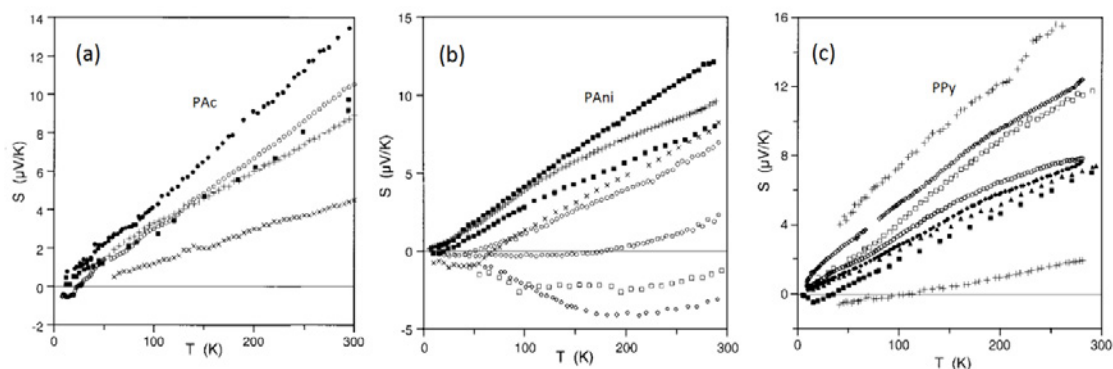


Figure 1.9: Thermopower for (a) highly doped PAC, (b) PANi, (c) PPy. [48]

applications:

- Electrochemical sensors, in form of organic electrochemical transistors (OECTs): Biosensors and Wearable Sensors;
- Devices controlling tissues and replication of living cells.

Examples of biosensors are implantable biological interfaces, such as cardiac patches, neural interfaces, electroceuticals and on-command drug delivery platforms.

One example of application is given by electrocorticography (ECoG) electrodes, which are increasingly used for functional mapping of cognitive processes, and for people with severe motor disabilities.

A micrograph of the electrodes is shown in Fig. 1.10a. The arrays consisted of a parylene substrate, gold contact pads and interconnects, and parylene insulation. A PEDOT:PSS film was deposited in appropriate holes in the insulation layer, defining the electrodes.

Fig. 1.10b shows a micrograph of an array conforming to the midrib of a small leaf. Regarding the wearable sensors, thanks to the use of a conducting polymer as active material, the OECT technology was successfully transferred on textile substrates, woven cotton and lycra.

An indisputable trend in biosensor technology is on-body continuous monitoring of metabolites using these wearable devices (Fig. 1.11).

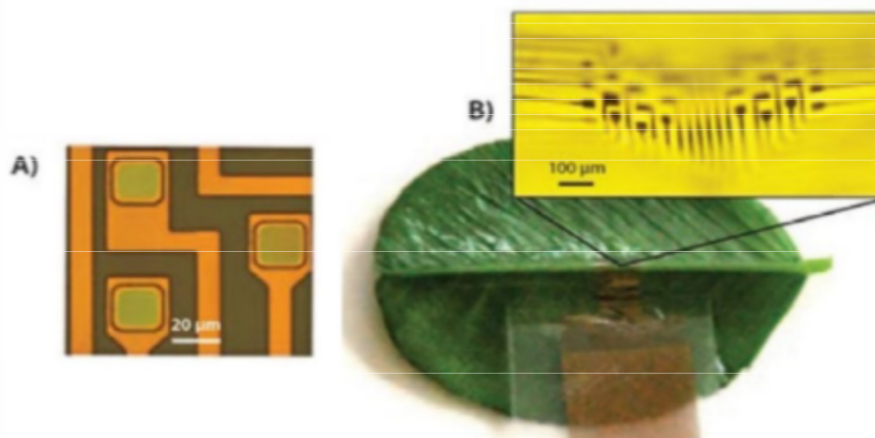


Figure 1.10: a) Micrograph of the electrodes. b) Micrograph of an array conforming to the midrib of a small leaf. [46]

Wearable biosensor applications aim to transform centralized hospital-based care systems to home-based personal medicine, reducing healthcare cost and time for diagnosis. Finally, for what it concerns the devices controlling tis-

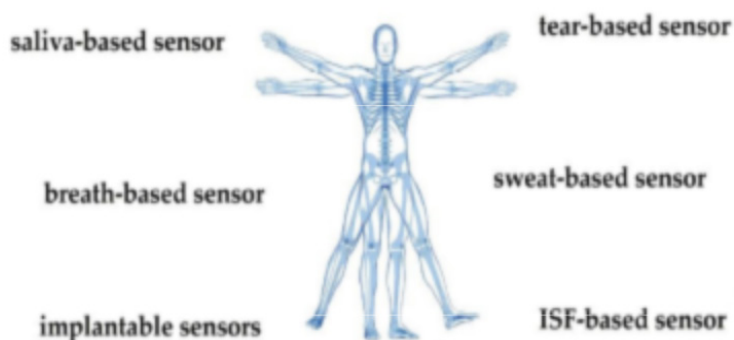


Figure 1.11: Examples of wearable sensors.[13]

sues and replication of living cells, we have that by integrating the OECT architecture into the cell layer (Fig. 1.12), the OECT technology is able to measure the ion flux allowed through the barrier tissue.

Barrier tissues (as the gastrointestinal (GI) tract and the blood brain barrier), act as the first line of defense of the body and block the passage of toxins and pathogens, but allow the passage of ions, water, and nutrients. So, devices able to measure the ion fluxes also give indications of anatomic integrity of the barrier.

As the cell proliferation rate is directly dependent on the electrochemical state of its substrate, devices based on OECT technology have been built, that through the variations of the redox state of the substrate act on cell growth; so have been tested different cell lines, such as human dermal fibroblasts (hDF) and human tumoral glioblastoma multiforme cells (T98G).

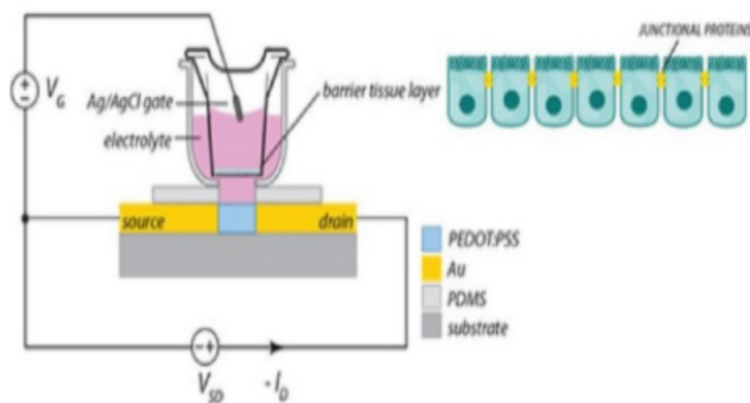


Figure 1.12: Architecture of an OECT integrated with barrier tissue layer; tissue is supported on a permeable membrane. On the right is showed a tightly packed epithelial cells with junctional proteins that regulate transport. [46]

Chapter 2

Molecular Dynamics Simulation

“An intelligence which could, at any moment, comprehend all the forces by which nature is animated and the respective positions of the beings of which it is composed, and moreover, if this intelligence were far-reaching enough to subject these data to analysis, it would encompass in that formula both the movements of the largest bodies in the universe and those of the lightest atom: to it nothing would be uncertain, and the future, as well as the past, would be present to its eyes. The human mind offers us, in the perfection which it has given to astronomy, a faint sketch of this intelligence. ”

— Pierre Simon de Laplace [56]

Science is based on experiments, and performed experiments can be in agreement or disagreement with models and theories.

By means of computer simulations we can think about the interplay between theory and experiments; the calculations that are performed in the computers are based on mathematical or theoretical models but the results obtained at the end of the calculations can be related with the physical quantities and properties that one can evaluate in an experiment, so that the expression “computer experiment” is sometimes used.

Computer simulations are performed in order to understand the behavior

and the properties of a relatively big amounts of atoms and molecules in terms of their structure and interactions, serving as a complement to conventional experiments [2].

What can be achieved is not only a posteriori verification of already existing experiments, but also the forecast of new and unexpected behaviors, especially those behaviors that cannot be found out in a different way [43].

Indeed many practical situations may require the support of a computer to avoid too dangerous, too expensive, too slow, too difficult etc. experiments, and for example in the pharmaceutical industry is commonly used to design drugs by means of computers [18].

Moreover a computer simulation acts as a bridge between (pico/nano/micro)scopic length and time scales and the macroscopic world through the statistical physics [71].

In particular, Molecular Dynamics is a computational technique for simulate a complex system at the atomic and molecular level, unlike other methods that consider the system as a continuum.

The equations of motion are solved numerically so that the evolution of the system can be followed in time, allowing the derivation of thermodynamic and kinetic properties of interest.

If we don't consider atoms of H and He, the dynamics of the nuclei can be described with very good accuracy by classical mechanics. More details are given in Section 2.9.

These approximation is enough to reduce the complexity of the calculations (that would be otherwise required for a truly quantum description of the particles involved), allowing us to simulate relative big systems for tens of nanoseconds [49].

Clearly the development of the Molecular Dynamics is related to the construction of faster and more efficient computers and also to the developments

of new methods.

Nowadays computers based on parallel architectures have improved considerably the simulation of increasingly complex atomic and molecular systems, also for longer times.

Molecular Dynamics methods can not only be based on a classical approach, in which the laws of classical mechanics define the evolution of the system: ‘first-principles’ Molecular Dynamics simulations indeed take explicitly into account the quantum nature of atoms, molecules and chemical bonds, allowing us to describe the electron density function for the valence electrons that determine bonding in the system by computing quantum equations.

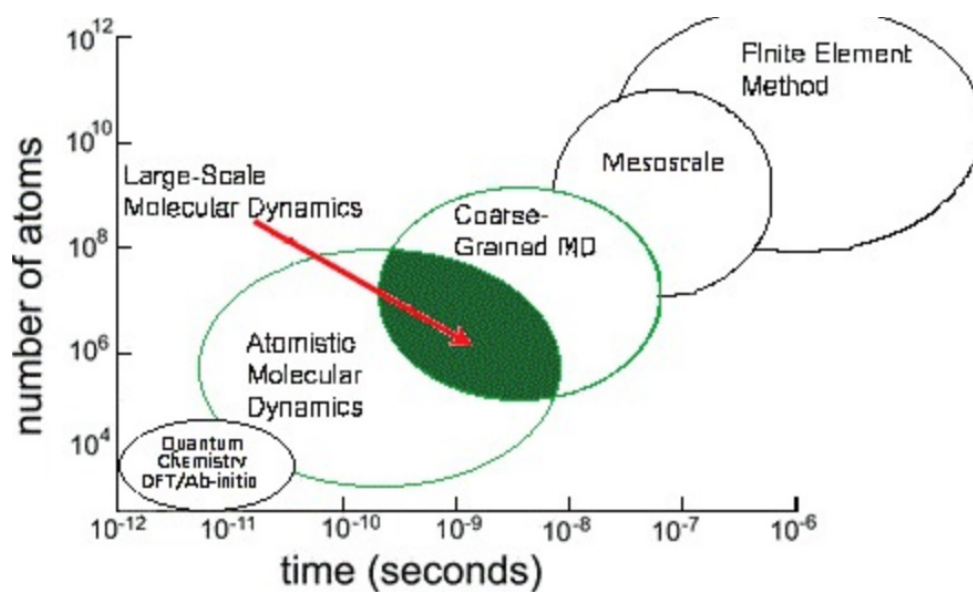


Figure 2.1: Time and length scales for computer simulations.

The optimization of the problem that one wants to solve must be taken into account so that, even if the quantum simulations represent a step forward towards a more precise description of the phenomena under examination, the computational resources required are bigger and at present only with classical Molecular Dynamics Simulations can be obtained information about

system comprising thousands of atoms over time scales of nanoseconds or microseconds.

Simulations may also need some specific input parameters to characterize the system under study, and they can be obtained either from theoretical considerations or by experimental data.

A simulation of a system containing water and ethanol molecules have been setup under the supervision of Prof. Andrei V. Komolkin, in order to learn the techniques of Molecular Dynamics.

2.1 Structure of the Simulations

A typical Molecular Dynamics Simulation is divided in different steps.

First of all it is necessary to define all the parameters useful for the simulation and read the initial coordinates; then the initial speeds are generated from a Maxwell-Boltzmann distribution (at a certain temperature).

Once that initial parameters are given, the calculations can proceed in a cycle; a time-step is given (e.g. ~ 1 fs), depending on the accuracy/efficiency that is more suitable for the problem, and the cycle last depending on the time of simulation needed. At each step the coordinates, speeds, forces and potentials of the atoms are calculated (based on the results of the previous step) and memorized on a disk with a certain frequency, that depends on how often the information on the trajectories are needed.

2.1.1 The Initial Configuration

In this stage it is created the configuration of the system we are interested in. The choices to do concern about size of the simulation box, the coordinate of atoms and molecules in the system, the partial charges to associate to every atom, the correct time-step, the cut-off radius and the way in which we want to treat the long-range interactions, the integration algorithm and

the working thermodynamic ensemble (NPT , NVT or NVE).

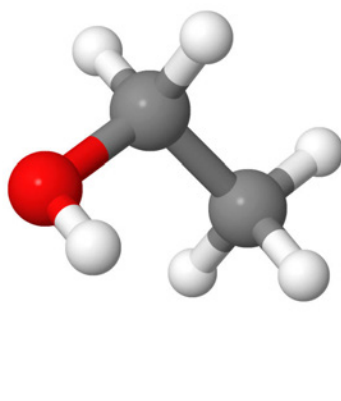


Figure 2.2: Ethanol molecule created with Jmol software.

ATOM	1	O1	SPI	1	-0.003	-0.013	-0.049	1.00	0.00	O
ATOM	2	C3	SPI	1	-0.824	0.829	-0.858	1.00	0.00	C
ATOM	3	H2	SPI	1	0.548	-0.554	-0.636	1.00	0.00	H
ATOM	4	C6	SPI	1	-1.729	-0.013	-1.740	1.00	0.00	C
ATOM	5	HC	SPI	1	-0.180	1.474	-1.460	1.00	0.00	H
ATOM	6	HC	SPI	1	-1.420	1.459	-0.196	1.00	0.00	H
ATOM	7	HC	SPI	1	-2.367	0.624	-2.365	1.00	0.00	H
ATOM	8	HC	SPI	1	-2.366	-0.659	-1.132	1.00	0.00	H
ATOM	9	HC	SPI	1	-1.141	-0.665	-2.388	1.00	0.00	H
TER										

Figure 2.3: Spatial coordinates of the above ethanol molecule.

The screenshot displays a multi-tabbed software interface. The top tabs include 'akmd.def', 'ak-PSS.data', and 'PSS_3minus.akmd'. The bottom tab, 'PSS_3minus.akmd', is active and shows a list of atom types and their corresponding parameters. The parameters are organized into columns: atom type, x, y, z coordinates, and other simulation parameters. The atom types listed include H, C, O, S, and P, with various subtypes like HC, CT, HA, HO, Su, Ou, Op, H, C, O, S, and P. The coordinates are given in scientific notation. The bottom right corner of the window shows a 'Plain Text' editor with 'Tab Width: 8' and 'Ln 1, Col 1'.

Figure 2.4: Some of the parameters needed in the initial stage of a simulation.

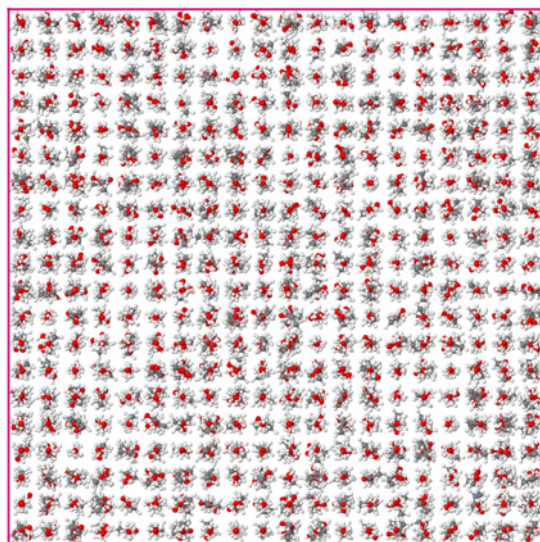


Figure 2.5: Initial atomic spatial configuration for the simulation of water/ethanol mixture (5 molecules of water for every ethanol molecule).

2.1.2 Equilibration Stage

The initial configuration is the starting point to obtain the desired physical quantities but it is not representative of the conditions we want to explore because it contains initial artifacts due to the starting configuration.

For example the initial atomic/molecular positions for the simulation of the water/ethanol mixture (Fig. 2.5) were determined randomly and arranged in an ordered structure: this is clearly not representative of the structure of a liquid, that instead is the physical aggregation state of the mixture at room temperature.

In that case we needed to wait at least an amount of time sufficient for the disappearance of the long range order.

Therefore, in general, this initial part of the simulation related to the equilibration is not used to compute any physical property.

The achievement of an equilibrium condition can be deduced by the analysis of the values of energy components (vibrational, translational etc.), pressure, temperature etc.; indeed at equilibrium this values should fluctuate around an average value. In particular one must first check that the total potential energy goes to a constant value with small fluctuations, usually in a relatively small amount of time. Then, one must check that kinetic energy distributes in equal proportions between degrees of freedom, usually in a slower way compared with the previous process. Lastly, the main criterion of equilibration for the systems consists in analyzing molecules positions: molecules must run away from the initial positions farther than one half of their length.

In any case, in general, the time of simulation must be also long enough to ensure the validity and applicability of the ergodic hypothesis.

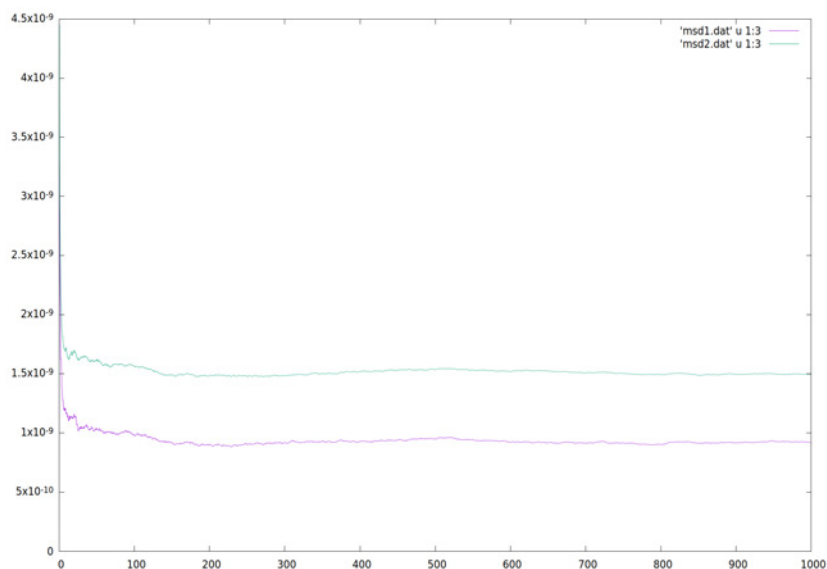


Figure 2.6: Diffusion coefficients of water molecules (green line) and ethanol molecules (purple line) in water/ethanol mixture, at $T = 25$ °C.

2.1.3 Output File

Once that we have obtained a situation of equilibrium, with the desired temperature and pressure that fluctuates around their equilibrium values, the system should continue to run in the simulation for an amount of time that is longer compared to the relaxation time of the physical property/process of interest, and in any case having in mind the ergodic hypothesis.

This means that the simulation time when simulating gasses or standard liquids can be relatively low (few nanosecond), while for glasses and large molecules/polymers the simulation must be long enough to ensure the exploration of all the possible configurations.

The simulated trajectories are finally analyzed to obtain properties/values of interest.

Statistical mechanics plays a fundamental role to link the information about positions, velocities and even forces as a function of time (that are the main output data that we have after a simulation), to the properties that we want

to study [65].

2.2 Periodic Boundary Conditions

Even if the use of computer simulations is a very useful and powerful bridge between theory and experiments, being also a valid forerunner of new ideas and results, it is always fundamental to think if and how we are legitimate to use the methods of Molecular Dynamics Simulations to study a biological/chemical/physical system. This topic will be considered also in section 2.9, but for the moment is important to stress again the fact that a large system cannot always be studied directly from the first principles of quantum mechanics despite the progresses of computers and that, even in a classical framework, the system that is studied by computers is usually restricted at most to several thousands of atoms, that corresponds to a subsystem respect to the physical system or object that one can study for example in a laboratory.

Anyway if we want to study a macroscopic object, or in general an object that is much bigger than the considered simulation box, it is of fundamental importance to relate what is measured in the cell box with the macroscopic system, even because the purpose of computer simulations is to describe the real world.

In a Molecular Dynamics Simulation, because one can be considered just a relative small number of atoms and molecules, some undesired surface effects can arise due to non-isotropic forces: the atoms/molecules on the surface are no longer surrounded by neighboring particles in all the possible directions and this means that the finiteness in size of the system is felt especially because of the presence of the boundaries.

Then how to measure the bulk properties of a physical system, due to the particles that are located far from the surface, even in (unavoidable) presence of surface particles?

Note that, if we consider 1000 atoms arranged in a cubic structure ($10 \times$

10×10), as many as 512 atoms are found on the surface of the cube (more than 50% of the total number of atoms), while if we consider 10^6 atoms in a cubic arrangement ($100 \times 100 \times 100$), just the 6% of this atoms lies on the surface of the cube.

A practical way to reduce this undesired effects, and that is adopted in most molecular dynamics simulations, consists in using periodic boundary conditions (PBC): this method assumes that the simulation box (often considered as cubic, but that in general is orthorhombic) in which the particles of the system are located, is periodically repeated in all the directions following the three directions of space by similar systems (ghost boxes) that have exactly the same configuration of particles of the “reference box”, at any time.

When and if a particle leaves the central box during the simulation, then one of the image particles enters in the central box from the opposite direction because every image particles of the other repeated boxes moves in the same way of the particles in the central box [93].

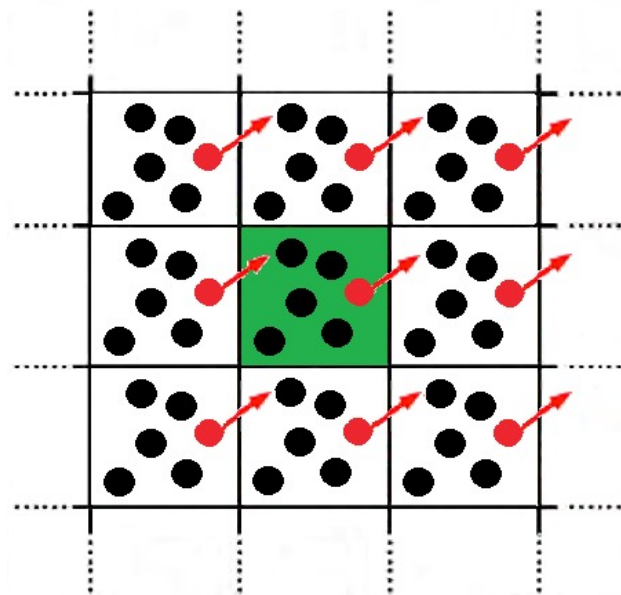


Figure 2.7: 2-dimensional periodic boundary conditions.

The features of this pseudo-infinite system generated in this way (we are essentially considering a system of a certain size embedded in an infinite system, composed of infinitely repeated systems that can be thought as ghost boxes) raises some questions about the method and the approximations that are more suitable to study the inter-molecular interactions, in view of a correct reproduction of the dynamic and thermodynamic quantities.

It turns out to be particularly useful the “minimum image” approximation, which supposes that each particle of the central simulation box interacts with the closest image of all other particles.

Indeed by introducing a cut-off sphere (that can be thought as a truncation sphere), the interactions beyond a certain distance can be ignored: typical distances are given by the half of the smallest dimension of the simulation box [10].

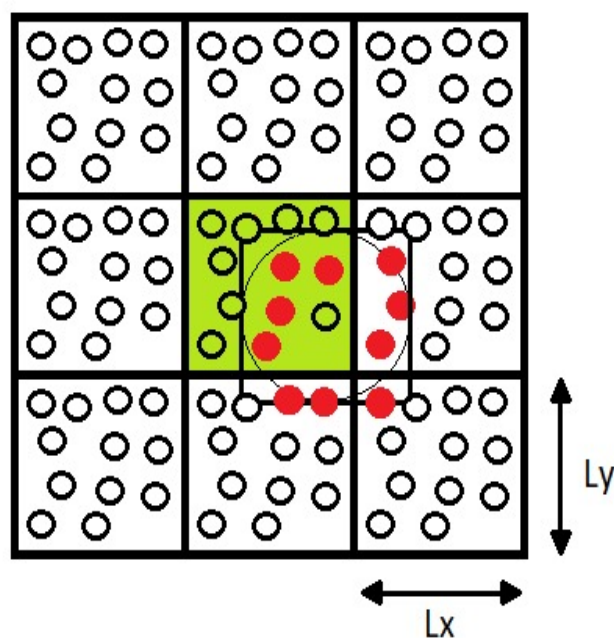


Figure 2.8: Minimum image convention interactions.

Because we are using an approximation, one must also consider how good it actually is and this in particular depends on the type of interaction that one is considering: short range and long range interactions requires a different level of attention. In particular, whereas short-range interactions don't require special care, for long-range interactions this is no longer true [83].

The $1/r^n$ interactions ($n < 3$) cannot be studied correctly with a cut-off radius, and that's why one should consider more suitable methods such as the Ewald Summation, as described in Section 2.7.

This method(s) are almost always indispensable for a correct physical description of long-range interactions, but on the other hand this has a cost in terms of computational performance [40].

2.3 Force Field Descriptions

The reliability and the accuracy of a Molecular Dynamics simulation strongly depends on the way in which we model the intra and the inter-molecular interactions and a comparison with already existing experimental results is always welcome for a validation or rejection of the model.

Because the utility of a simulation is not only to reproduce known results, but also to understand and predict from a quantitative and qualitative point of view the microscopic origin of the observed physical effects, very detailed information about positions, velocities and forces are of paramount importance.

A good idea for an optimal description of the inter-atomic forces is to obtain them from first principles, studying the electronic structure of a certain configuration of the nuclei, and consequently calculate the resulting forces on each atom. If the spatial and time-scales that one want to simulate are prohibitive, however, a different approach must be taken into account and empirical methods based on Force Field are used.

A force field is then a functional mathematical expression that describes the intra- and inter-molecular energy of an atomic/molecular system, consisting of the analytical form of the inter-atomic energy and of a set of parameters that enter into this form.

The parameters can be obtained from quantum mechanical calculations, as stated above, or from experimental data (e.g. from NMR or neutron spectroscopy).

Calculations must be fast enough to obtain the results in a reasonable amount of time but also accurate enough to provide satisfactory results, and that's why many force fields are available, so that one can choose the most appropriate degree of accuracy and complexity.

A more accurate description of some existing Force Field will be done in Section 2.3.3: for the moment it is good to know that a typical example of a Force Field used in many simulations is the following:

$$\begin{aligned}
 \mathcal{V}(\mathbf{r}_1, \dots, \mathbf{r}_N) &= \mathcal{V}_{bonded} + \mathcal{V}_{non-bonded} \\
 &= \sum_{bonds} \frac{1}{2} k_{el} (r - r_0)^2 + \sum_{angles} \frac{1}{2} k_{\theta} (\theta - \theta_0)^2 + \sum_{impr} \frac{1}{2} k_{\xi} (\xi - \xi_0)^2 \\
 &+ \sum_{dihedral} k_{\phi} [1 + \cos(n\phi - \delta)] \\
 &+ \sum_{non-bonded\ pairs} \left[\frac{q_i q_j}{4\pi\epsilon_0 r_{ij}} + \frac{A_{ij}}{r_{ij}^{12}} - \frac{B_{ij}}{r_{ij}^6} \right] \\
 &+ \text{special terms}
 \end{aligned}
 \tag{2.1}$$

2.3.1 Bonded Interactions

Bonded interactions are described through 2-, 3- and 4-body energy terms, usually considered to be harmonics.

The first term in eq. 2.1 represents the vibrational energy of the bonds and the bond stretching is represented with a simple harmonic expression: the choice of an harmonic potential is an advantage in terms of computational costs but it can result in a quite poor approximation if the bond displacement is larger than a certain threshold (e.g. 10-15%) from the equilibrium value.

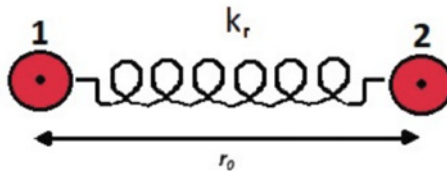


Figure 2.9: 2-body harmonic interaction between two particles.

From a physical point of view, using an harmonic function means that the bonds cannot be broken and therefore the existence of unbound states is forbidden: no chemical processes can be studied in this way.

The Morse potential $\mathcal{V}_{Morse}(r) = D_e(1 - e^{-a(r-r_e)})^2$ can be used to improve the accuracy and to have a better physical description but clearly this happens at the expense of computing time, and that is why in many circumstances the harmonic approximation is used.

Also the process of angle bending is usually represented by an harmonic potential.

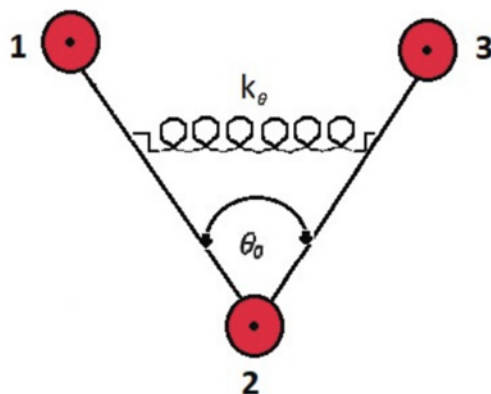


Figure 2.10: 3-body harmonic angle bending.

If the molecule contains more than four atoms in a row, also dihedral/torsional terms must be included for a correct description of the system.

It is good to note that in molecular systems the bond stretching and the angle bending are high frequency motions, compared with the other processes involved; this means that it is possible to use a rigid approximation (SHAKE method for intra-molecular constraints), especially when we want to use a larger time step in the simulation for efficiency reasons and if we are interested in physical properties that are not related to these high frequency motions.

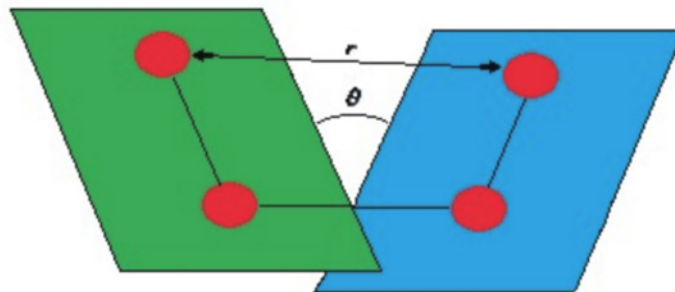
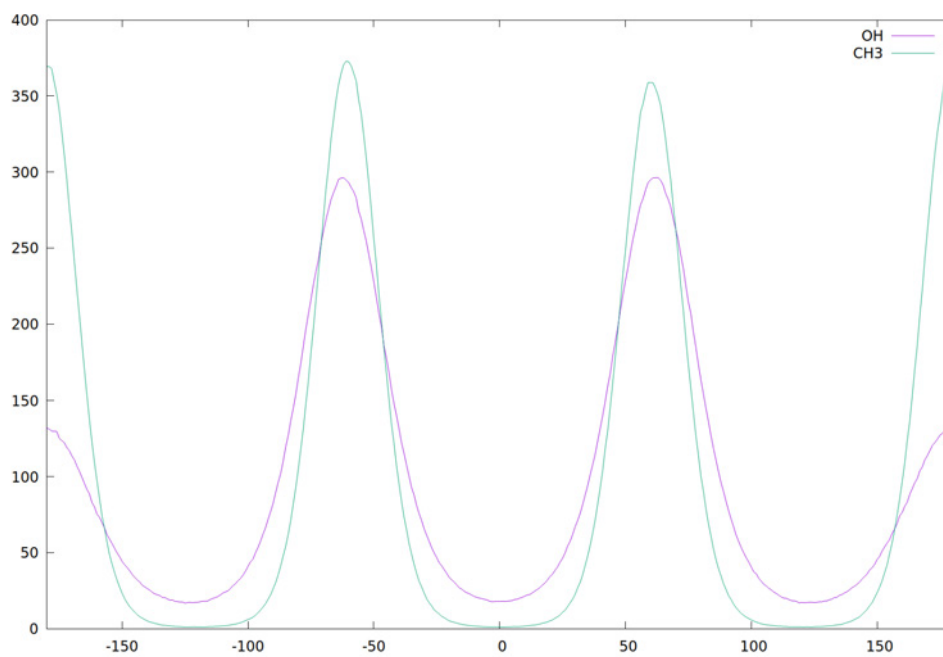


Figure 2.11: 4-body torsional interaction.

Figure 2.12: Dihedral angle distribution of ethanol molecules in water/ethanol mixture, $T = 25\text{ }^{\circ}\text{C}$.

For the torsional terms we have to do a different reasoning, due to the fact that this torsional motion is of paramount importance to determine the local structure of the molecules and to reproduce the dynamics of its conforma-

tional changes.

The rotations around the chemical bond is characterized by periodic energy terms, with periodicity determined by n and heights of rotational barriers given by k_ϕ [45].

2.3.2 Non Bonded Interactions

The “non-bonded pairs” term in equation 2.1 describes the interactions between pairs of atoms that are not bound: in particular these are the Lennard-Jones and Coulomb interactions between the atoms i and j , respectively with charges q_i and q_j at distance r_{ij} .

Lennard-Jones term describes an interaction characterized by a short-range repulsion (due to the overlapping of electron orbitals) and a long(er)-range attraction (due to electrons fluctuations in neutral atoms and molecules):

$$\mathcal{V}_{LJ} = \frac{A_{ij}}{r_{ij}^{12}} - \frac{B_{ij}}{r_{ij}^6} \quad (2.2)$$

which can be expressed also as:

$$\mathcal{V}_{LJ} = 4\epsilon \left(\left(\frac{\sigma}{r} \right)^{12} - \left(\frac{\sigma}{r} \right)^6 \right) \quad (2.3)$$

where σ is the distance at which the potential is zero, ϵ is the depth of the potential well and r is the distance between the particles.

The values of σ and ϵ related to different atoms can be combined to obtain the interaction values between the pair of atoms.

A typical way to obtain this values is the following:

$$\sigma_{ij} = \frac{\sigma_{ii} + \sigma_{jj}}{2} \quad (2.4)$$

$$\epsilon_{ij} = \sqrt{\epsilon_{ii}\epsilon_{jj}} \quad (2.5)$$

Note that it is as well often used the Buckingham potential terms to describe the repulsive part in the 12-6 Lennard-Jones potential:

$$\mathcal{V}_{rep} = A \exp(-Br) \quad (2.6)$$

Electrostatic interaction instead is generally described by a Coulomb term. To each atom of the system is then associated an atomic partial charge (for practical reasons the partial charges are assigned to the atomic sites, but as well we can place them outside the atomic positions) that can be calculated for example with quantum mechanical methods (e.g. Mulliken and Löwdin atomic charges calculations) .

The use of fixed partial charges however cannot fully describes the polarization effects. Moreover, as the electrostatic interaction is long-ranged it requires a special treatment during the computation of the forces; the techniques to deal with this interactions will be discussed in Section 2.7.

The special terms of Eq. 2.1 are referred to all the terms that, based on experimental data or theoretical considerations, gives a conformational contribution to the system.

2.3.3 Classical Force Fields

The first Force Fields date back to the 1960's and were mainly oriented to study small organic molecules, even if some of them are still developed and used.

Very popular Force Fields are GROMOS, AMBER, CHARMM, OPLS and COMPASS: all of them are quite general but in different situations each of them may be more or less appropriate.

In general they are divided into three classes, based on they functional form.

For Class I Force Fields the functional form is of the type:

$$\begin{aligned}
\mathcal{V} = & \sum_{bonds} \frac{1}{2} k_r (r - r_0)^2 + \sum_{angles} \frac{1}{2} k_\theta (\theta - \theta_0)^2 + \sum_{torsion} \sum_n k_{\phi,n} [1 + \cos(n\phi + \delta)] \\
& + \sum_{non-bonded\ pairs} \left[\frac{q_i q_j}{4\pi\epsilon_0 r_{ij}} + \frac{A_{ij}}{r_{ij}^{12}} - \frac{B_{ij}}{r_{ij}^6} \right]
\end{aligned}
\tag{2.7}$$

Among them we can find for example the OPLS Force Field for peptides and small organics, CHARMM27 Force Field for RNA, DNA and lipids and GAFF Force Field for drug design.

Class II Force Fields functional form is characterize by being anharmonic, and this reflects the fact that bonds, angles and torsions are not independent in molecules. COMPASS Force Field can be used for small molecules and polymers, and clayFF Force Field can be used for hydrated minerals.

Lastly, Class III Force Fields include also the polarizability. AMOEBA Force Field can be used to study distributed multipoles, while ReaxFF Force Field is used for chemical reactions.

2.4 The Importance of Water

Water is one of the most studied substances, also from a computational point of view [47].

Even if it is everywhere in our everyday life, its modeling is still an hard challenge because of non-trivial and unusual behaviors, due in particular to the formation of hydrogen bonding and its polar nature.

An accurate description of water molecules is of interest not only from a theoretical point of view, but also in view of the applications: indeed the presence of water is related to many degradation phenomena in organic semiconductors and in general is something that strongly influence and characterize the properties of a system, and the possibility to simulate its thermodynamical, dynamical and structural properties is a great help [50].

Despite the complex behavior of the aqueous systems, relatively simple models (that are still being improved) can be used to correctly predict the quantities of interest.

In many situations, for example when the number of molecules is big, one can ignore the polar and flexible nature of water molecules and consider a rigid model. Clearly more details in a simulation means more accurate results, but also a bigger computational effort [90].

Some of the most important water models are the SPC (simple point charge) and TIPXP-type (Transferable Inter-molecular Potential XP: TIP3P, TIP4P, TIP5P) ones, that have also been extended in SPC/E and TIP4P/2005 models [76].

TIP3P and SPC(/E) have three site of interactions whereas TIP4P have four site of interactions to improve the electronic distribution within the molecule with an extra auxiliary atom (very close to the Oxygen atom and without any mass), but all the SPC and TIPXP models have both Lennard-Jones and Coulombic terms.

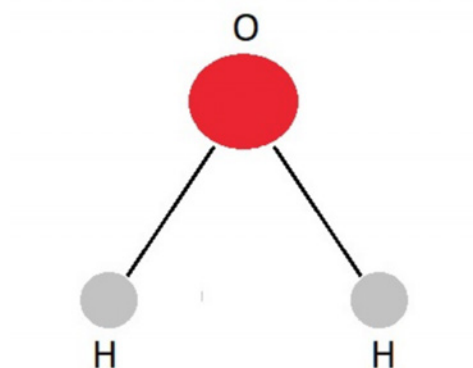


Figure 2.13: Example of three particles water model.

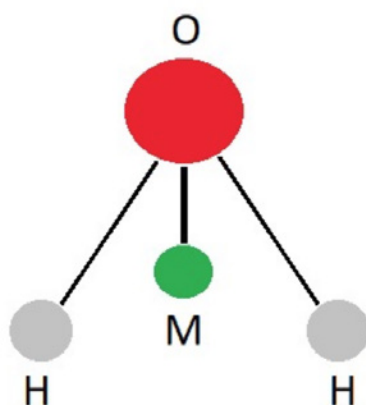


Figure 2.14: Example of four particles water model. The particle M is very near to the Oxygen atom (few Å), so the distances of the image are not representative.

2.5 Equations of Motion and Algorithms

In Molecular Dynamics simulations the evolution as a function of time of a set of an atomic/molecular system is followed via the solution of Newton's equations of motion [49]:

$$\mathbf{F}_i = m_i \frac{d^2 \mathbf{r}_i}{dt^2} \quad (2.8)$$

where \mathbf{F}_i is the force acting upon the i^{th} particle at time t , $\mathbf{r}_i(t)$ is the position of the i^{th} particle and m_i is the mass of the particle.

The integration of a second-order differential equation requires the specification, and so the knowledge, of the instantaneous positions and velocities of the particles: the equations of motion are discretized and solved numerically. The Molecular Dynamics trajectories are so defined by both position and velocity and they describe the system's evolution in phase space as a function of time: as the particles move their trajectories can be displayed and analyzed and the system can be directly traced at the atomic level [57].

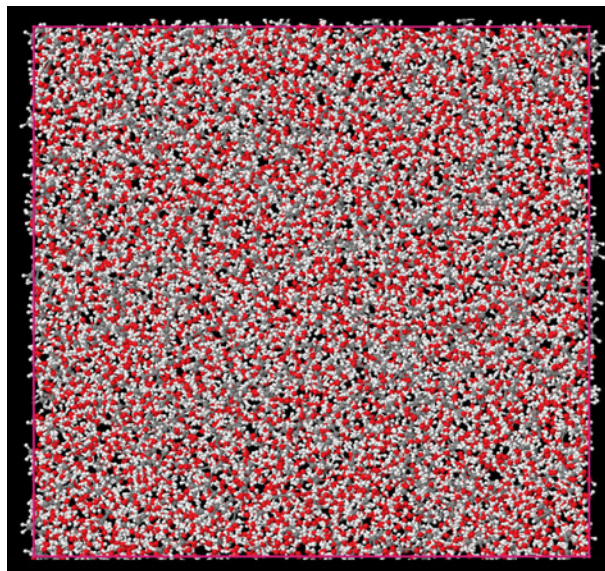


Figure 2.15: Snapshot of a .PDB file of water/ethanol mixture simulation model at $T = 25$ °C, after ~ 3 ns.

The description given by the Newton's equation of motion is the simplest that one can use, but in general the motion can be formulated/described in different ways.

The Lagrangian formulation and the Hamiltonian formulation can be used to describe in a elegant and mathematical way some aspects of Molecular Dynamics such as constraints and thermal coupling.

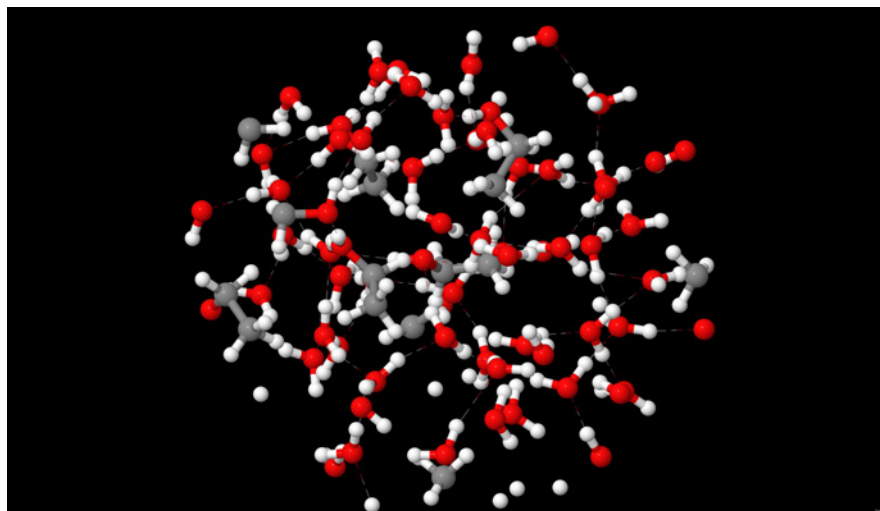


Figure 2.16: Zoom of the snapshot of a .PDB file of water/ethanol mixture simulation model at $T = 25\text{ }^{\circ}\text{C}$, after ~ 3 ns. Details on the hydrogen bonding are showed.

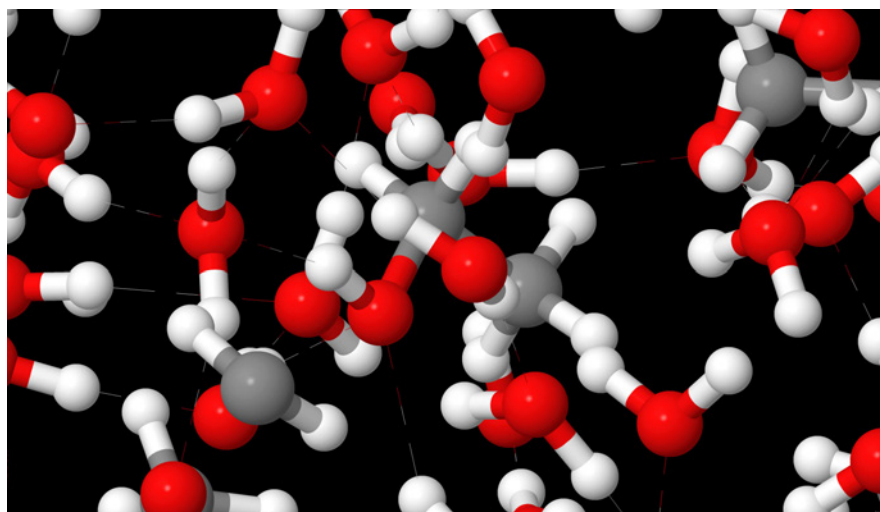


Figure 2.17: Zoom of the snapshot of a .PDB file of water/ethanol mixture simulation model at $T = 25\text{ }^{\circ}\text{C}$, after ~ 3 ns. Details on the hydrogen bonding are showed.

The non-Newtonian formulations of classical mechanics can be expressed through the Hamilton variational principle, which states that the trajectory followed by a mechanical system in the phase space is the one for which the integral over time $\int \mathcal{L} dt$ (\mathcal{L} is the Lagrangian of the system) takes its minimum value.

Given a conservative force field, a set of N generalized coordinate and generalized velocities q_i , \dot{q}_i , and $\mathcal{L} = \mathcal{L}(\{q_i\}, \{\dot{q}_i\}, t)$ we have that:

$$\frac{d}{dt} \left(\frac{\partial \mathcal{L}}{\partial \dot{q}_i} \right) - \frac{\partial \mathcal{L}}{\partial q_i} = 0, \quad i = 1, \dots, N \quad (2.9)$$

where the Lagrangian of the system is defined as:

$$\mathcal{L} = \mathcal{K} - V \quad (2.10)$$

The advantage Lagrange equations formalism is that it allows to treat the constraints in a simple and direct way.

The Hamiltonian formulation of the equation of motion is very useful both for Classical Physics and Quantum Mechanics.

The Hamiltonian of a system is defined as:

$$\mathcal{H}(\{q_i\}, \{p_i\}, t) = \sum_i p_i \dot{q}_i - \mathcal{L} \quad (2.11)$$

and the equations of motion of the system are given by the Hamilton's equations:

$$\begin{bmatrix} \frac{d\mathbf{q}}{dt} \\ \frac{d\mathbf{p}}{dt} \end{bmatrix} = \begin{bmatrix} 0 & 1 \\ -1 & 0 \end{bmatrix} \begin{bmatrix} \frac{\partial \mathcal{H}}{\partial \mathbf{q}} \\ \frac{\partial \mathcal{H}}{\partial \mathbf{p}} \end{bmatrix} \quad (2.12)$$

The motion of a system of particles is then described by the temporal evolution of the phase space variables (\mathbf{q}, \mathbf{p}) , and the phase space $\Gamma(\mathbf{q}, \mathbf{p}) \in \mathbb{R}^6$ contains all the combinations of coordinates and momenta of the system.

Because the system is evolving in time, it exist a flow map:

$$\Phi_{t, \mathcal{H}} : \mathbb{R}^6 \rightarrow \mathbb{R}^6 \quad (2.13)$$

such that

$$\Phi_{\delta t, \mathcal{H}}(\mathbf{q}(t), \mathbf{p}(t)) = (\mathbf{q}(t) + \delta\mathbf{q}(t), \mathbf{p}(t) + \delta\mathbf{p}(t)) \quad (2.14)$$

and

$$\mathbf{q} + \delta\mathbf{q} = \mathbf{q}(t + \delta t), \quad \mathbf{p} + \delta\mathbf{p} = \mathbf{p}(t + \delta t) \quad (2.15)$$

A certain number of finite difference schemes may be used for integrate the equation of motion.

Because this schemes must be useful for molecular dynamics simulations, it is important for practical reasons that they fulfill some requirements such as stability, accuracy and effectiveness.

Anyway the numerical flow $\phi_{\delta t, \mathcal{H}}$ is not completely equivalent to $\Phi_{\delta t, \mathcal{H}}$.

A good starting point to find the expressions that define the positions (let us consider cartesian coordinates) $\mathbf{r}_i(t + \delta t)$ at time $(t + \delta t)$ in terms of already known positions at time t is based on Taylor series expansions, and leads to an higher order scheme from which first order accurate schemes, second order accurate schemes etc. can be obtained.

$$\mathbf{r}(t + \delta t) = \mathbf{r}(t) + \mathbf{v}(t)\delta t + \frac{1}{2}\mathbf{a}(t)\delta t^2 + \frac{1}{6}\mathbf{b}(t)\delta t^3 + \frac{1}{24}\mathbf{c}(t)\delta t^4 + \dots \quad (2.16)$$

$$\mathbf{v}(t + \delta t) = \mathbf{v}(t) + \mathbf{a}(t)\delta t + \frac{1}{2}\mathbf{b}(t)\delta t^2 + \frac{1}{6}\mathbf{c}(t)\delta t^3 + \dots \quad (2.17)$$

$$\mathbf{a}(t + \delta t) = \mathbf{a}(t) + \mathbf{b}(t)\delta t + \frac{1}{2}\mathbf{c}(t)\delta t^2 + \dots \quad (2.18)$$

An example of first order method is given by the Euler's method:

$$\mathbf{r}(t + \delta t) = \mathbf{r}(t) + \mathbf{v}(t)\delta t \quad (2.19)$$

$$\mathbf{v}(t + \delta t) = \mathbf{v}(t) + \mathbf{a}(t)\delta t \quad (2.20)$$

while an example of second order method is given by the Verlet algorithm (eq. 2.23), obtained simply by adding eq. 2.21 to eq. 2.22:

$$\mathbf{r}(t + \delta t) = \mathbf{r}(t) + \mathbf{v}(t)\delta t + \frac{1}{2}\mathbf{a}(t)\delta t^2 \quad (2.21)$$

$$\mathbf{r}(t - \delta t) = \mathbf{r}(t) - \mathbf{v}(t)\delta t + \frac{1}{2}\mathbf{a}(t)\delta t^2 \quad (2.22)$$

$$\mathbf{r}(t + \delta t) = 2\mathbf{r}(t) - \mathbf{r}(t - \delta t) + \mathbf{a}(t)\delta t^2 \quad (2.23)$$

The latter is one the most used algorithm to calculate the atomic trajectories in Molecular Dynamics Simulations because it offers a better stability than the Euler method and it is symplectic (so include time-reversibility and preservation of phase space).

Other very commons methods are the leap-frog algorithm and the velocity-Verlet algorithm.

2.6 Thermodynamic ensembles

Different thermodynamic ensembles are classified and characterized according to the interactions of the system with the surroundings: this interactions can take place because of energy exchange or matter exchange (variation of the total number of particles) [29].

When the equations of motion 2.8 are integrated the total energy is conserved, together with the number N of particles and the volume V of the simulation box. This leads to the so called NVE (microcanonical) ensemble, that is not always the optimal choice.

Because we want to compare the computational results with experimental conditions of laboratory, it can be convenient to introduce other statistical ensembles such as the canonical ensemble (NVT) and the isothermal-isobaric ensemble (NPT).

Summarizing, a macroscopic state is described by: number of particles N , chemical potential μ , volume V , pressure P , energy E and temperature T .

The thermodynamic ensembles are:

- Microcanonical, fixed N, V, E
- Canonical, fixed N, V, T
- Constant $P - T$, fixed N, P, T
- Grand Canonical, fixed μ, P, T

In a Molecular Dynamics simulation it is possible to control certain thermodynamics quantities, and then to realize different thermodynamic ensembles, by means of algorithms, rescaling of atomic velocities, modified equations of motion etc., that fixes the property to the right value.

We can decide to work with with constant temperatures or pressure by using one of the available barostats and/or thermostats.

2.6.1 Thermostat and Barostat Algorithms

Nosé algorithm is a useful way to maintain the system at constant temperature by a reformulation of the equations of motion, and in particular by considering a Lagrangian that contains additional coordinates and velocities. We introduce an extra-variable η as a scaling factor for the velocities, and we introduce as well an associated momentum $p_\eta = Q\dot{\eta}$, where Q can be thought as the mass of the extra degree of freedom [69].

The equations of motion are:

$$\dot{q}_i = \frac{p_i}{m} \quad (2.24)$$

$$\dot{p} = F(q) - p \frac{p_\eta}{Q} \quad (2.25)$$

$$\dot{p}_\eta = \sum \frac{p_i^2}{2m_i} - nk_B T \quad (2.26)$$

Because of the non-ergodic behavior of the Nosé-Hoover thermostat, a modification of this one called Nosé-Hoover chain thermostat has been proposed.

The Berendsen thermostat is as well an algorithm that simulates the coupling of the system with an external thermal bath at a certain temperature T_{bath} , and this is done by the re-scaling of the velocities of the particles.

$$\frac{dT}{dt} = \frac{T_{bath} - T}{\tau} \quad (2.27)$$

It can be seen that the temperature T is scaled to the reference temperature T_{bath} via an exponential law.

About the control of pressure and the related barostat algorithm, the various methods are based on the same ideas and principles for the constant temperature methods; the only essential difference is that now the role of the temperature is played by the pressure.

2.7 Long-Range Interactions Calculation

The treatment and the calculations of long-range interactions, i.e. of that spatial interactions that falls of no faster than $1/r^d$ (d : dimension of the system) in a Molecular Dynamics Simulation represents a challenging problem; indeed the time of calculation of the interactions between non-bonded atoms and of non-bonded interactions in general is proportional to N^2 : we must therefore think of various methods to speed up the calculation of long-range interactions [83].

The simplest way to deal with this problem is based on the cut-off criterion and consists in calculating the interactions between particles that are within a sphere of a certain radius $R_{cut-off}$, so that if the distance between them is larger than $R_{cut-off}$ the interaction is neglected.

It is clear that this procedure introduces an artificial discontinuity of the interactions at $r = R_{cut-off}$, but the problem can be treated by considering a switching function $S(R)$ that bring the potential to zero continuously in correspondence of the cut-off distance by starting to reduce the potential at some distance $R_{sf} < R_{cut-off}$.

The long-range interaction between two particles A and B is then:

$$V_{A,B}(R) = \begin{cases} V_{A,B}(R), & R \leq R_{sf} \\ V_{A,B}(R) \times S(R), & R_{sf} \leq R \leq R_{cut-off} \\ 0, & R \geq R_{cut-off} \end{cases} \quad (2.28)$$

An interesting way to reduce the distance of action of the Coulombian forces is to assemble the atoms of the simulated molecules into appropriate groups having a zero net charge because, when the sum of the partial atomic charges of a group of particles is zero, then we have a multipolar resulting interaction between two groups of particles of this type and the energy is proportional to r^{-n} , $n \geq 3$.

Moreover, a twin range cut-off method can be used, in which a particle inter-

acts at every step with all the particles that are within a sphere of radius R_1 , and with the particles that are within a sphere of radius R_2 every n steps.

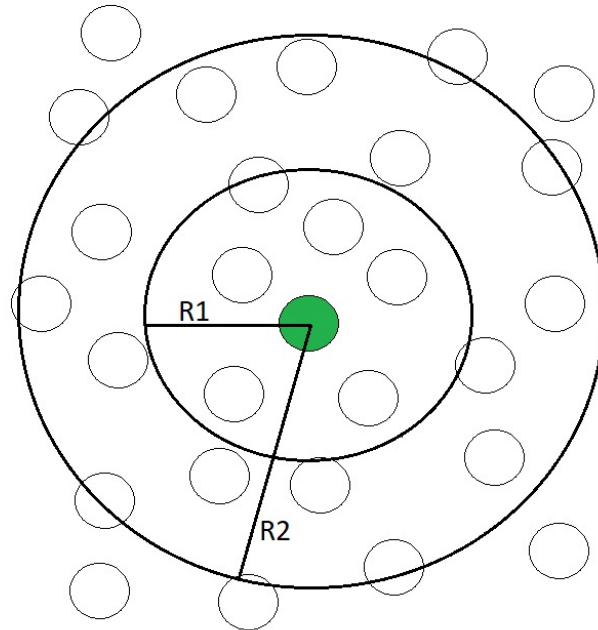


Figure 2.18: Twin range cut-off method.

Anyway, in general, it is not clear whether a potential with a cut-off can be considered, so that one might hope that screening effects could justify this method.

2.7.1 Ewald Summation

When dealing with the electrostatic potential of eq. 2.1 in general we are not allowed to use safely a simple truncation scheme and Ewald's method helps us to treat efficiently the electrostatic interactions of the system (and of the infinite number of periodic images). It is convenient to think in terms of a cubic box of side L , but the method can be extended to be more general.

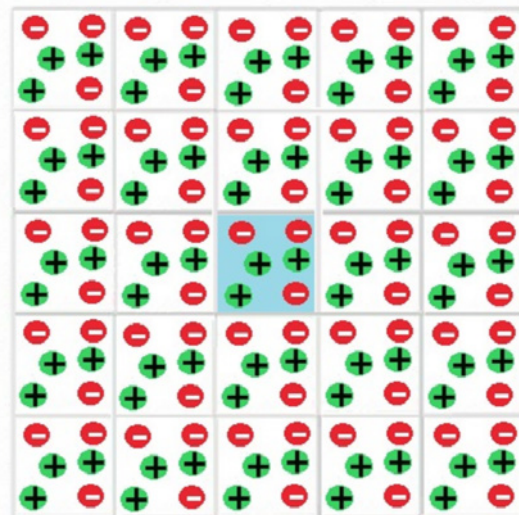


Figure 2.19: Schematic representation of a 2-D system with Periodic Boundary Conditions and electric charges.

The total Coulomb energy of a system of N particles and their infinite replicas is then given by:

$$U = \frac{1}{2} \sum_n' \sum_i^N \sum_j^N \frac{q_i q_j}{|\mathbf{r}_i - \mathbf{r}_j + \mathbf{n}L|} \quad (2.29)$$

where $\mathbf{n} = (n_x, n_y, n_z) = n_x L\mathbf{x} + n_y L\mathbf{y} + n_z L\mathbf{z}$ is the cell-coordinate vector and the original cell is placed in $\mathbf{n} = (0, 0, 0)$, so that the images cells are located at $L\mathbf{n}$ intervals (\mathbf{n} goes to infinity).

In the first summation there is a prime because the terms with $i = j$ are omitted when $\mathbf{n} = \mathbf{0}$ so as to prevent interaction of atoms with themselves but not with their images.

The potential energy of eq. (2.29, expressed as a single slowly and conditionally convergent series, can be recast into the sum of two rapidly converging

series plus a constant term: this was the idea of Ewald.

$$\begin{aligned}
U_{Ewald} &= U^r + U^F + U^0 = \\
&= \frac{1}{2} \sum_{i,j}^N \sum_{\mathbf{n}} q_i q_j \frac{\operatorname{erfc}(\alpha |\mathbf{r}_i - \mathbf{r}_j + \mathbf{n}L|)}{|\mathbf{r}_i - \mathbf{r}_j + \mathbf{n}L|} \\
&+ \frac{1}{2\pi V} \sum_{i,j}^N q_i q_j \sum_{\mathbf{m} \neq 0} \frac{\exp(-(\pi \mathbf{m}/\alpha)^2 + 2\pi i \mathbf{m} \cdot (\mathbf{r}_i - \mathbf{r}_j))}{\mathbf{m}^2} \\
&+ \frac{-\alpha}{\sqrt{\pi}} \sum_{i=1}^N q_i^2
\end{aligned} \tag{2.30}$$

where V is the volume of the simulation box and $\mathbf{m} = (j, k, l)$ is a reciprocal-space vector.

The eq. 2.29 is then recast in the sum of a real space sum, the reciprocal (Fourier) sum and a self-term.

The physical idea behind this method is that to each point charge we add a isotropic charge distribution of equal magnitude and opposite sign which surrounds and spreads out radially from the charge. In other words, the eq. 2.29 is reformulated by adding to the infinite distribution of point charges $\rho(\mathbf{r}) = \sum_n \sum_i q_i \delta(|\mathbf{r} - \mathbf{r}_i + \mathbf{n}L|)$ a charge distribution with the above specified characteristics for each point charge. In this way the electrostatic potential caused by the screened charges becomes short-ranged.

In the Ewald method the extended charge distribution is taken to be a Gaussian (but in general is arbitrary), with charge density:

$$\rho_i(\mathbf{r}) = q_i \left(\frac{\alpha}{\pi} \right)^{3/2} e^{-\alpha |\mathbf{r} - \mathbf{r}_i|^2} \tag{2.31}$$

where the normalization factor is for the three-dimensional case and α is a positive parameter that determines the width of the distribution (the bigger is α , the more the charge distribution tends to a Dirac δ function).

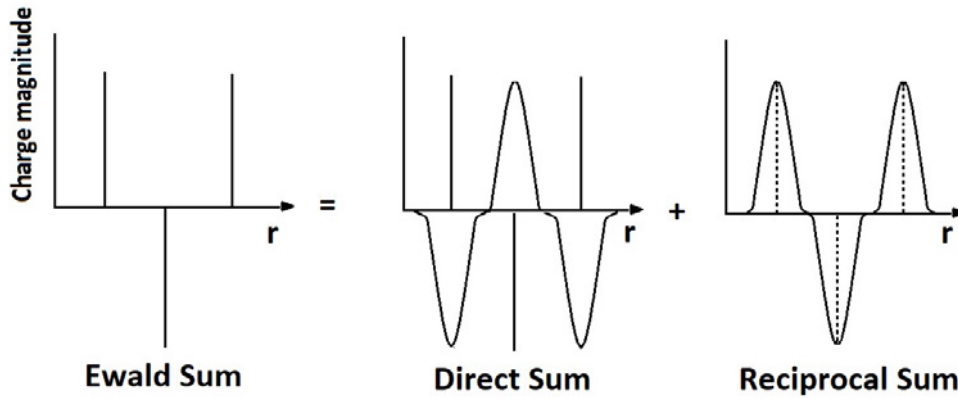


Figure 2.20: Schematic view of the Ewald method.

The interaction between neighboring point-charges is screened by the introduced charge distribution, limiting it to a short range interaction, and the total charge distribution is given by:

$$\rho_i(\mathbf{r}) = \rho_i^q(\mathbf{r}) + \rho_i^G(\mathbf{r}) \quad (2.32)$$

with $\rho_i^G(\mathbf{r})$ that is the Gaussian distribution corresponding to the $\rho_i^q(\mathbf{r})$ point charge distribution of the i -th particle.

To obtain again the original charge distribution, for each point charge a second Gaussian distribution of the same magnitude and sign as the original one is added, and the sum is performed in the reciprocal space by solving the resulting Poisson's equation through the Fourier transforms.

Remember that

$$\frac{1}{r} = \int \frac{d^3k}{(2\pi)^3} \frac{4\pi}{k^2} e^{i\mathbf{k}\mathbf{r}} \quad (2.33)$$

and

$$\sum_{\mathbf{R}} e^{i\mathbf{k}\mathbf{R}} = \frac{(2\pi)^3}{V} \sum_{\mathbf{K}} \delta^3(\mathbf{k} - \mathbf{K}) \quad (2.34)$$

2.8 Properties of the System from the Trajectories

The goal is to analyze the trajectories, and so the output files, of a Molecular Dynamics Simulation, deriving different macroscopic properties of thermodynamic, kinetic, structural or dynamical nature.

This is done in terms of statistical mechanics, considering the mean value of a quantity along the trajectory.

Typical quantities that can (must) be calculated are the temperature T and the pressure P , that are respectively related to the kinetic energy \mathcal{T} and to the virial:

$$T = \frac{2\mathcal{K}}{(3N - N_c)k_B} = \frac{1}{(3N - N_c)k_B} \sum_{i=1}^N |\mathbf{p}_i|^2/m_i \quad (2.35)$$

$$P = \frac{1}{V} \left[Nk_B T - \frac{1}{3k_B T} \sum_i \sum_{j>i} \mathbf{F}_{ij} \mathbf{r}_{ij} \right] \quad (2.36)$$

where N_c is the number of internal constraints and N is the number of atoms. In the definition of T (2.35) also the angular velocities may appear. From the kinetic and potential contributions, also the total energy can be obtained:

$$E = \langle \mathcal{H} \rangle = \langle \mathcal{K} \rangle + \langle \mathcal{V} \rangle \quad (2.37)$$

While running a simulation it can be convenient to separate the rotational and the translational contributions of the kinetic energy, and also separate the different contributions given by different types of atoms and molecules to the kinetic energy and to the total temperature. Moreover, it can be convenient to separate the different contributions to the total energy (van der Waals' energy, electrostatic intermolecular energy etc.): dividing a problem in its smallest part will help to check the eventual presence of errors or

anomalies in the simulation.

For example:

	Mean Value	Fluctuations
Temperature (K)	297.99 ±	0.98
Partial temp. of PEDOT-6 (K)	295.86 ±	5.94
P. trans. temp. of PEDOT-6 (K)	299.48 ±	43.15
P. rotat. temp. of PEDOT-6 (K)	299.67 ±	44.76
P. intra. temp. of PEDOT-6 (K)	295.71 ±	6.06
Partial temp. of PSS-12 (K)	293.53 ±	3.71
P. trans. temp. of PSS-12 (K)	299.90 ±	45.99
P. rot. temp. of PSS-12 (K)	298.98 ±	44.56
P. intra. temp. of PSS-12 (K)	293.45 ±	3.73
Partial temp. of Na+ (K)	299.80 ±	14.25
P. trans. temp. of Na+ (K)	299.80 ±	14.25
Partial temp. of SPC/E-aqua (K)	298.43 ±	1.06
P. trans. temp. of SPC/E-aqua (K)	299.56 ±	1.50
P. rot. temp. of SPC/E-aqua (K)	297.28 ±	1.51

Table 2.1: Contributions to the total temperature T of the system.

	Mean Value	Fluctuations
Pressure (total) (atm)	0.970 ±	101.263
Pressure (external) (atm)	2694.987 ±	9.681
Pressure (internal) (atm)	-2694.017 ±	100.341

Table 2.2: Contributions to the total pressure P of the system.

The heat capacity (at constant volume V) can be obtained through the expression:

$$C_V = \left(\frac{\partial U}{\partial T} \right) \quad (2.38)$$

	Mean Value	Fluctuations
Total energy (kJ/mol)	-45.18 ±	0.05
Total potential energy (kJ/mol)	-52.58 ±	0.04
Total kinetic energy (kJ/mol)	7.40 ±	0.03
van der Waals' energy (kJ/mol)	9.54 ±	0.05
Electrostatic energy (kJ/mol)	-62.12 ±	0.07

Table 2.3: Contributions to the total energy of the system.

	Mean Value	Fluctuations
Intramolecular kinetic energy (kJ/mol)	0.82 ±	0.01
Translational kinetic energy (kJ/mol)	3.74 ±	0.02
Rotational kinetic energy (kJ/mol)	3.67 ±	0.02

Table 2.4: Contributions to the kinetic energy of the system.

	Mean Value	Fluctuations
Lennard-Jones intermol. energy (kJ/mol)	8.45 ±	0.05
Electrostatic intermol. energy (kJ/mol)	181.03 ±	0.07
Total intermolecular energy (kJ/mol)	189.48 ±	0.04

Table 2.5: Contributions to the energy of the system.

and so can be calculated changing the temperature T and repeating the simulation.

RMS fluctuations have their importance in the calculation of the desired parameters, and can be used also to obtain the heat capacity at constant V in a canonical ensemble:

$$\langle \delta \mathcal{H}^2 \rangle_{NVT} = k_B T^2 C_V \quad (2.39)$$

Transport and dynamical properties are without any doubt come of the most important properties that must be calculated.

The two fundamental laws that describe the diffusion processes are the 1st

and 2^{nd} Fick's laws, that respectively reads (in one dimension):

$$J_x = -D \frac{\partial c(x, t)}{\partial x} \quad (2.40)$$

$$\frac{\partial c(x, t)}{\partial x} = D \frac{\partial^2 c(x, t)}{\partial x^2} \quad (2.41)$$

where the constant D that appears in eq. 2.40 and 2.41 is the Diffusion Coefficient ($[D] = [L]^2[T]^{-1}$).

In three dimensions the Diffusion Coefficient is given by:

$$D = \frac{1}{3} \int_0^\infty dt \langle \mathbf{v}_i(t) \cdot \mathbf{v}_i(0) \rangle \quad (2.42)$$

where $\mathbf{v}_i(t)$ represents the velocity of the center of mass of a single molecule.

For long times we have:

$$D = \lim_{t \rightarrow \infty} \frac{d}{dt} \frac{1}{6} \left\langle |\mathbf{r}_i(t) - \mathbf{r}_i(0)|^2 \right\rangle \quad (2.43)$$

where $\mathbf{r}_i(t)$ is the molecule position.

The final result is the mean value obtained considering the averages computed for each of the particles in the simulation, that are then added together and divided by N (the total number of particles in the system).

Among the structural properties, the Radial Distribution Function $g(r)$ have a fundamental importance because the knowledge of the distribution of molecules and atoms relative to each other (especially in a fluid) permits to extrapolate information on the structures; indeed it describes how the density varies as a function of distance from a reference particle.

If we consider a particle in $\mathbf{r} = \mathbf{0}$, then $g(r)\rho 4\pi r^2 dr$ gives the mean number of particles between r and $r + dr$, where ρ is the density.

In the canonical ensemble

$$g(\mathbf{r}_1, \mathbf{r}_2) = \frac{N(N-1)}{\rho^2 Z_{NVT}} \int d\mathbf{r}_3 \dots d\mathbf{r}_N \exp[-\beta \mathcal{V}(\mathbf{r}_1, \dots, \mathbf{r}_N)] \quad (2.44)$$

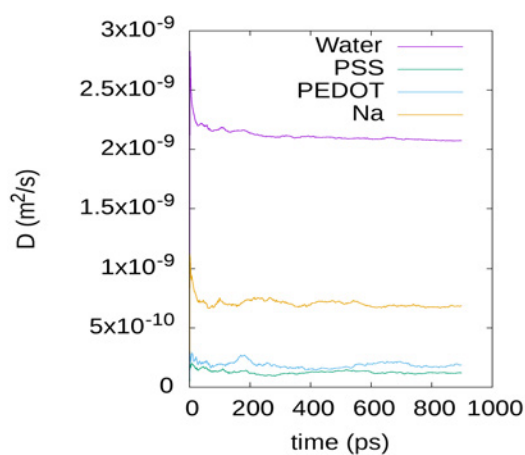


Figure 2.21: Diffusion Coefficients of PEDOT oligomers, PSS polymers, water molecules and Na^+ counterions in PEDOT:PSS bulk system ($T = 25$ °C), at the very beginning of a simulation (equilibration stage, $t_{\text{simulation}} < 1$ ns). Values obtained from the analysis of the trajectories.

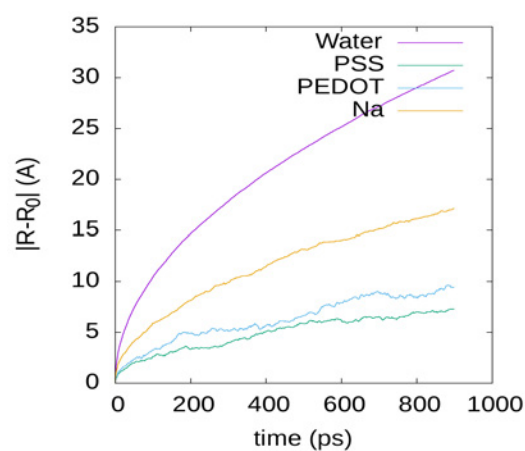


Figure 2.22: Mean Squared Displacements of PEDOT oligomers, PSS polymers, water molecules and Na^+ counterions in PEDOT:PSS bulk system ($T = 25$ °C), at the very beginning of a simulation (equilibration stage, $t_{\text{simulation}} < 1$ ns). Values obtained from the analysis of the trajectories.

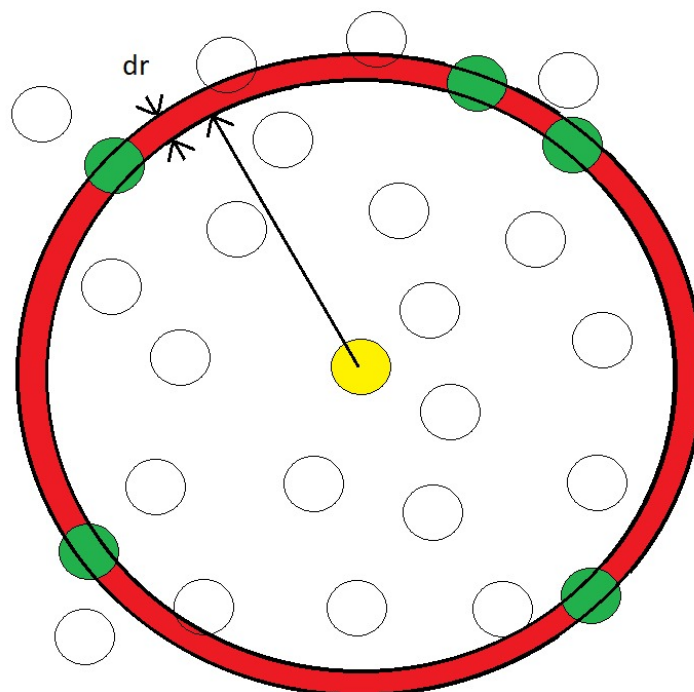


Figure 2.23: Calculation of the Radial Distribution Function.

2.8.1 Ergodic Hypothesis

One of the most fundamental aspects of Molecular Dynamics Simulations is given by the Ergodic hypothesis: indeed the results obtained from a simulation are interpreted in the framework of Statistical Mechanics, and what must be true (if the hypothesis is fulfilled) is that the time average of the simulated particles is the same as the ensemble average.

The averaged in time observable is expressed as:

$$\bar{A}_t = \lim_{t \rightarrow \infty} \frac{1}{t} \int_0^t dt' A(\Gamma, t') \quad (2.45)$$

where $\Gamma(q^{3N}, p^{3N})$ is a point in the $6N$ -dimensional phase space ($3N$ coordinates and $3N$ momenta).

The statistically averaged observable is expressed by:

$$\langle A \rangle_{ensemble} = \frac{\int d\Gamma e^{-\beta\mathcal{H}(\Gamma)} A(\Gamma)}{\int d\Gamma e^{-\beta\mathcal{H}(\Gamma)}} \quad (2.46)$$

The ergodicity holds if

$$\bar{A}_t = \langle A \rangle_{ensemble} \quad (2.47)$$

i.e. that the trajectory explores all the possible conformations of the system in the phase space.

When an initial configuration is chosen, we expect after a certain amount of time, especially after the initial equilibration, that the system reaches the thermal equilibrium, but for a rigorous analysis one should also consider that the simulated system may have several potential wells that are not reached during the simulation time.

For example glasses, due to fast cooling, are blocked in one of the possible disordered configurations and the system does not have time to minimize the free energy by exploring ergodically all accessible configurations.

Because we want to be sure about the simulated system, a possible solution can consist in using some extra information obtained for example from X-ray experiments to force our system in a certain conformation [44].

In general one can increase the accuracy of the estimations by considering different simulations that start from different points of the phase space and then obtain the values of the thermodynamic properties of the system from the partition function.

2.9 Limits of Molecular Dynamics Simulations

There are some important limitations about the use of Molecular Dynamic Simulations that one must take into account for a better understanding of the obtained results and to have in mind the directions and the strategies for possible future works and developments.

Indeed the principle of Molecular Dynamics consists in studying and analyzing the trajectories of a distribution of atoms and molecules by the numerical integration of the classical equations of motion, and a priori this can be an arguable approach because it must be true that quantum effects and quantum mechanical considerations can be neglected without any problems.

The very big problem about Molecular Dynamics Simulations arises from the time limitations: dealing with a system that contains a number of atoms that is greater than 10000 or even 100000 units is computationally demanding in terms of time performances, for every single time step.

The presence of light atoms (e.g. Hydrogen atoms) or in general of very fast motions forces us to choose a time step value, usually of the order of the femtosecond, that allows to sample the studied system sufficiently well, avoiding too large fluctuations in the physical control parameters of the simulation program [79].

Moreover, the time scales of the processes that one want to study can be several orders of magnitude greater than the chosen time step; the time scale needed for this thesis work is of the order of tens of nanoseconds, but there are several biological, chemical and physical processes that need a time scale of microseconds (e.g. proteins dynamics) [28].

About the physical considerations on the studied system, the most important questions are:

- Is the classical description still valid/is the quantum description mandatory?

- If the quantum description is necessary, how it will influence a classical description of the dynamics of the system? Can it be considered just as a (possibly small) correction?

The dynamics of heavy atoms and molecules at room temperature can be studied without any problems by means of pure classical mechanics, but processes of tunneling or changes in chemical bonding requires a pure quantum description.

If the presence of light atoms in the system is abundant, especially at low temperatures, and/or if the quantum wavelength of the particle is not negligible compared to the physical conditions of the system (e.g. respect to the spatial changes of the potentials), then the quantum behaviors must be considered at least as a perturbation to the classical behaviors; typical solutions that one can take into account consist in starting from a pure classical simulation and in the aftermath add the quantum corrections to the unmodified physical values previously calculated, or by directly including the quantum corrections into the equations of motions.

Quantum considerations can be taken into account by using first-principles (ab-initio) Molecular Dynamics, in which the trajectories are generated through the forces resulting from ‘on-the-fly’ electronic structure calculations. Quantum (ab-initio) simulations however are still impractical for large systems [9].

2.10 Molecular Dynamics Simulations for Polymer Composites

The physical properties of polymeric materials arise from their chemical complexity and from their variability of structures and constituent molecules. This results in a broad range of applications, but also in a broad range of

time scales (from femtoseconds to hours) and length scales (from nanometers to millimeters, and even more) of the relevant processes involved.

Computer simulations are an optimal tool in this field of research, due to the levels of complexity involved, both to predict the properties of a polymeric material/nanocomposite and also to compare the results with experimental data [38].

Different scales also means the need for different computational techniques, in order to catch all the essential physical elements of the problem that have to be anyway computed in a reasonable amount of time.

The most fundamental modeling of a polymeric system clearly involves a quantum mechanical description of the nuclear and electronic degrees of freedom; the typical lengths of a huge number of polymer and nanocomposites of practical interest, however, exceed by far the dimensions of atoms and molecules, resulting in very expensive and slow calculations [23].

A separation between the nuclear and electronic degrees of freedom can also be considered in order to obtain a purely electronic Hamiltonian, where the position of the nuclei only acts as a parameter for the dynamical description of the system.

Chemical reactions then can be studied at the electronic level with great accuracy, together with the effects of quantum fluctuations of the nuclear coordinates on the properties of polymers.

Simulations of polymers, involving an accurate chemical model, can be performed via Molecular Dynamics and Monte Carlo methods, parametrizing the energies with the Force Fields. Depending on the particular situation, one can choose to constraints the bond lengths that give rise to high frequency and small amplitude motions.

When chemical details are not particularly influential, the use of coarse

grained and mesoscopic methods represents an optimal choice: the freely-jointed tangent hard-sphere chain or models of polymers linked by anharmonic springs represents some typical examples.

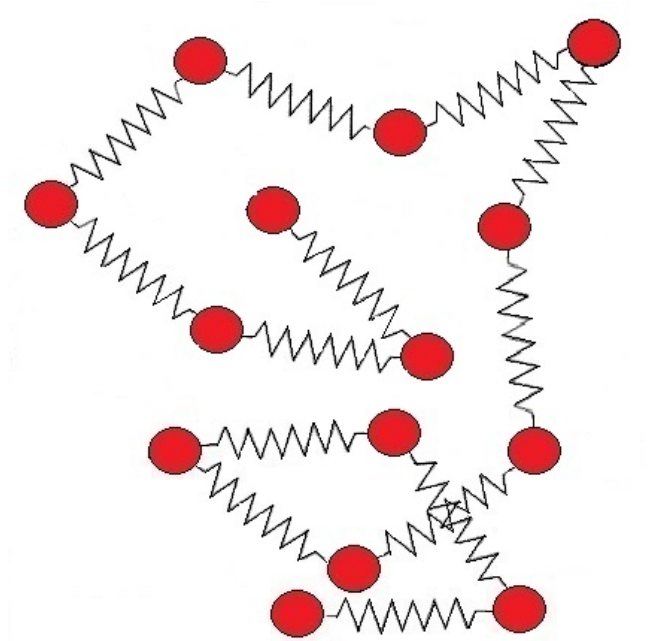


Figure 2.24: Rouse model for polymers.

Also models typical of continuum mechanics can be used, where hydrodynamic descriptions of the flow of polymeric materials on a processing scale are employed [70].

Anyway in simulations of nanocomposites it is of great usefulness the possibility of combining models that span from an atomistic/molecular description to a macroscopic one.

One of the first approaches to this method is given by the study of crack propagation in Silicon: a tight-binding model was used near the crack tip, then Molecular Dynamics methods was employed farther away and finite element calculations were performed when the continuum approximation was valid [42].

The concept of multiscale modeling have been also successfully applied in the framework of polymer physics, for example to polymer-organoclay nanocomposites, to immiscible polymer blends and to polymer-carbon nanotubes [33].

2.10.1 Molecular Dynamics Simulations for Polymer Composites/Interface

There is a growing interest in the study of interactions among polymeric materials and a substrate [85]. This is also due to the potential applications, that span from renewable energy production structures to electronic devices. New techniques for the preparation of polymer thin film devices can be developed by understanding the behavior of polymers at surfaces and interfaces. A complex interplay between the polymers and the surface arises because of the new geometrical constraints, that can result in a change of the polymers properties, leading for example to layer-like demixing patterns or to microphase segregation [22].

This is a challenging task to deal with, and again computer simulations turn out to be an useful tool to solve this problems by using Molecular Dynamics methods or Monte Carlo models.

Same methods and ideas can be used also to study the interactions and the dynamics of polymers in presence of nanoparticles. This interaction indeed not always results in a nanocomposite.

Moreover polymers-nanoparticles interactions may result in a phase separation, and hence in a deterioration of the properties of the composite as a whole.

Also in view of the applications, is then important to study and analyze the differences between the properties of a certain material in the bulk phase, and in presence of an interface.

In recent years have been studied linear polymer melts in bulk and confined systems under shear flow via Molecular Dynamics Simulations: the simulation show that the interfacial chain dynamics near the boundary solid walls in the confined system are significantly different from the corresponding bulk chain dynamics [16].

Molecular Dynamics Simulation have been also employed to study the transport of methane and n-butane molecules in the bulk and interface region of polyethylene (PE), poly(4-methyl-2-pentyne) (PMP) and polydimethylsiloxane (PDMS), or to study a dense polymer melt adsorbed on a solid substrate on the one side and exposed to vacuum on the other [6].

2.10.2 Molecular Dynamics Simulations for PEDOT:PSS

Molecular Dynamics simulations concerning PEDOT and PEDOT:PSS have already been performed due to the growing interest that this polymeric blend is gaining [34].

Over-simplified models consisting of single oligomers or perfect periodic crystals of PEDOT have already been presented. An adequate realistic description of the morphology of PEDOT thin films cannot be obtained by this models.

Many others research groups investigated the structural and electronic properties of PEDOT and PEDOT:PSS. Ab initio Hartree-Fock (HF/6-31G) and density functional theory (DFT/6-31G) methods have been used by Dkhissi et al. to exhibit relative stability of the aromatic and quinoid forms of neutral PEDOT in the ground state [24]. Structural and electronic properties of n-EDOT with $n = 1-8$ have been reported by Aleman et al [3]. The influence of the degree of doping on the reflectivity and optical properties of PEDOT:PSS based on GGA PW91 functional has been studied by Lenz et al [58]. The nature of the interaction between PEDOT and PSS using B3LYP/6-31G** has been studied by Gangopadhyay [35]. Theoretical studies of PEDOT:PSS for ammonia sensing applications have been performed by Marutaphan et al

[5].

In recent years, Zozoulenko et al. worked on the morphology and crystallization of doped conducting polymer PEDOT:TOS (Fig. 2.25), focusing on the role of water and on the changes in morphology under the transition from the aqueous solution to the dry phase [34].

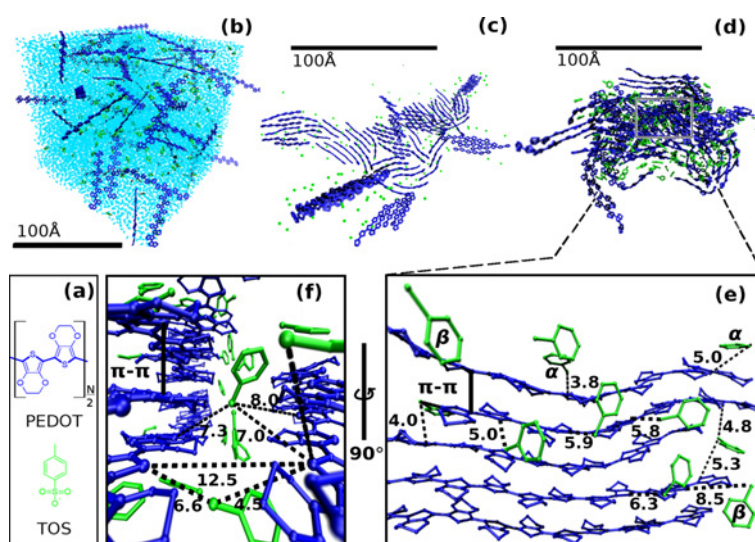


Figure 2.25: (a) Molecular structure of PEDOT and TOS. (b-e) Snapshots of the PEDOT:TOS structures. PEDOT is shown in blue, TOS in green, and water in light blue; water is not shown in parts c-f. (b) Random initial position of PEDOT chains, TOS and water in $12 \times 12 \times 12 \text{ nm}^3$ computational box; PEDOT chain length $N = 12$, carrier concentration $c_h = 33\%$. (c) Aqueous PEDOT:TOS solution after equilibration time of 20 ns; water content is 82% w/w (only thiophene rings and sulfur atoms from TOS are shown). (d) PEDOT:TOS in a dry phase after five steps of water evaporation (H and O atoms and methyl groups from TOS are not shown). (e) Zoom of a representative crystallite from part d with the indicated distances r_{SO_3-S} (in Å) between Sulfur atoms of PEDOT and TOS. α and β mark TOS molecules. (f) Previous crystal rotated 90° (left) and a neighboring crystallite (right).

The authors of the work started with a diluted water solution of PEDOT

chains and TOS (molecular tosylate) counterions and gradually evaporate water molecules in order to reach a dry phase. They considered PEDOT chains with a relative concentration of holes up to one charge per three monomers with the distribution of charges in the PEDOT chains that has been calculated by density functional theory.

Chains with a number of monomers $N = 3, 6, 12,$ and 18 have been considered, and they have been randomly located in a cubic computational box $12 \times 12 \times 12 \text{ nm}^3$ together with TOS counterions.

The main results of this work are:

- PEDOT comprises crystallite aggregates consisting of 3-6 $\pi - \pi$ stacked chains;
- The size of the crystallites depends on the water content, but the stacking distance does not depend particularly on the chain length, charge concentration and water content;
- PEDOT chains and crystallites exhibit bending that depends on their length and water content;
- TOS counterions are located either on the top of the chains or on the side of the crystallites and their distribution depends on the charge concentration but is practically independent of the water content.

Chapter 3

Problem Statement

In this thesis work the problem that have been addressed concern the development and the use of Molecular Dynamics methods, in order to provide a quantitative description (through Diffusion Coefficients, Bending of the PSS polymers expressed by Probability Density Function, distribution of molecules along the z axes and Radial Distribution Functions, depending on the specific simulation) of the conducting polymer PEDOT:PSS. Moreover, the local structure of the polymer blend has been visualized using MRI (magnetic resonance tomography) software.

We investigated structural models of this organic semiconductor in different physical conditions (see next in this section), analyzing the relationship among the structure and the properties of the system.

Extending the comparison with experimental results and understanding the influence of certain parameters on the dynamics of the material are the goals of the work; several simulations hence have been considered and other simulations are in progress.

The importance of the work lies in the concernment of this material in the field of organic conducting polymers, being by far one of the most used in bioelectronics and being often the material of choice for many applications.

Even if its morphology and electronic properties have already been clarified by several experiments, there is a difficulty in obtaining experimental data about the micro-structure due to its disordered and nano-crystalline nature. Furthermore, a consistent theoretical description of the structure has not been presented yet.

Molecular Dynamics methods hence appeared to be suitable to provide atomistic structures of the polymer blend, giving access to structural models of such composite and overcoming the limitations.

Different physical conditions were considered, obtained by:

- changing the temperature of the system;
- changing the amount of charge on the PEDOT oligomers;
- introducing the presence of a surface.

We focused on these parameters/physical conditions because of their relevance in experimental conditions (see Chapter 1).

Computer simulations have therefore been used to analyze the relationships that exist among the structure of the system (influenced by the above mentioned parameters and geometry) and the resulting properties.

Progresses beyond the state of the art has been achieved by considering atactic PSS polymers in the calculations, by studying this conducting nanocomposite in presence of a surface and considering the evaporation process both in the bulk phase and with a PEDOT:PSS/solid interface.

Further optimizations of polymeric nanocomposites with mixed ionic and electronic properties can be obtained by overcoming the experimental limitation (due to the disordered and nano-crystalline morphology) with structural models obtained through these simulations.

Chapter 4

Discussion and Results

4.1 Computational Details

As the Molecular Dynamics Simulations is a semi-empirical method, the quality of the results will depend on the chosen inputs. Great importance so is given to the choice and the determination of the initial configuration, as it will influence all the subsequent steps.

About the atomic charges, ab initio molecular orbital calculations have been performed by using GAMESS US quantum chemistry package. The simulations presented in this thesis involve both PEDOT and PEDOT²⁺, hence the charge distribution has been calculated for both molecules by using Löwdin population with 6-311G basis.

Simulations have been carried out using the AKMD simulation program of Prof. Andrei V. Komolkin and research was carried out using computational resources provided by Resource Center “Computer Center of SPbU” (<http://cc.spbu.ru>).

Using NVIDIA GeForce 970 and NVIDIA GeForce 1070 graphics cards, the simulations in presence of a surface required a little over 4 months of calculations (because of the long process of evaporation) and the simulations in

bulk phase required \sim 2-3 months of calculations.

JMOL software has been used to visualize the resulting .pdb files.

In order to be close to experimental conditions, PEDOT molecules (Fig. 4.1, 4.2) are taken shorter in the linear direction compared to PSS polymers (Fig. 4.3, 4.4, 4.5). In particular the oligomers of PEDOT are composed by 6 monomers (Fig. 4.2) and the polymers of PSS are composed by 12 monomers (Fig. 4.5, 4.6, 4.7).

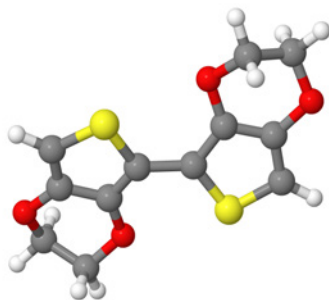


Figure 4.1: Dimer of PEDOT. Yellow spheres are Sulfur atoms, red spheres are Oxygen atoms, gray spheres are Carbon atoms and white spheres are Hydrogen atoms.

For this work we considered atactic PSS polymers randomly generated (Fig. 4.6, 4.7) so that every one of this polymers have its own particular structure, that is (very likely) different from all the other PSS polymers.

Both structures of PEDOT and PSS have been created using Jmol software and the bond lengths have been chosen both considering experimental data and geometry optimization calculations.

Simulations was performed both in NVE , NpT and NVT ensembles, in systems consisting of about 85000-100000 atoms; in the bulk phase and without

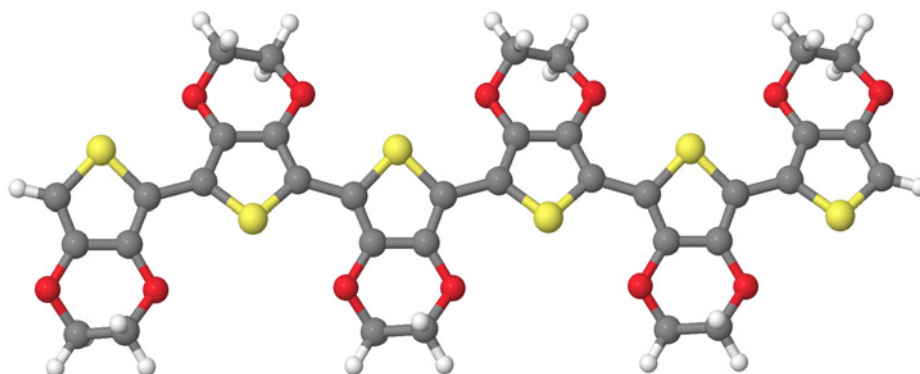


Figure 4.2: Oligomer of PEDOT, used during the simulations. Yellow spheres are Sulfur atoms, red spheres are Oxygen atoms, gray spheres are Carbon atoms and white spheres are Hydrogen atoms.

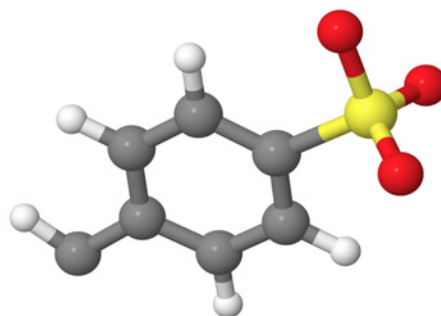


Figure 4.3: Monomer of Styrene Sulfonate.

any evaporation process there are 180 PEDOT monomers, 360 PSS polymers, 29000 water molecules and 300 or 360 Na⁺ counterions (their number depend on the charge of PEDOT oligomers).

The amorphous SiO₂ surface that we used has been obtained starting from optimized coordinates of an amorphous silica slabs [87] and it contains about 11000 atoms.

The number of water molecules instead is not constant in the simulations that involve the evaporation process, as this molecules are removed from the simulations at every step once they fulfill a certain condition, i.e. they are

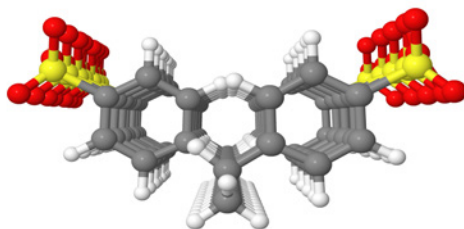


Figure 4.4: Side view of a PSS polymers. Note the structure obtained from polystyrene by the addition of sulfonate functional groups. Yellow spheres are Sulfur atoms, red spheres are Oxygen atoms, gray spheres are Carbon atoms and white spheres are Hydrogen atoms.

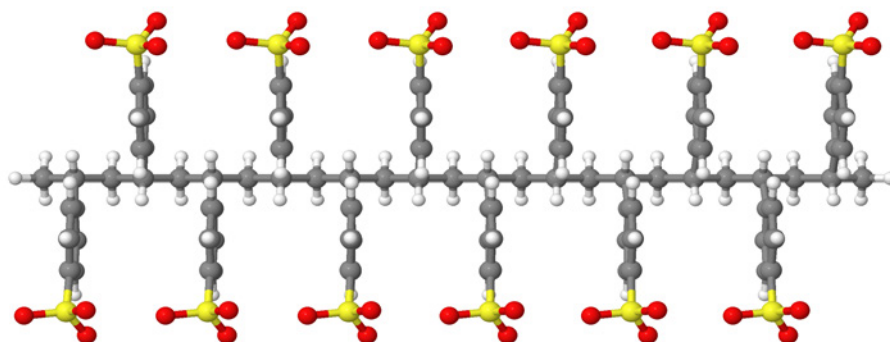


Figure 4.5: Top view of a syndiotactic PSS polymers. Note the structure obtained from polystyrene by the addition of sulfonate functional groups. Yellow spheres are Sulfur atoms, red spheres are Oxygen atoms, gray spheres are Carbon atoms and white spheres are Hydrogen atoms.

deleted from the simulations if their value of the z -coordinate is bigger than a certain threshold (that is progressively changed with the evolution of the simulation).

The simulations without a surface (in bulk phase) are performed in a cubic box of $\sim 100 \times 100 \times 100 \text{ \AA}^3$ and the density of the system is $\sim 1 \text{ g/cm}^3$, i.e. the density of pure water, due to the big amount of water molecules

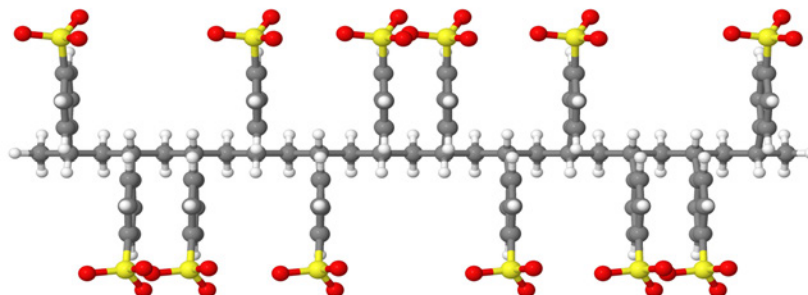


Figure 4.6: Top view of atactic PSS polymers. Note the structure obtained from polystyrene by the addition of sulfonate functional groups. Yellow spheres are Sulfur atoms, red spheres are Oxygen atoms, gray spheres are Carbon atoms and white spheres are Hydrogen atoms.

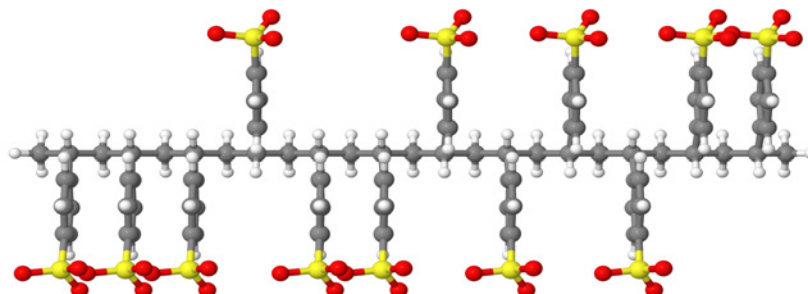


Figure 4.7: Top view of another atactic PSS polymers. Note the structure obtained from polystyrene by the addition of sulfonate functional groups and the differences with the above PSS polymer. Yellow spheres are Sulfur atoms, red spheres are Oxygen atoms, gray spheres are Carbon atoms and white spheres are Hydrogen atoms.

compared to the other components.

In presence of the (rigid) surface we consider about 25 angstrom of vacuum above the system (polymer blend + surface), so that the surface results to be periodic in the $x - y$ plane and sandwiched between vacuum layers in the z -direction.

During the process of evaporation the density of the system increase, because of the decreasing of the ratio of water molecules to PEDOT:PSS.

When the evaporation process is not considered the temperature of the system is $T = 25\text{ }^\circ\text{C}$ (room temperature), otherwise it is $T = 90\text{ }^\circ\text{C}$. In any case the target temperature was maintained using the Nosé-Hoover thermostat.

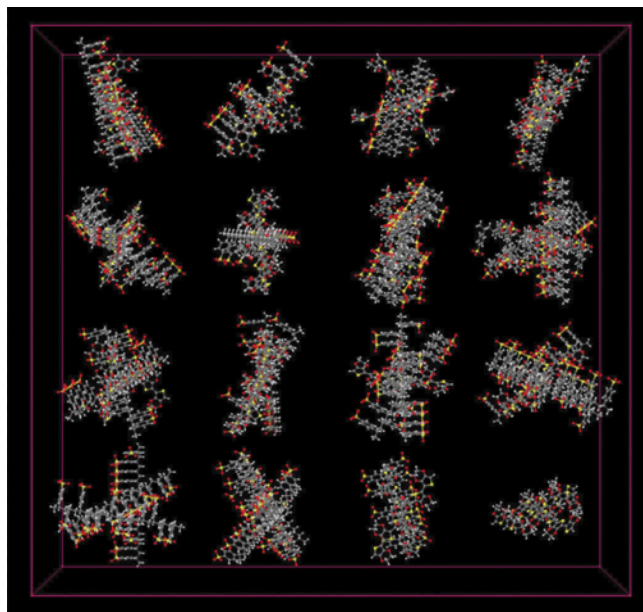


Figure 4.8: Initial atomic spatial configuration for the simulation of PEDOT:PSS in bulk phase from a top view. Water molecules are not shown.

The equations of motion are integrated using the Verlet algorithm, with a time step of $\tau = 1\text{ fs}$ and $\tau = 2\text{ fs}$. Every simulation last at least 20 ns, enough to be sure that we have reached the equilibration stage. In our case indeed the presence of heavy molecules (PEDOT and PSS) required longer

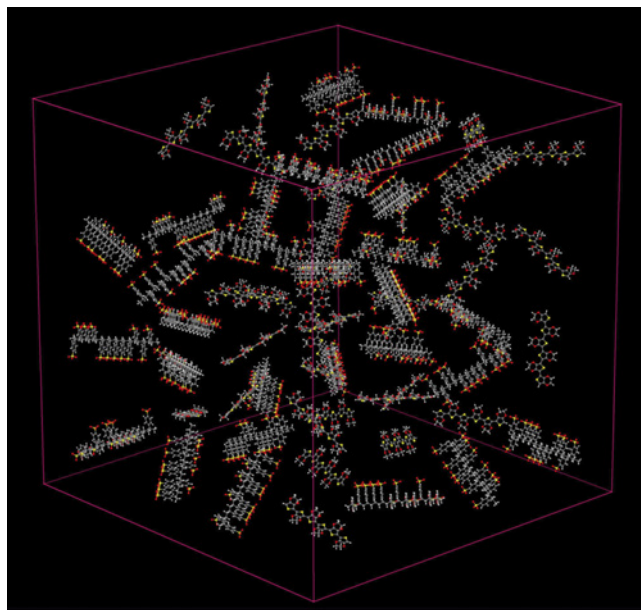


Figure 4.9: Initial atomic spatial configuration for the simulation of PE-DOT:PSS in bulk phase from a side view. Water molecules are not shown.

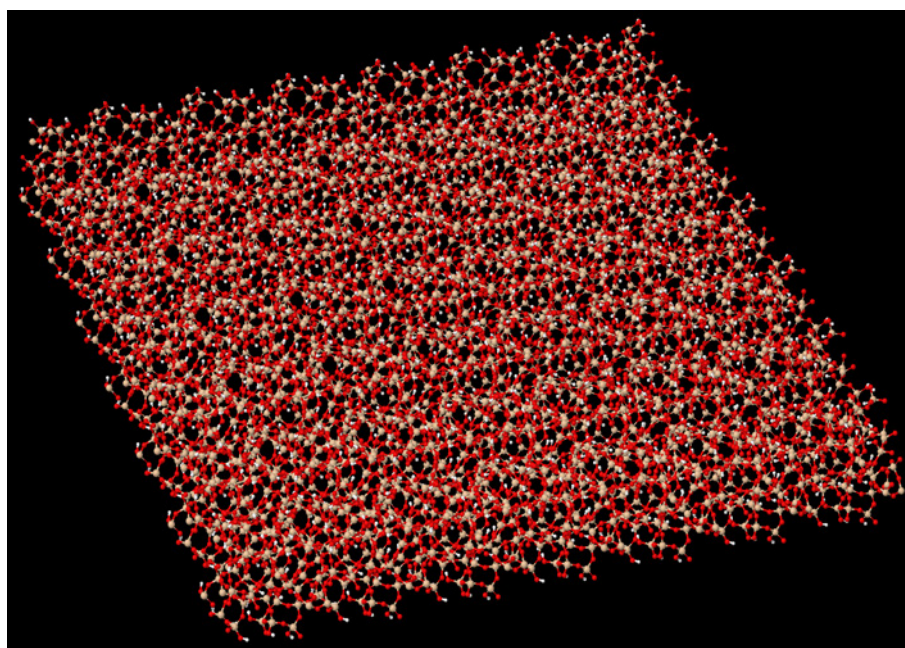


Figure 4.10: Amorphous glass surface used for the simulations.

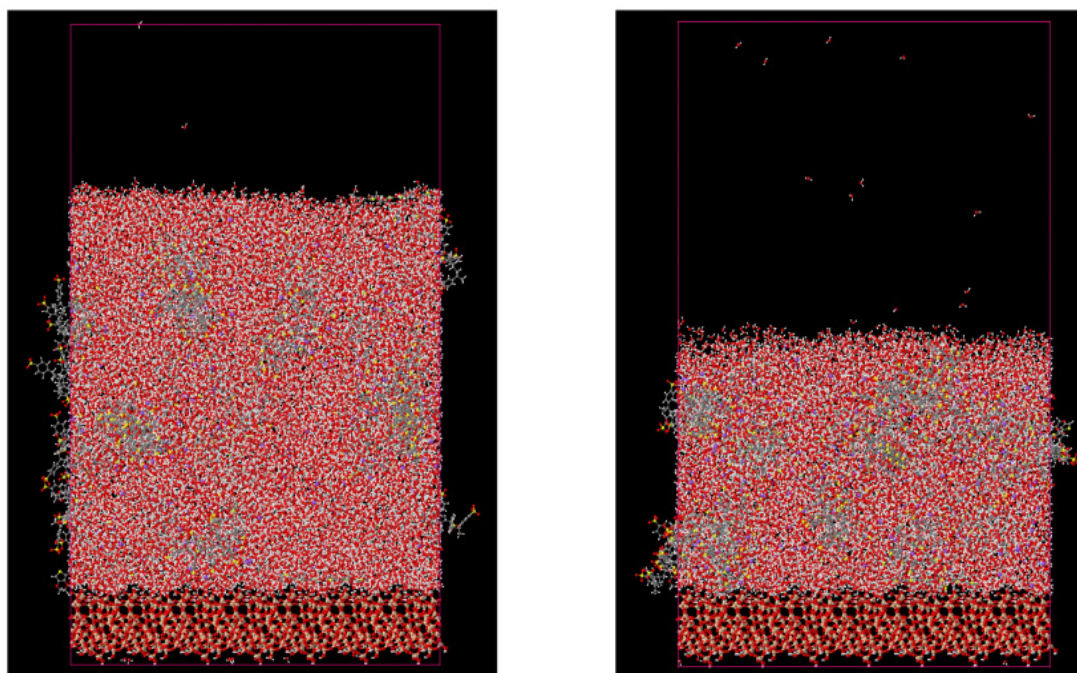


Figure 4.11: Evaporation of water for PEDOT:PSS in contact with the glass surface. Note the non-cubic simulation box.

time for the equilibration, compared for example to the case of water/ethanol mixture.

The equilibration of the simulated system can be estimated step by step checking the following parameters:

- The total potential energy goes to a constant value, with small fluctuations;
- The kinetic energy distributes in equal proportions between degrees of freedom. In this step, partial temperatures of each species should be equal to the mean value of the temperature, in the range of standard deviation. Moreover the temperatures of different kinds of degrees of freedom (translational, rotational and intra-molecular) should be approximately the same (see e.g. Tab. 2.1).

- The molecules run away from the initial positions farther than one half of their length.

The first two criteria are reached after a few picosecond of simulation, but molecules are still in the initial positions, i.e. where they were placed during the creation of the system. The third point is the main criterion of the equilibration of the systems.

Water molecules, in all the simulations, were modeled using the SPC/E model. To model PEDOT oligomers and PSS polymers, OPLS Force Field was used; this means that the potential energy of the system consist of bond energy, bond angles, dihedral and non-bonded interactions:

$$E = E_{bonds} + E_{angles} + E_{dihedrals} + E_{non-bonded} \quad (4.1)$$

The calculations of interaction energy between different atoms/molecules are so based on a combination of van der Waals and electrostatic energies, where negative values represent an attractive interaction.

The standard Ewald summation method was used and, before starting to simulate, the accuracy and the cut-off for the long-range interactions have been choosen. Three-dimensional periodic boundary conditions have been used.

All systems were initially equilibrated in a NVE ensemble, checking in the meanwhile the output files and looking at the mean values of the physical values and at their fluctuations. When the latter start to be small enough the calculations are switched to a NpT or NVT ensemble, hence making use of a thermostat and/or a barostat, and the system is gradually warmed up until the target temperature is reached.

Jmol software have also been used to visualize the output of the calculations.

The quantities that have been calculated are useful to quantify what is qualitatively found out from this visualization software; in particular we obtained, from the analysis of the trajectories, information about the Diffusion Coefficients, the Probability Density Function regarding the bending of PSS polymers (to discover if the *freely jointed chain* could be an optimal model in this framework), the approaching of the Na^+ counterions to the SO_3 group of PSS, the formation of the lamellar ordering concerning the PEDOT oligomers (Fig. 4.12) and the interactions among PEDOT and PSS (Fig. 4.13).

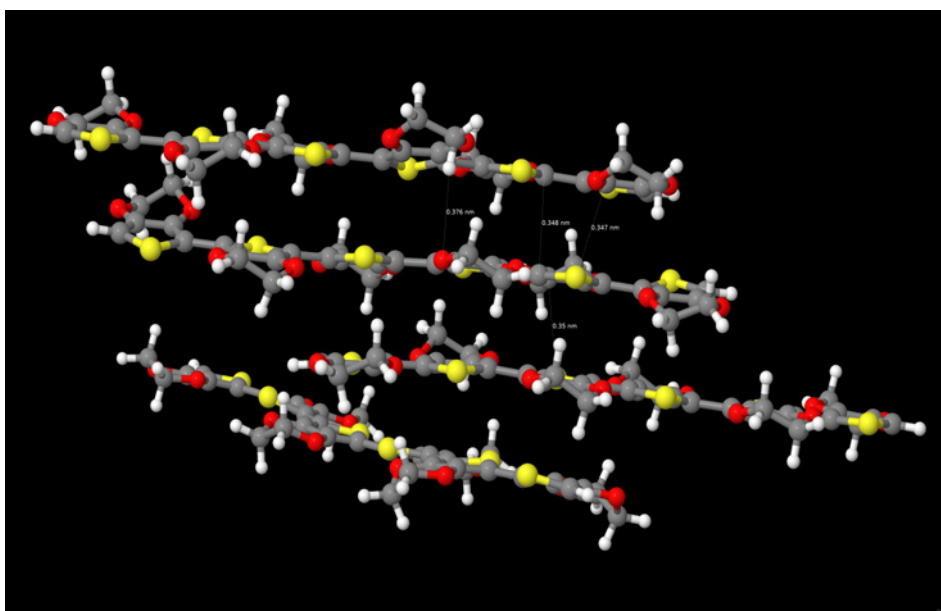


Figure 4.12: Lamellar structure of PEDOT oligomers in PEDOT:PSS. The typical distance between the plane is of $\sim 3.5 \text{ \AA}$.

Diffusion Coefficients D are calculated through the Einstein formula 2.43. This coefficient depends on the starting time of analysis t_{start} and on the final time of analysis t_{final} ; when the curve (plot of D as a function of time) reaches a constant value at the end of the simulation (t_{final}), D is correctly calculated and this final value can be accepted as an optimal estimation. Otherwise one should continue the simulation.

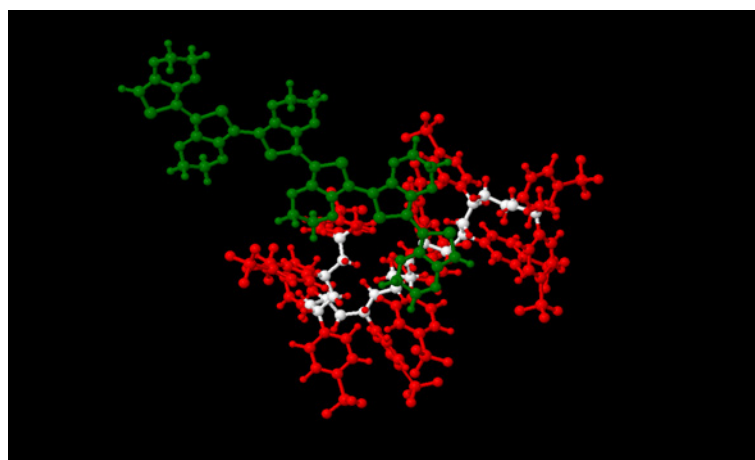


Figure 4.13: Interaction among a charged PEDOT oligomer (2+) and a charged PSS polymer (12-). The PEDOT oligomer is green, PSS polymer is red and its backbone is white.

The results have been obtained as a function of different physical conditions (charge on PEDOT oligomers, different temperatures and presence of a surface).

The visualization of the local structure of the polymer blend deals with a new method invented by Prof. Andrei V. Komolkin, and it is based on the use of MRI (magnetic resonance tomography) software.

The results concerning the computational tomography of the structure of PEDOT molecules in the simulation can be seen from x , y and z directions. They show both the intra-molecular and the inter-molecular interactions: the green color is about the inter-molecular interactions and the intensity is related to the probability of finding another PEDOT oligomer at a certain distance and in a certain configuration, taken one of the PEDOT oligomer as a reference.

Then the calculations are performed following the trajectories of every oligomer in the system, and so what is represented is the mean behavior of every PEDOT oligomer.

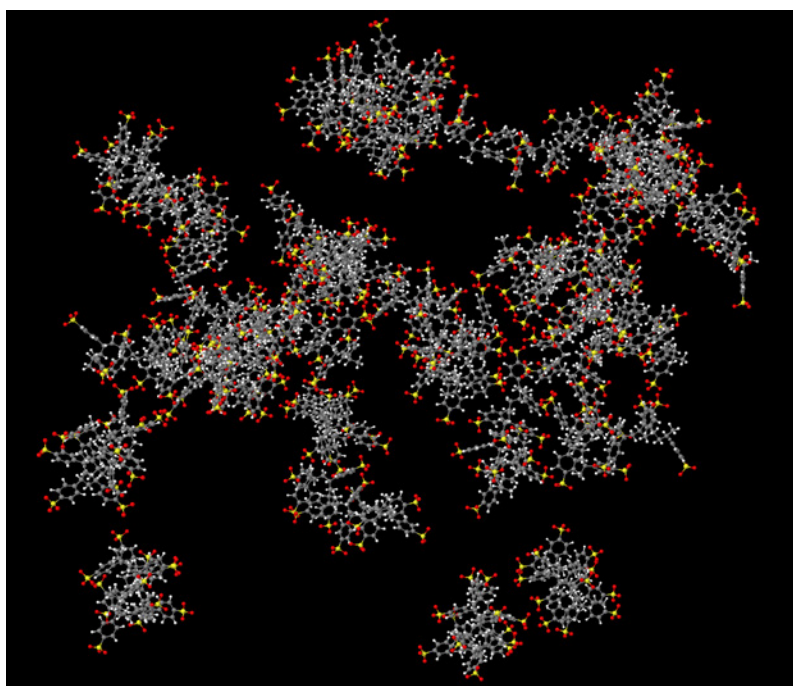


Figure 4.14: Example of PSS bending during the simulation run. PEDOT oligomers, water molecules and Na^+ counterions are not shown in this image.

The images give us information about the structures that arise, and they clearly show that in every simulation is very likely that an oligomer is embedded in a lamellar structure (stacking order).

Anyway, some differences arise in this lamellar structure because of different physical conditions, and this details will be discussed in next sections.

The resulting intra-molecular interactions are given by the following colors: yellow for Sulfur, white for Carbon and red for Oxygen.

Also in this case the intensity of the color is related to probability of finding a certain atom at a certain distance respect to the other atoms of the PEDOT oligomer; the calculations, again, are performed following the trajectories of the atoms of every PEDOT oligomers.

What it can be observed are the bonds oscillations and the mean distance of every atom respect to the other atoms of the same oligomer (so we can observe the internal structure).

Visualization of the 3-D densities of Oxygen atoms of PSS polymers and Carbon atoms of PSS backbone around PEDOT are considered as well.

4.1.1 Visualization of the 3D structures

Visualization of the local structure of the material is done through DICOM files. This format is used for the exchange of images in medical systems like tomographs.

Inside the file one can find either one slice of a 3-D image, or the whole 3-D image.

To calculate and represent the local structure of the PEDOT oligomers, a molecular frame has been allocated on one of the molecule. This is done in such a way that the origin is in the center of mass, and the axes coincide with the principal axes of inertia tensor.

x -axis is along molecular axis, y -axis is along the molecule plane and z -axis is perpendicular to this plane.

The space around the molecule is subdivided into cubic *voxels*, whose side is $l = 0.2 \text{ \AA}$. The number of voxels is $128 \times 128 \times 128$, corresponding to 128 slices of 128×128 color pixels.

Attention is focused on the heavy atoms of PEDOT, on the Oxygen atoms of SO₃ groups of PSS and on the backbone carbons of PSS.

For each PEDOT molecule, on each step of the trajectory, is calculated the number of interesting atoms (i.e. those cited in the previous sentence) in the voxels.

This is done for every molecule of PEDOT, on each step of the simulation.

The final step is to normalize the calculated average density of the interesting atoms.

There is a correspondence among the color of the voxel and the corresponding

average density, as the black is related to the absence of atoms, the medium green to the mean density of these atoms in the sample and the bright green to the double mean density.

The color corresponds so to probability of finding the atoms around the reference PEDOT molecule.

The color 3-D picture so obtained is stored in the DICOM file, in order to use tomography visualization software.

We used PixelMed software; it allows us to draw slices in $x - y$, $x - z$ and $y - z$ planes to visualize the local structure of the PEDOT molecules.

4.2 Analysis of PEDOT:PSS in Bulk Phase

The first results have been obtained studying the PEDOT:PSS without any surface, hence in the bulk phase.

A simulation box of about $100 \times 100 \times 100 \text{ \AA}^3$ (dimensions may slightly change in a NpT ensemble, as the volume is not fixed) have been used and the simulations involve 2400 atoms belonging to the 30 PEDOT oligomers, 6990 atoms belonging to the 30 PSS polymers, 78366 atoms belonging to 26122 water molecules and 300 Na^+ sodium counterions in systems containing charged PEDOT, otherwise 360 Na^+ sodium counterions for uncharged PEDOT.

Water molecules have been modeled with SPC/E model and the evolution of the whole system is given by inter-molecular interactions among the different components (electrostatic and van der Waals), together with bonded interactions (both 2-body harmonic interactions, 3-body angle bending and 4-body torsional interaction).

After the generation of the initial atomic/molecular spatial configuration, simulations have been launched and the systems have been equilibrated. The simulation for neutral PEDOT ran for ~ 33 ns and the one for charged PEDOT ran for ~ 40 ns.

For bulk PEDOT:PSS system with neutral PEDOT we found out that PEDOT oligomers moves about (average motion) 16.3 Å during 20 ns of simulation, and that PSS polymers moves about (average motion) 23.5 Å in the same period (Fig. 4.15). According to what have been said in Section 4.1 regarding the equilibration, we conclude that 20 ns of simulation is enough to equilibrate the positions of the molecules in the system.

Then, only after 20 ns of simulation one can analyze trajectories of the simulation.

For bulk PEDOT:PSS system with charged PEDOT the required time increases (Fig. 4.16)

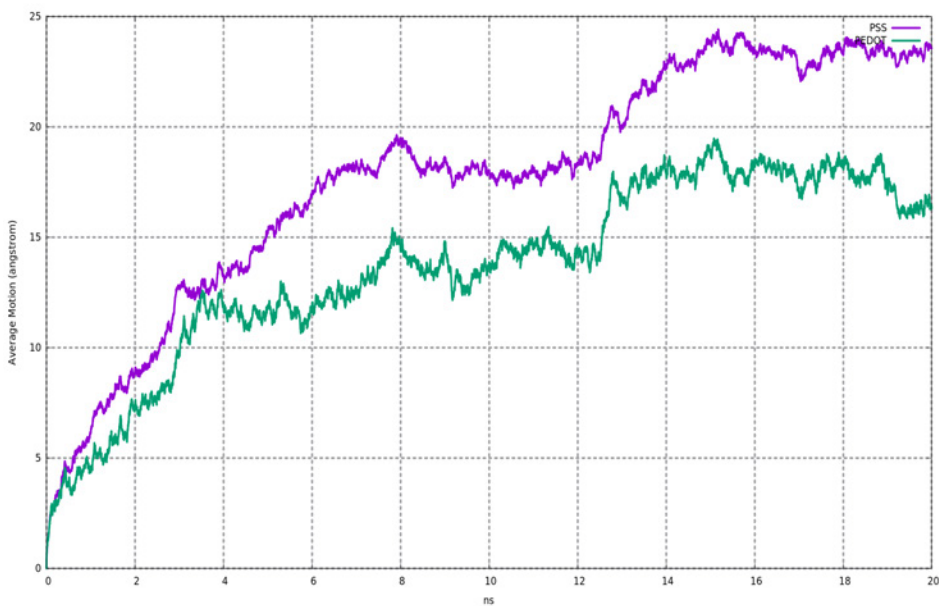


Figure 4.15: Average motion of PEDOT and PSS for bulk system at $T = 25$ °C, with uncharged PEDOT.

Simulations until 3.25 ns are performed in NpT ensemble with a time step of 1 fs; from 3.25 ns we switched to NVT ensemble with a time step of 2 fs, as we assured that the fluctuations of the mean values was not so big, in order to have faster calculations (3 times).

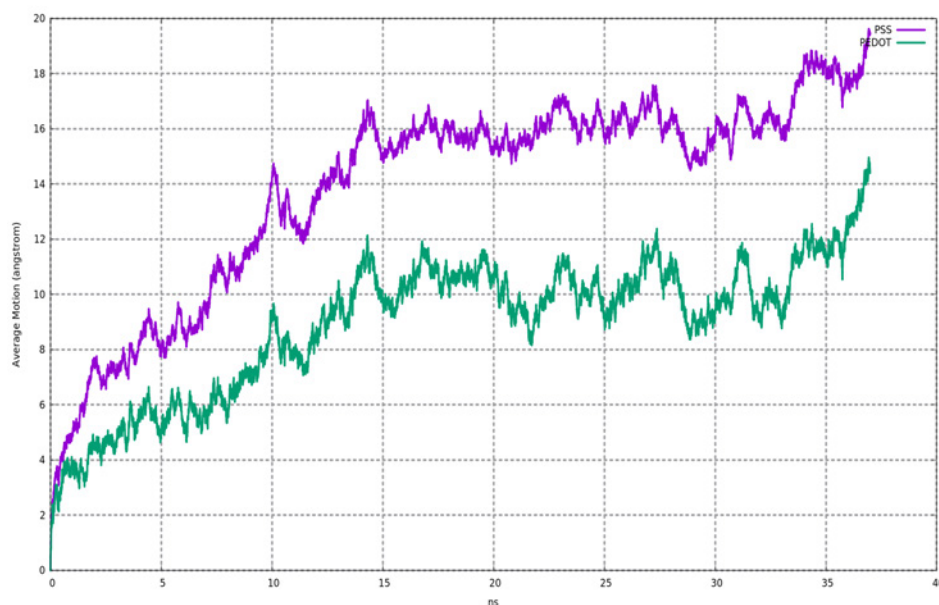


Figure 4.16: Average motion of PEDOT and PSS for bulk system at $T = 25$ °C, with charged PEDOT.

All data have been obtained by analyzing the output files of the simulations containing the trajectories. The results that are presented in the next subsections (4.4.1 and 4.2.2) concern the study of Diffusion Coefficients, useful to get fundamental information about the dynamics of the different components of the system and to make comparison with already existing experimental data.

From the qualitative observation of the pdb files, we noted that during the evolution of the systems the PSS polymers start to bend, and for this reason have been calculated the probability density function of the distance between the Carbon atoms at the extremes of the polymer, for every polymer in the simulation box; in this way the conformation of the PSS have been analyzed, allowing us to compare the data with already existing models (freely-jointed chain model, in particular).

As one of the main advantage of organics materials is to support efficient

ion transport at room temperature, the radial distribution function of the equilibrium positions of the Na^+ counterions, respect to the SO_3 group of PSS, have been calculated from the trajectories. Together with the diffusion coefficient, it give us information about the dynamic of the counterions inside the polymer blend.

Great attention is devoted to the visualization of the local structure with the MRI software.

Many similarities arise from the observation of data, between the two simulations in bulk phase (with charged PEDOT oligomers and neutral PEDOT oligomers).

Regarding the visualization of the local structure, for both charged and uncharged PEDOT in bulk phase at $T = 25^\circ \text{C}$, a lamellar structure appears with a spacing between planes of $\sim 3.6 \text{ \AA}$.

Indeed the PEDOT oligomers are relatively big, and 2 missing electrons in the charged configuration don't influence considerably the distance between planes in lamellar structure. However, differences can be observed in the size of the lamellar structure, that appears to be bigger in the charged configuration (4.43 and 4.42 compared with 4.30).

In the case of uncharged PEDOT oligomers, it can be seen (4.27, 4.28) that there is a certain probability of observing perpendicular/transverse structures.

Moreover, for both simulations, the green probability regions for the intermolecular interactions are longer compared to the central oligomer. This is representative of the appearance of slide between oligomers inside the same lamellar structure (4.12).

From the analysis of the 3-D densities of Oxygen atoms of the SO_3 groups of PSS (Fig. 4.33, 4.34, 4.46, 4.47) and Carbon atoms of PSS backbone around PEDOT (Fig. 4.31, 4.32, 4.44, 4.45), we can conclude that in both

bulk simulations at $T = 25$ °C the Oxygen atoms are mainly located at the edge of the PEDOT oligomers, while under the plane their density is much lower. Vice versa, the Carbon atoms of the backbone are located under the PEDOT oligomers, while in the plane they are practically absent.

However, signals appears to be brighter (in the sense discussed in Subsection 3.2.1) for charged PEDOT oligomers, reflecting a stronger electrostatic interaction among them and PSS polymers.

Moreover, the distributions of Carbon atoms of phenyl rings of PSS around show that, in the system with charged PEDOT oligomers, the contact of phenyl rings with PEDOT in the plane of the oligomer is more emphasized (Fig. ??).

Regarding the conformation of PSS polymers, the presence of charged PEDOT leads to a more ordered structure in the bending process (4.48 compared with 4.35), but in both case it is clear that the freely-jointed chain model cannot be applied.

Indeed, from theory, one have that:

$$\sqrt{\langle \vec{R}^2 \rangle} = \sqrt{N} \times b = \sqrt{L \times b} \quad (4.2)$$

where $\sqrt{\langle \vec{R}^2 \rangle}$ is the average end-to-end distance, b is the length of the monomer, L the length of the polymer and N the number of monomers.

In our case it would be:

$$\sqrt{\langle \vec{R}^2 \rangle} = (2.47 \times \sqrt{12}) \text{ \AA} = 8.56 \text{ \AA} \quad (4.3)$$

but the images 4.35 and 4.48 clearly show that the probability is not localized only around this value, reflecting the interactions between PEDOT and PSS oligomers and resulting in a smaller number of bent PSS around the average value of 8.56 Å.

According to the freely-jointed chain model one would expect a Gaussian distribution, hence with a single maximum, in the limit of large N . This is

not our case, where several maxima appears in both cases in the simulated distribution.

This maxima reflect the equilibrium conformation for the bending of PSS polymers, resulting from the balancing of electrostatic forces, van der Waals interactions and thermal motion.

Every PSS polymer is embedded in the same environment of the others PSS but, because of small statistical fluctuations and non periodic distributions of polymers/components of the system in the simulation box, each one will feel a slightly different potential field that result in different equilibrium conformations.

It is our opinion that, however, for a complete statistical analysis of the bending/conformation one would need more than 30 PSS polymers, as we are far from the limit of large N .

Regarding the equilibrium positions of the Na^+ counterions, their distance from the Oxygen atoms of the SO_3 groups of PSS doesn't depends on the charge of PEDOT oligomers (Fig. 4.17), and the same is true for the distance between the ions and the Sulfur atoms of the SO_3 groups (Fig. 4.18). This means that the ions are more influenced by the polar SO_3 groups, respect to the charge distribution of the PEDOT oligomers.

The distance of the counterions from the Sulfur of the SO_3 groups is bigger compared to the their distance from the Oxygen atoms of the same groups (Fig. 4.36 and 4.49), and this is due to the geometric conformation of the functional SO_3 group, where the Sulfur atom is closer to the backbone, compared to the Oxygen atoms that are more peripheral.

It's interesting to analyze the obtained values for the Diffusion Coefficients, as they show some dependence on the PEDOT charge (Tab. 4.1 and Figg. 4.37, 4.50, 4.19, 4.20).

The only quantity that is not influenced by the electronic state of PEDOT

is the Diffusion Coefficient for water, that is also the main component of the simulated systems, and whose value can be compared with the experimental and computational results that have been already calculated in other works. The data of Diffusion Coefficients for PEDOT and PSS in the PEDOT 2+ configuration show a big difference compared with the neutral PEDOT configuration: the order of the coefficients is the same for both (10^{-11} m²/s), but their magnitude is 3 times larger for the neutral PEDOT configuration. This reflects the electrostatic interaction that exist between polymers and oligomers in the system, and hence it become bigger when the PEDOT is positively charged (leading to a smaller Diffusion Coefficient).

Finally, it is worthwhile to note that in both cases the Diffusion Coefficient for Na⁺ counterions in the PEDOT:PSS polymer blend approaches the Diffusion Coefficient for Na⁺ ions in pure water (1.334×10^{-9} m²/s).

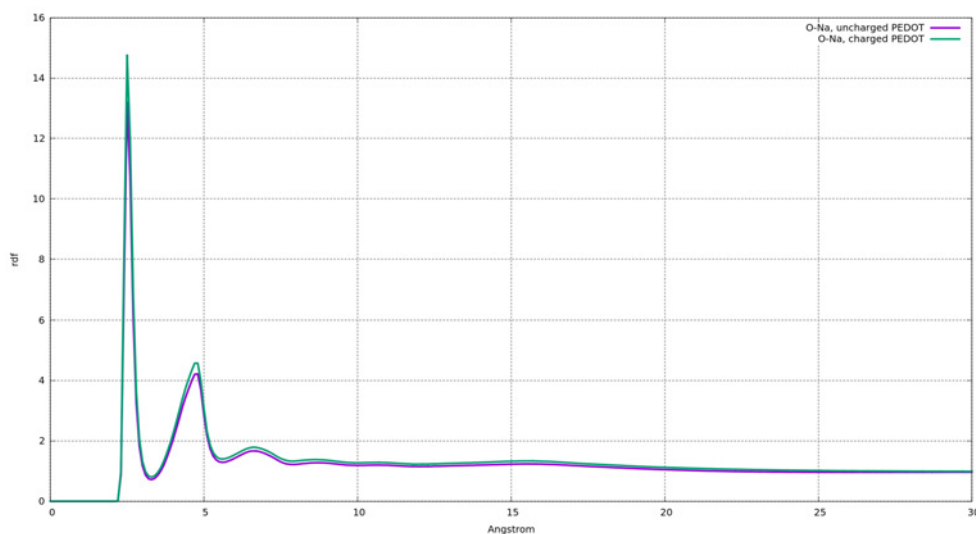


Figure 4.17: Radial distribution function of the distance between Oxygen atoms of the SO₃ group of PSS, and the Na⁺ counterions, for the bulk phase system at $T = 25$ ° C and neutral/charged PEDOT.

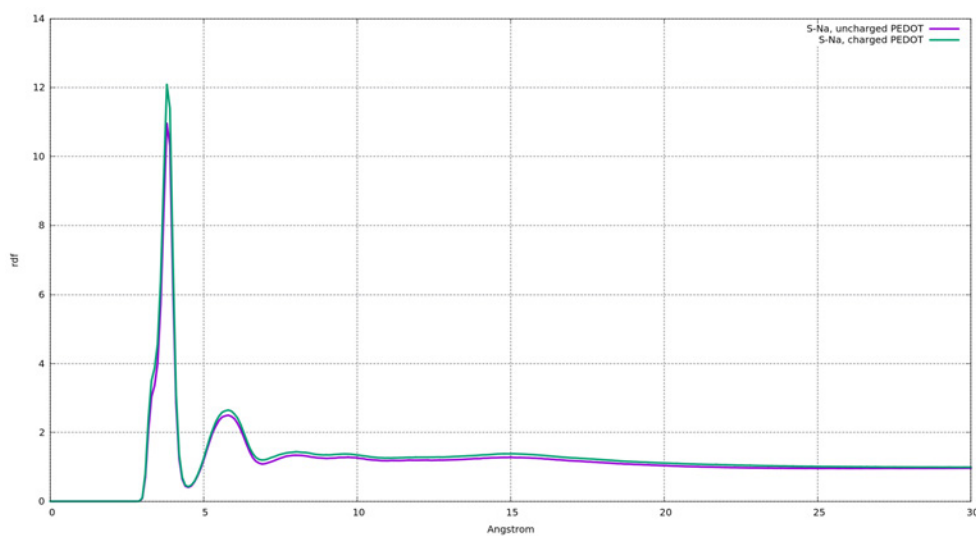


Figure 4.18: Radial distribution function of the distance between Sulfur atoms of the SO₃ group of PSS, and the Na⁺ counterions, for the bulk phase system at $T = 25^\circ\text{C}$ and neutral/charged PEDOT.

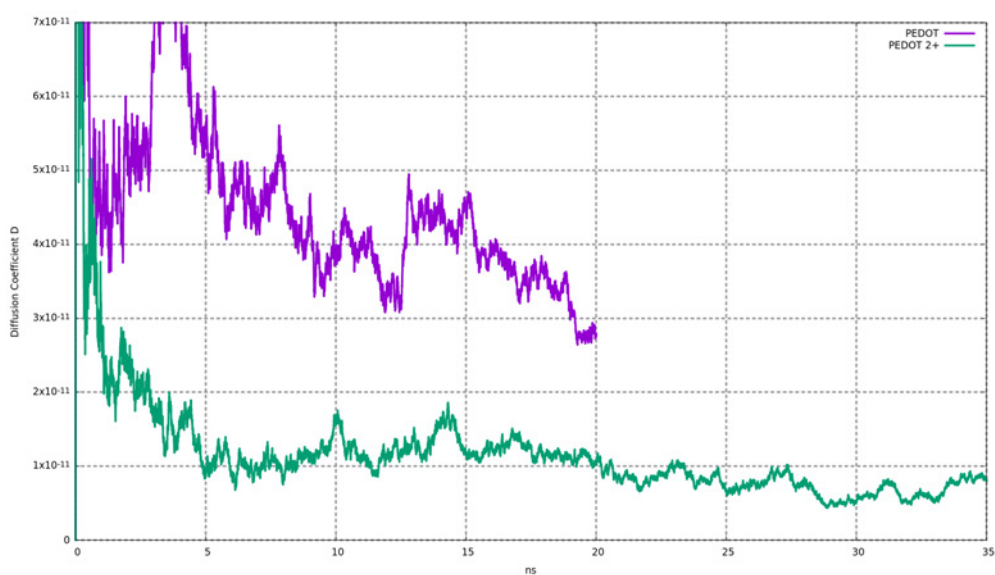


Figure 4.19: Graphical comparison among the Diffusion Coefficients of the PEDOT oligomers in bulk system at $T = 25^\circ\text{C}$ (uncharged and charged PEDOT).

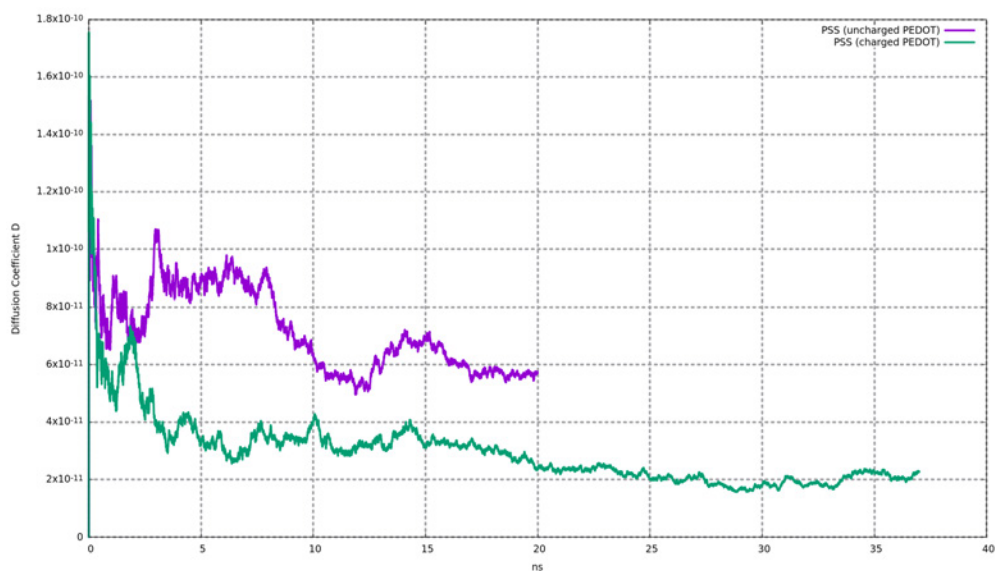


Figure 4.20: Graphical comparison among the Diffusion Coefficients of the PSS polymers in bulk system at $T = 25\text{ }^{\circ}\text{C}$ (uncharged and charged PEDOT).

$T = 25\text{ }^{\circ}\text{C}$, bulk phase	Charged PEDOT (2+)	Uncharged PEDOT
PEDOT	$1 \times 10^{-11}\text{ m}^2/\text{s}$	$3 \times 10^{-11}\text{ m}^2/\text{s}$
PSS	$2 \times 10^{-11}\text{ m}^2/\text{s}$	$6 \times 10^{-11}\text{ m}^2/\text{s}$
Na^+	$6.6 \times 10^{-10}\text{ m}^2/\text{s}$	$8 \times 10^{-10}\text{ m}^2/\text{s}$
Water	$2.1 \times 10^{-9}\text{ m}^2/\text{s}$	$2.1 \times 10^{-9}\text{ m}^2/\text{s}$

Table 4.1: Values of Diffusion Coefficient for bulk systems at $T = 25\text{ }^{\circ}\text{C}$, for charged and neutral PEDOT oligomers.

Fig. 4.21 is a superfigure representing a comparison among the experimental findings for uncharged (top row) and charged (bottom row) PEDOT in bulk phase at $T = 25$ °C. They concern the visualization of the local structure along z direction ($x - y$ plane) by MRI software, focusing on the stacking order of PEDOT oligomers. Detailed images related to the superfigure are Figg. 4.27, 4.28, 4.39 and 4.40.

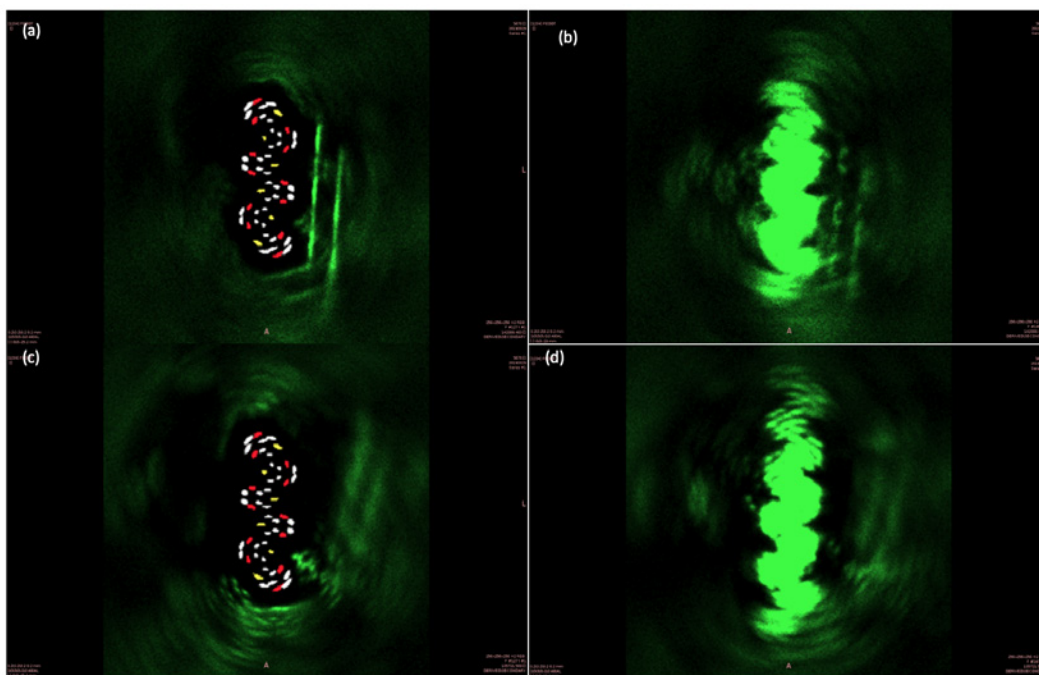


Figure 4.21: a) Computational tomography of uncharged PEDOT, in the $x - y$ plane ($z = 25.2$ Å) b) Computational tomography of uncharged PEDOT, in the $x - y$ plane ($z = 29.0$ Å) c) Computational tomography of charged PEDOT, in the $x - y$ plane ($z = 25.2$ Å) d) Computational tomography of charged PEDOT, in the $x - y$ plane ($z = 29.2$ Å).

Fig. 4.22 is a superfigure representing a comparison among the experimental findings for uncharged (left) and charged (right) PEDOT in bulk phase at $T = 25\text{ }^\circ\text{C}$. They concern the visualization of the local structure along y direction by MRI software, focusing on the stacking order of PEDOT oligomers. Detailed images related to the superfigure are Figg. 4.30 and 4.42.

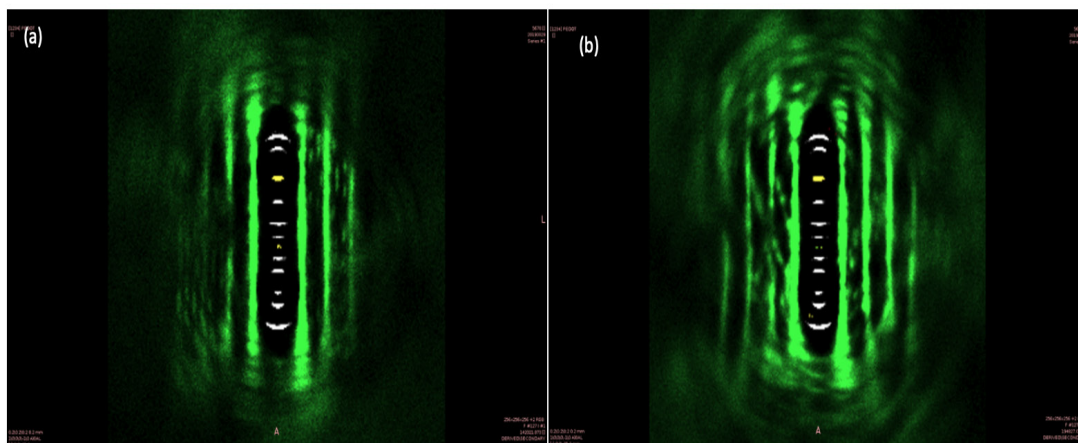


Figure 4.22: a) Computational tomography of uncharged PEDOT, along y direction ($x - z$ plane, $y = 25.2\text{ \AA}$) b) Computational tomography of charged PEDOT, along y direction ($x - z$ plane, $y = 25.2\text{ \AA}$).

Fig. 4.23 is a superfigure representing a comparison among the experimental findings for uncharged (top row) and charged (bottom row) PEDOT in bulk phase at $T = 25\text{ }^\circ\text{C}$. They concern the visualization of the local structure along x direction by MRI software, focusing on the 3-D densities of Carbon atoms of PSS backbone around the oligomers. Detailed images related to the superfigure are Figg. 4.31, 4.32, 4.44 and 4.45.

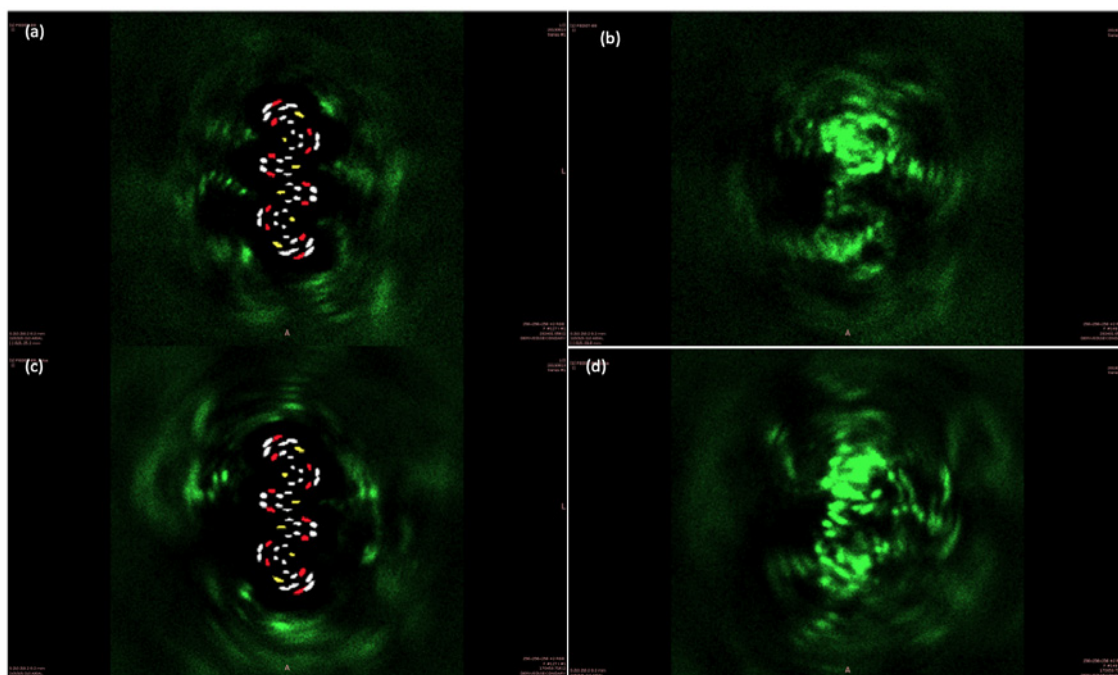


Figure 4.23: a) 3-D densities of Carbon atoms around uncharged PEDOT b) 3-D densities of Carbon atoms around uncharged PEDOT, at a distance of 4.4 \AA from the molecule plane c) 3-D densities of Carbon atoms around charged PEDOT d) 3-D densities of Carbon atoms around charged PEDOT, at a distance of 4.4 \AA from the molecule plane.

Fig. 4.24 is a superfigure representing a comparison among the experimental findings for uncharged (top row) and charged (bottom row) PEDOT in bulk phase at $T = 25 \text{ }^\circ\text{C}$. They concern the visualization of the local structure along x direction by MRI software, focusing on the 3-D densities of Oxygen atoms of SO_3 groups around the oligomers. Detailed images related to the superfigure are Figg. 4.33, 4.34, 4.46 and 4.47.

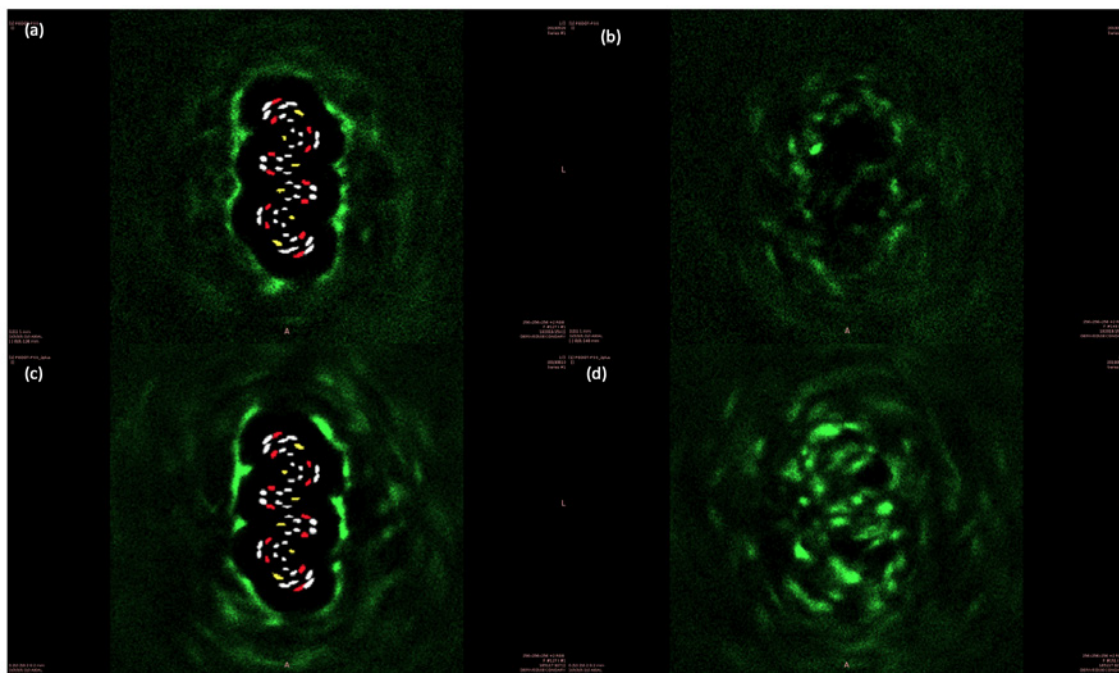


Figure 4.24: a) 3-D densities of Oxygen atoms around uncharged PEDOT b) 3-D densities of Oxygen atoms around uncharged PEDOT, at a distance of 4.4 \AA from the molecule plane c) 3-D densities of Oxygen atoms around charged PEDOT d) 3-D densities of Oxygen atoms around charged PEDOT, at a distance of 4.4 \AA from the molecule plane.

Fig. 4.25 is a superfigure representing a comparison among the experimental findings for uncharged (left column) and charged (right column) PEDOT in bulk phase at $T = 25 \text{ }^\circ\text{C}$. They concern the visualization of distributions of Carbon atoms of phenyl rings of PSS around PEDOT.

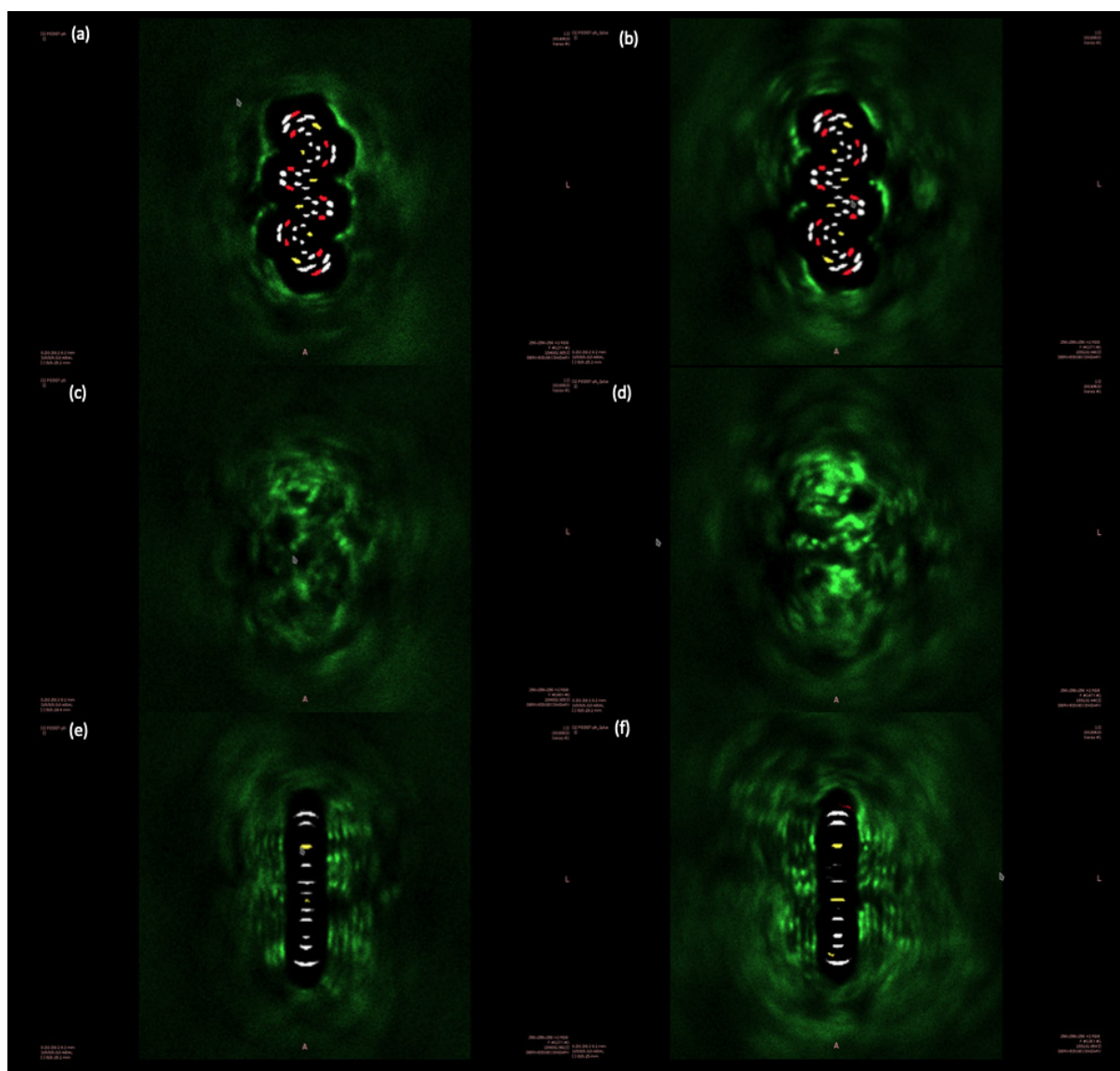


Figure 4.25: a) Distributions of Carbon atoms of phenyl rings of PSS around neutral PEDOT in the $x - y$ plane, at $z = 25.2 \text{ \AA}$ b) Distributions of Carbon atoms of phenyl rings of PSS around charged PEDOT in the $x - y$ plane, at $z = 25.2 \text{ \AA}$ c) Distributions of Carbon atoms of phenyl rings of PSS around neutral PEDOT in the $x - y$ plane, at $z = 29.4 \text{ \AA}$ d) Distributions of Carbon atoms of phenyl rings of PSS around charged PEDOT in the $x - y$ plane, at $z = 29.2 \text{ \AA}$ e) Distributions of Carbon atoms of phenyl rings of PSS around neutral PEDOT in the $x - z$ plane, f) Distributions of Carbon atoms of phenyl rings of PSS around charged PEDOT in the $x - z$ plane

4.2.1 System at $T = 25$ °C with neutral PEDOT

Fig. 4.26 is a superfigure representing some experimental findings concerning the simulation of the system at $T = 25$ °C with neutral PEDOT in bulk phase. Detailed images related to the superfigure are Figg. 4.15, 4.37, 4.35 and 4.36.

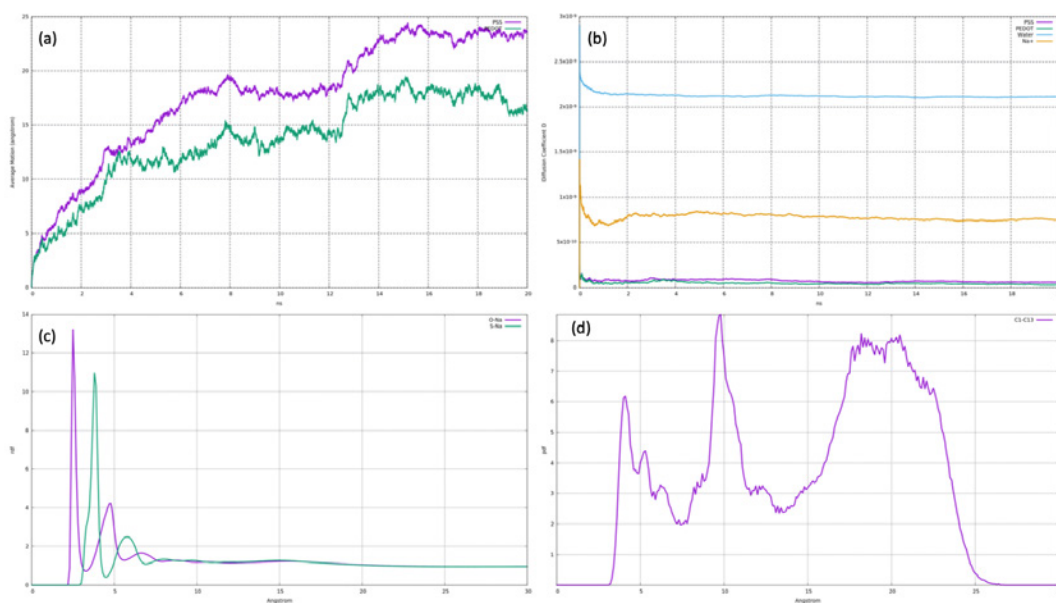


Figure 4.26: a) Average motion of PEDOT and PSS b) Diffusion Coefficients for the different components of the system c) Radial Distribution Function for the distances of Na^+ counterions from the SO_3 group of PSS d) Probability Density Function concerning the bending of PSS (distance among the extremal Carbon atoms).

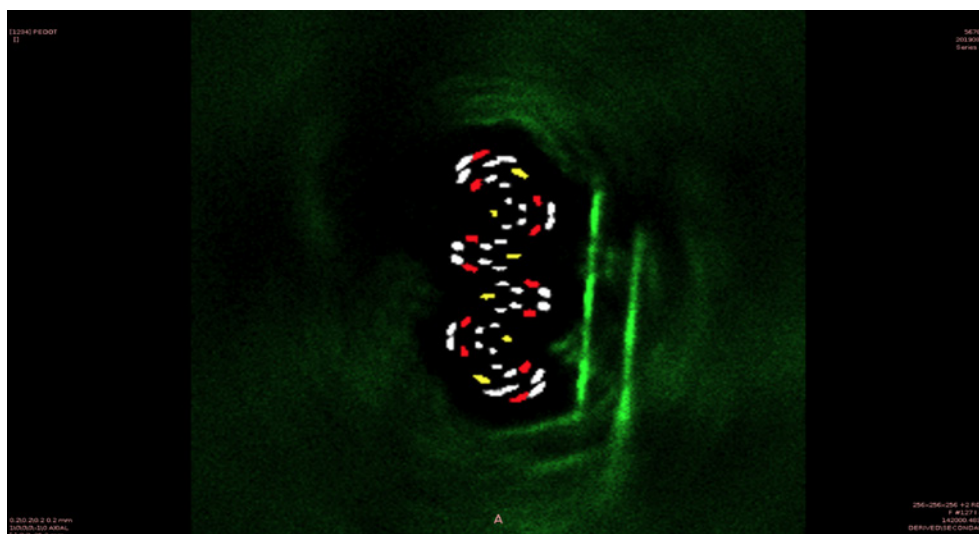


Figure 4.27: Computational tomography of uncharged PEDOT in the $x - y$ plane, with height in z direction of 25.2 \AA , for neutral PEDOT and $T = 25 \text{ }^\circ\text{C}$.

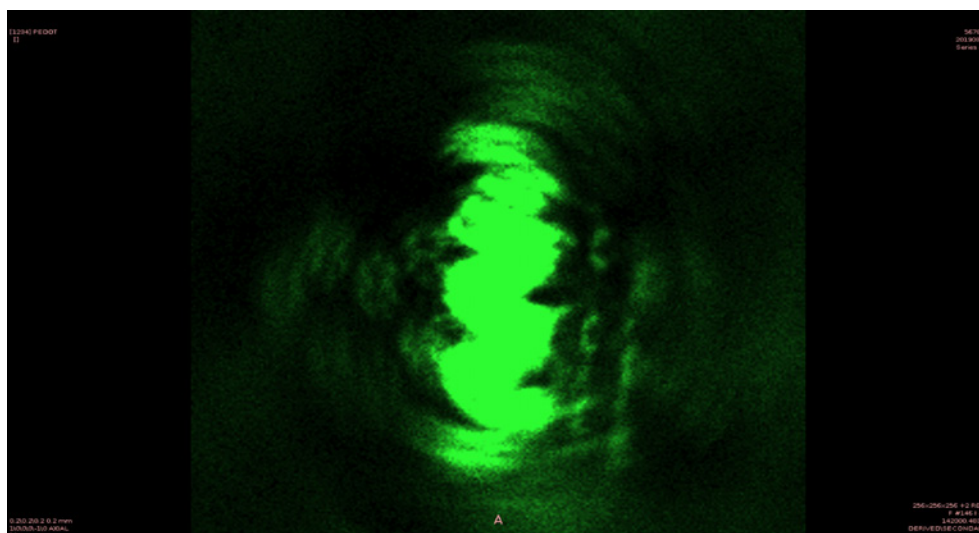


Figure 4.28: Computational tomography of uncharged PEDOT in the $x - y$ plane, with height in z direction of 29.0 \AA , for neutral PEDOT and $T = 25 \text{ }^\circ\text{C}$.

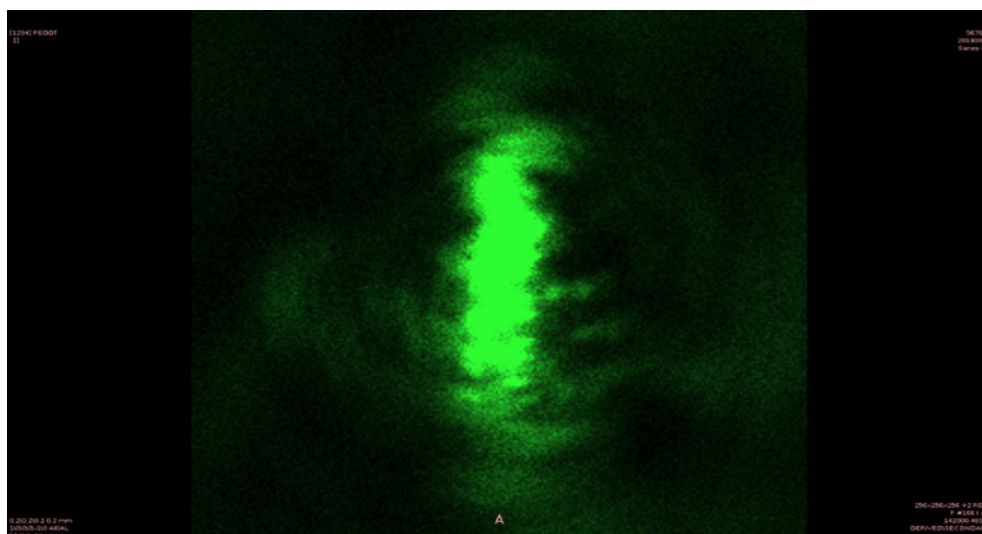


Figure 4.29: Computational tomography of uncharged PEDOT in the $x - y$ plane, with height in z direction of $x=33.0 \text{ \AA}$, for neutral PEDOT and $T = 25 \text{ }^\circ\text{C}$.

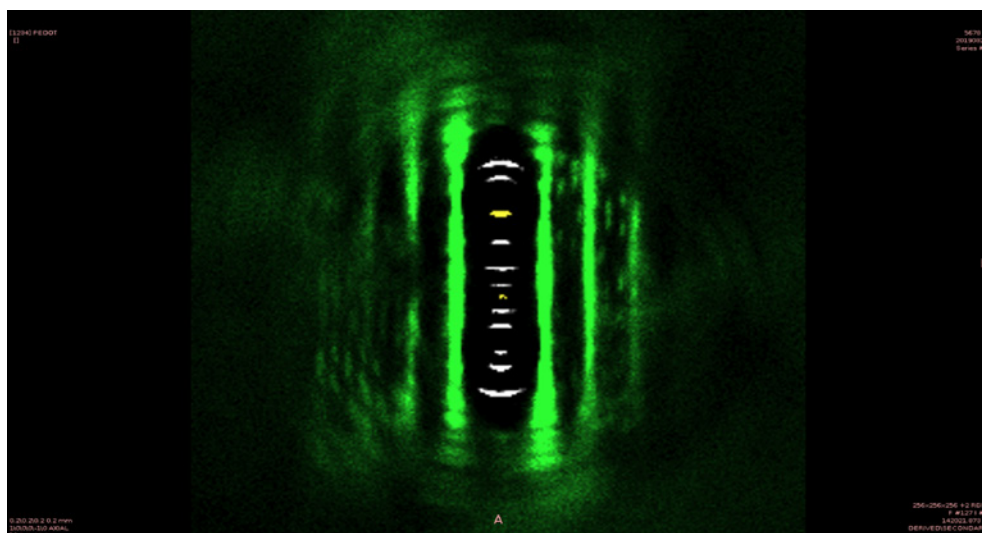


Figure 4.30: Computational tomography of uncharged PEDOT in the $x - z$ plane, with position along the y direction in $y = 25.2 \text{ \AA}$, for neutral PEDOT and $T = 25 \text{ }^\circ\text{C}$.

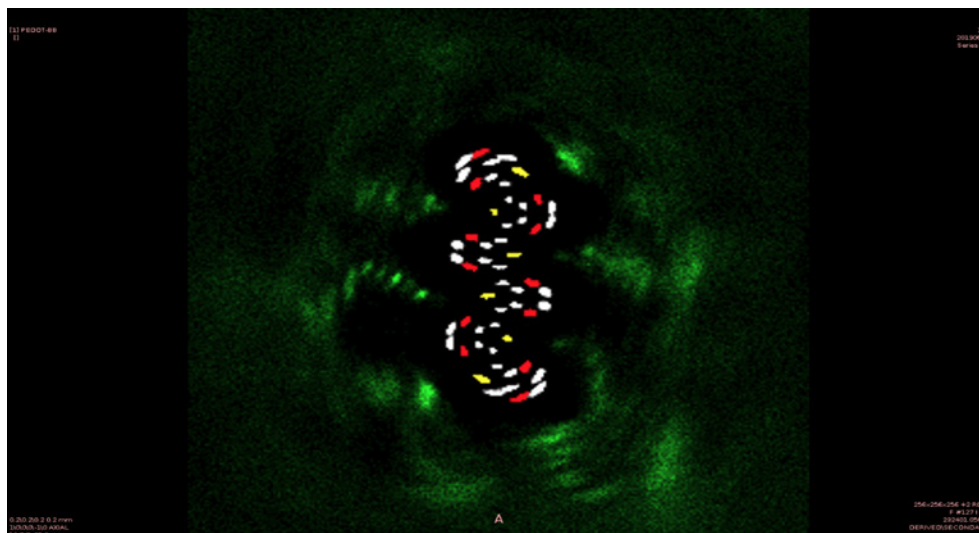


Figure 4.31: 3-D densities of Carbon atoms of PSS backbone around uncharged PEDOT, seen in $x - y$ plane.

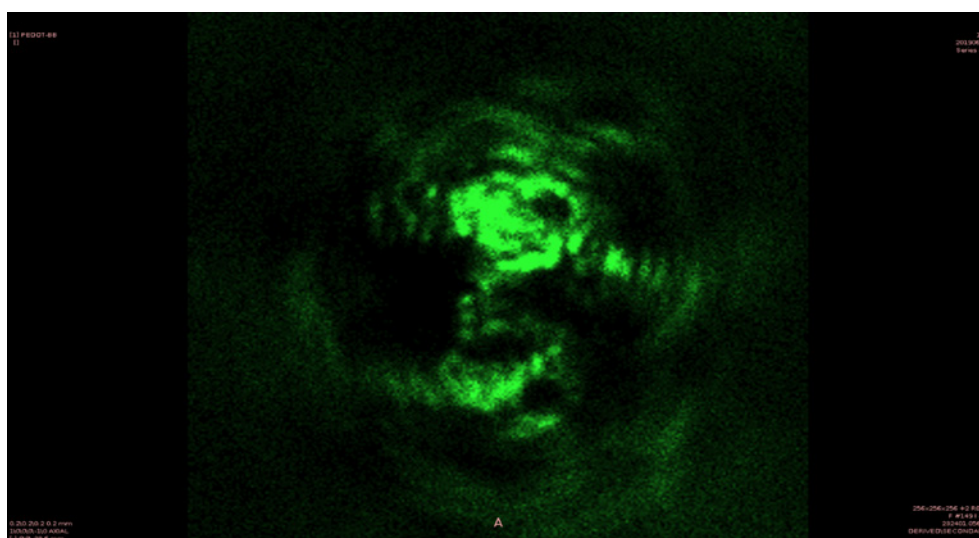


Figure 4.32: 3-D densities of Carbon atoms of PSS backbone around uncharged PEDOT, out of the $x - y$ plane (4.4 \AA under the plane of PEDOT).

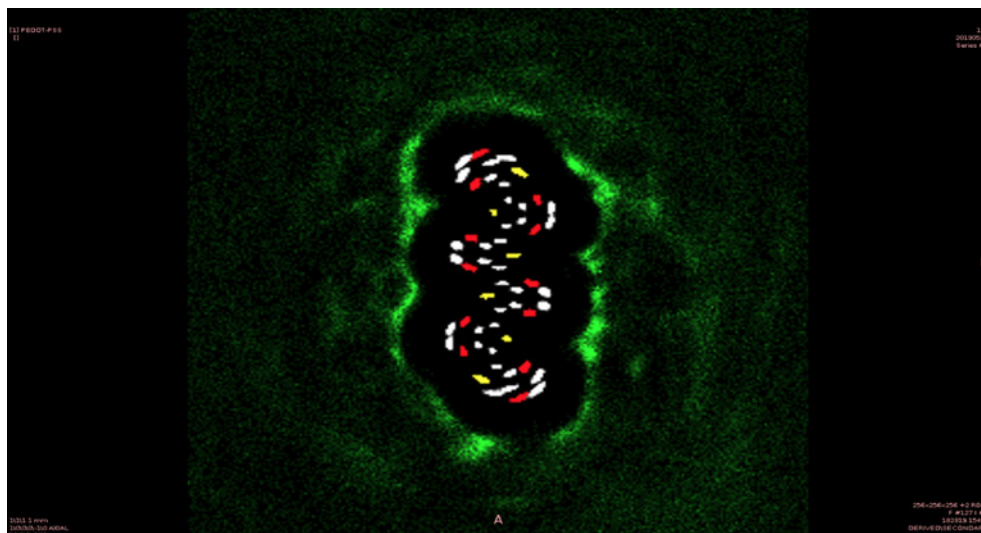


Figure 4.33: 3-D densities of Oxygen atoms of PSS around uncharged PEDOT, seen in $x - y$ plane.

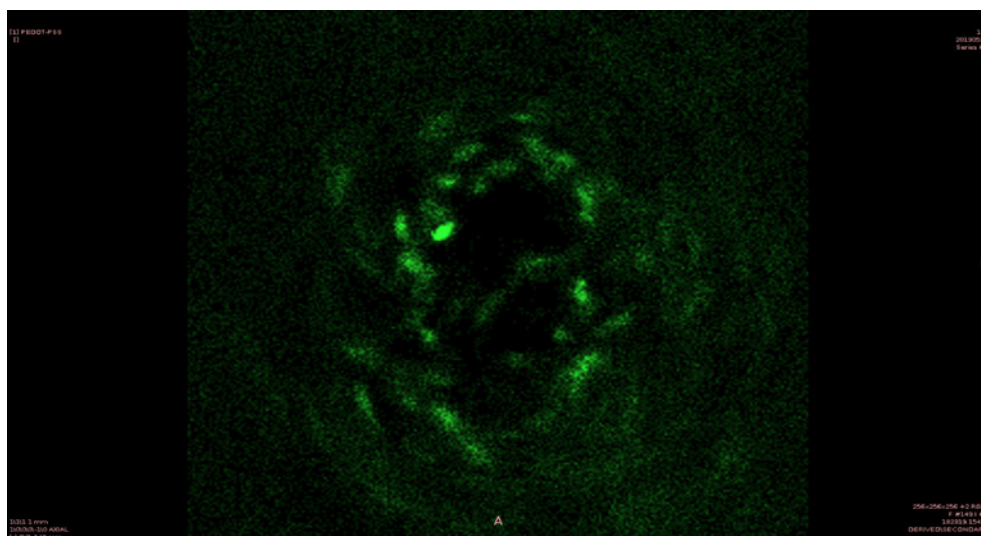


Figure 4.34: 3-D densities of Oxygen atoms of PSS around uncharged PEDOT, out of the $x - y$ plane (4.4 \AA under the plane of PEDOT).

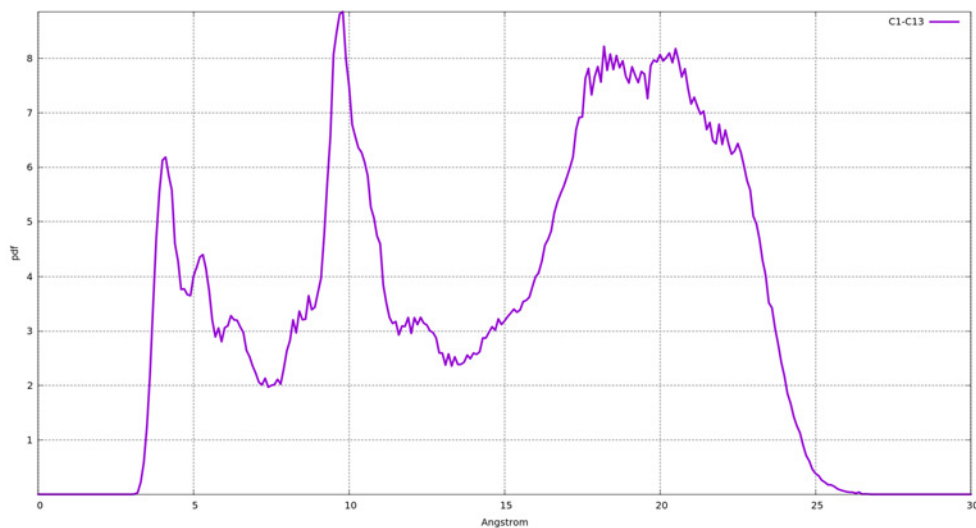


Figure 4.35: Probability density function of the distance between the Carbon atoms at the extremes of PSS for a system in the bulk phase at $T = 25\text{ }^{\circ}\text{C}$ and neutral PEDOT.

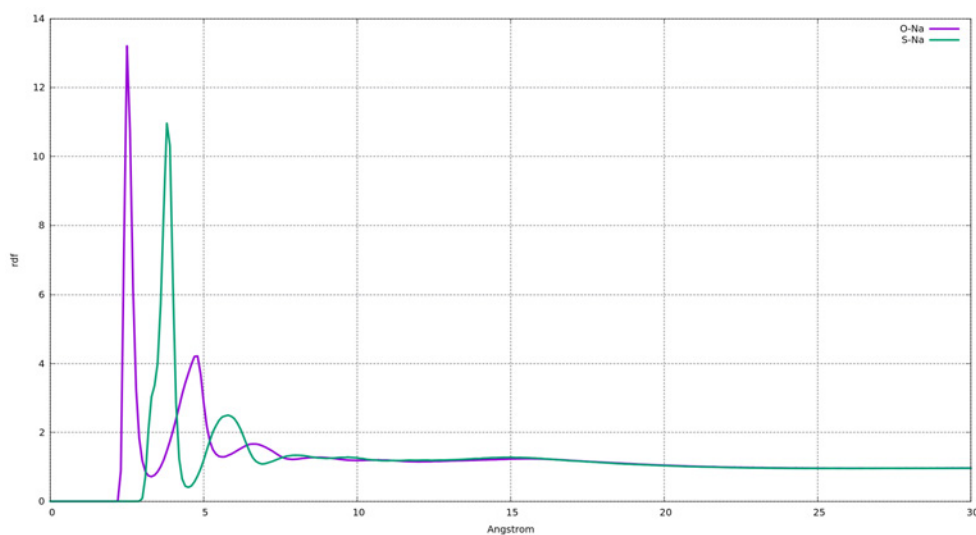


Figure 4.36: Radial distribution function of the distance between Oxygen and Sulfur atoms of the SO₃ group of PSS, and the Na⁺ counterions, for the bulk phase system at $T = 25\text{ }^{\circ}\text{C}$ and neutral PEDOT.

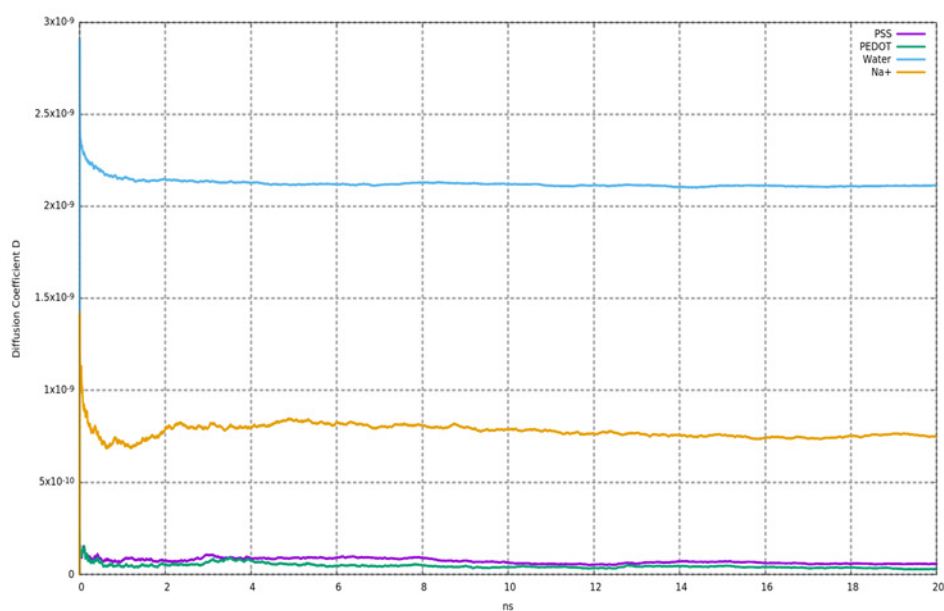


Figure 4.37: Diffusion Coefficients of the components of bulk system at $T = 25$ °C, with uncharged PEDOT.

4.2.2 System at $T = 25\text{ }^{\circ}\text{C}$ with PEDOT 2+

Fig. 4.38 is a superfigure representing some experimental findings concerning the simulation of the system at $T = 25\text{ }^{\circ}\text{C}$ with charged PEDOT in bulk phase. Detailed images related to the superfigure are Figg. 4.16, 4.50, 4.48 and 4.49.

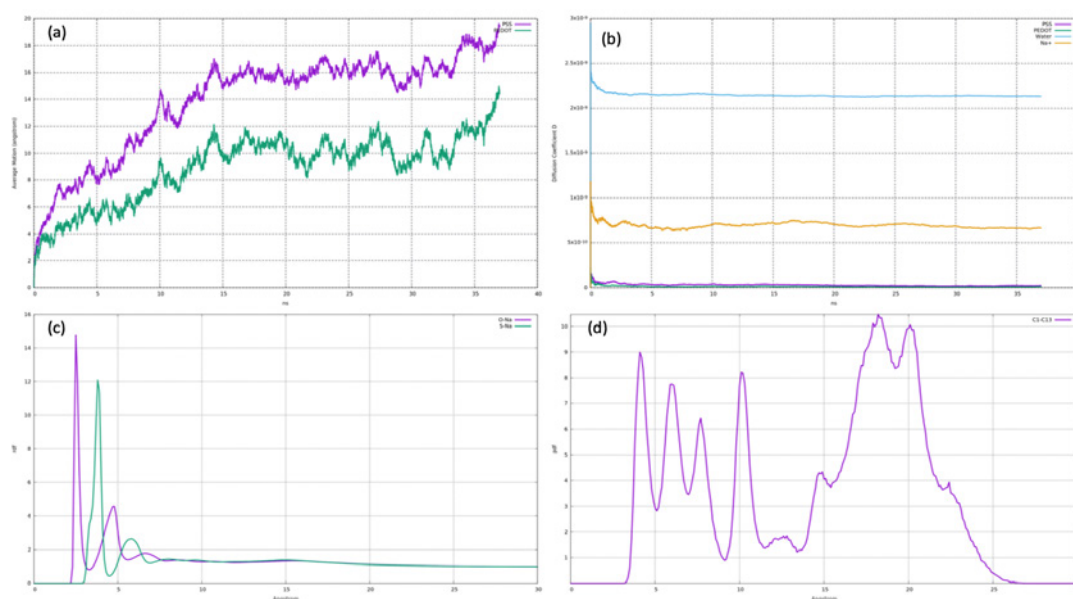


Figure 4.38: a) Average motion of PEDOT and PSS b) Diffusion Coefficients for the different components of the system c) Radial Distribution Function for the distances of Na^+ counterions from the SO_3 group of PSS d) Probability Density Function concerning the bending of PSS (distance among the extremal Carbon atoms).

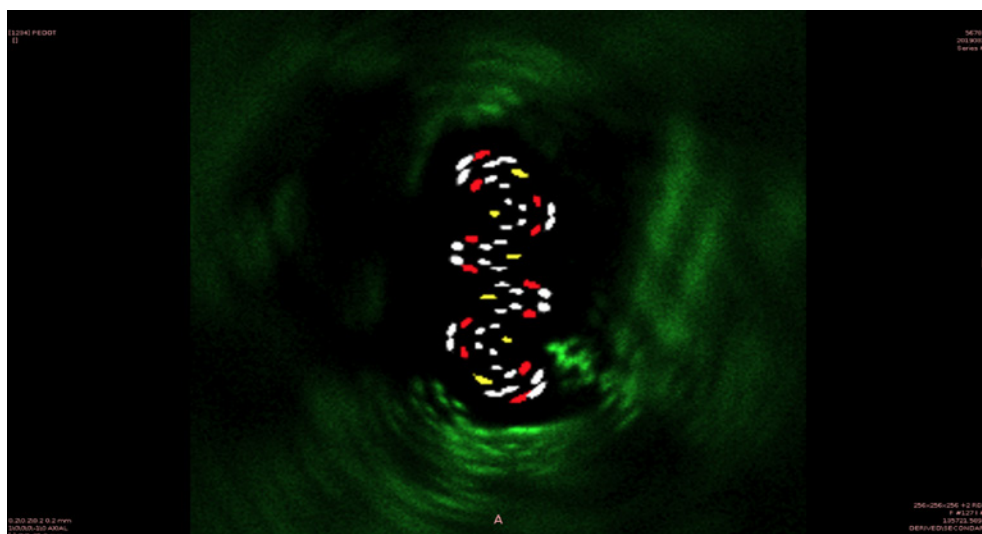


Figure 4.39: Computational tomography of PEDOT:PSS in the $x - y$ plane, with height in z direction of 25.2 \AA , for charged PEDOT ($2+$) and $T = 25 \text{ }^\circ\text{C}$.

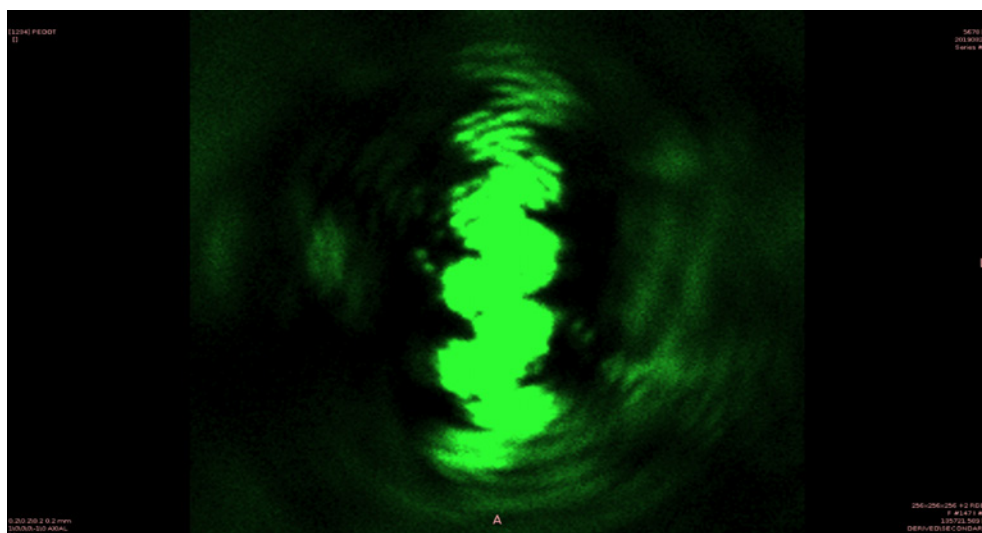


Figure 4.40: Computational tomography of PEDOT:PSS in the $x - y$ plane, with height in z direction of 29.2 \AA , for charged PEDOT ($2+$) and $T = 25 \text{ }^\circ\text{C}$.

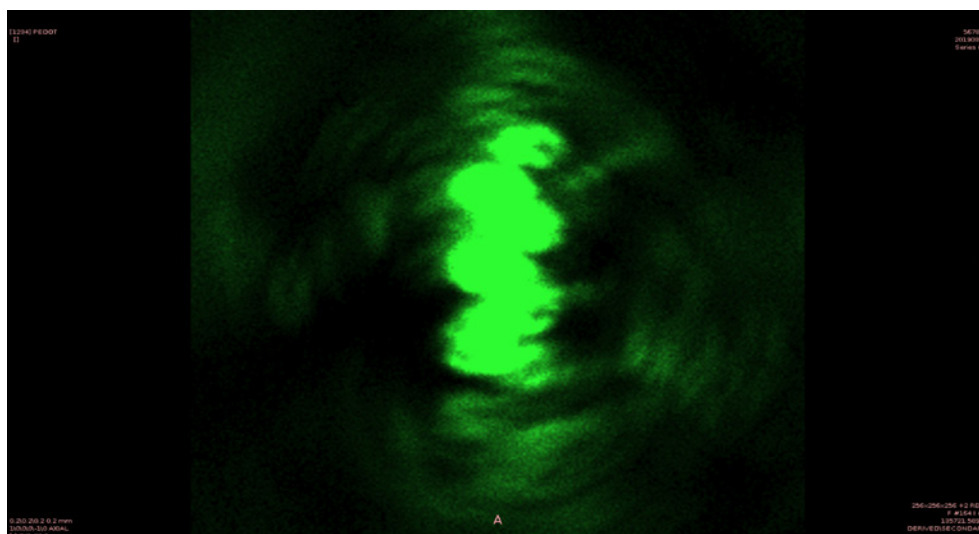


Figure 4.41: Computational tomography of PEDOT:PSS in the $x - y$ plane, with height in z direction of 32.6 \AA , for charged PEDOT ($2+$) and $T = 25 \text{ }^\circ\text{C}$.

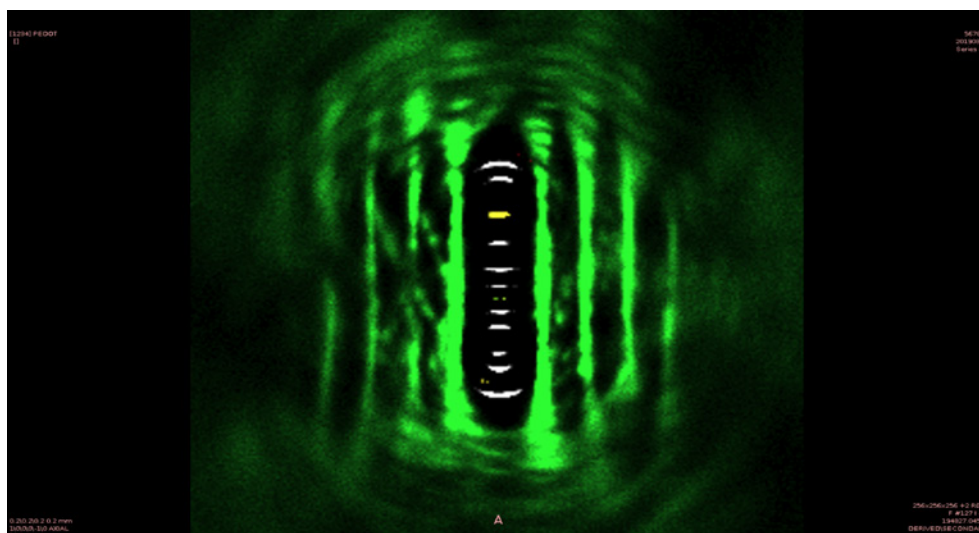


Figure 4.42: Computational tomography of PEDOT:PSS in the $x - z$ plane, with position along the y direction in $y = 25.2 \text{ \AA}$, for charged PEDOT ($2+$) and $T = 25 \text{ }^\circ\text{C}$.

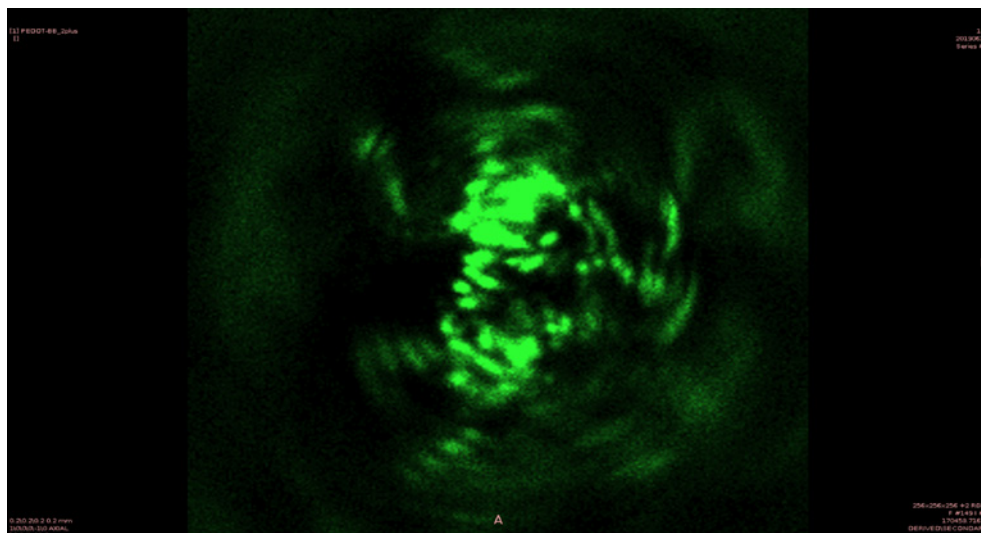


Figure 4.45: 3-D densities of Carbon atoms of PSS backbone around charged PEDOT, out of the $x - y$ plane (4.4 \AA under the plane of PEDOT).

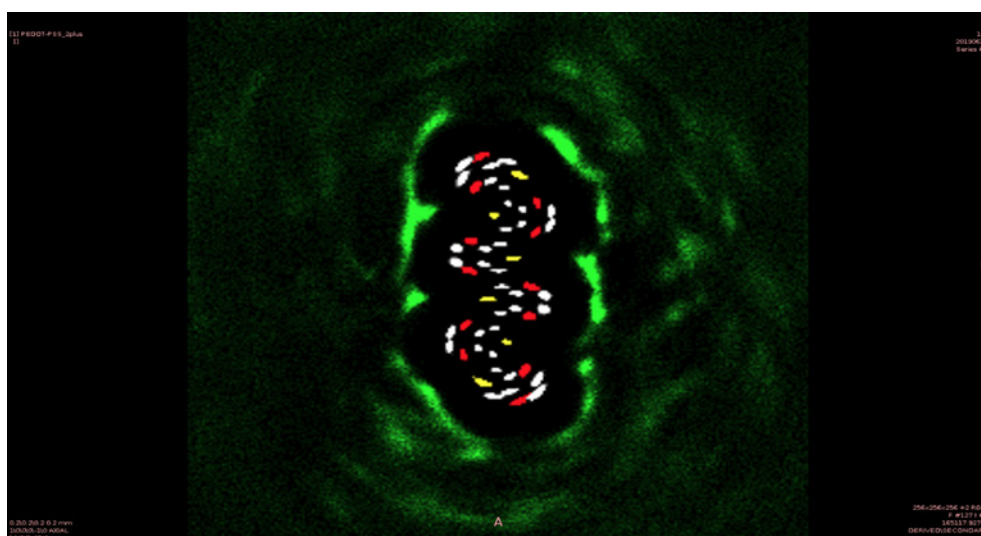


Figure 4.46: 3-D densities of Oxygen atoms of PSS around charged PEDOT, seen in $x - y$ plane.

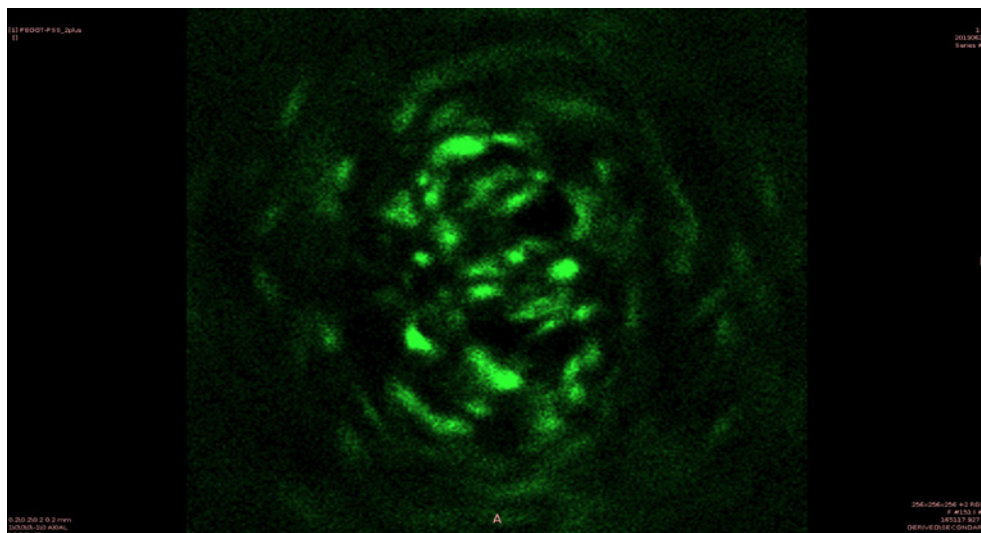


Figure 4.47: 3-D densities of Oxygen atoms of PSS around charged PEDOT, out of the $x - y$ plane (4.4 \AA under the plane of PEDOT).

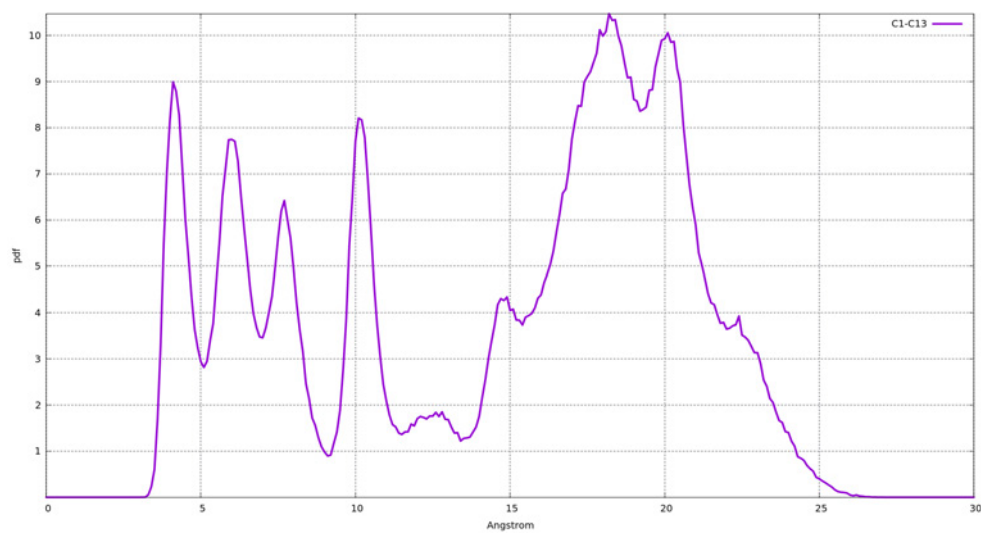


Figure 4.48: Probability density function of the distance between the Carbon atoms at the extremes of PSS for a system in the bulk phase at $T = 25 \text{ }^\circ\text{C}$ and charged PEDOT (2+).

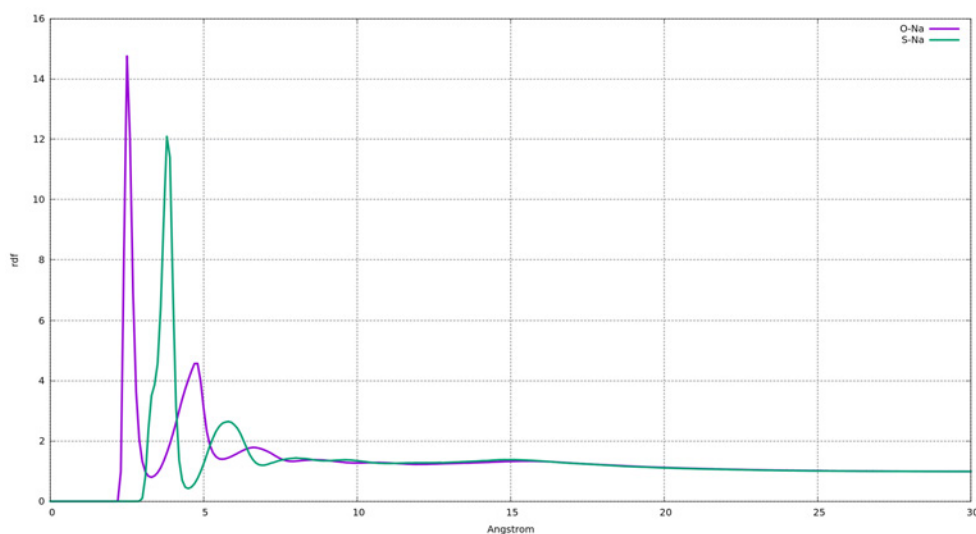


Figure 4.49: Radial distribution function of the distance between Oxygen and Sulfur atoms of the SO₃ group of PSS, and the Na⁺ counterions, for the bulk phase system at $T = 25$ °C and charged PEDOT (2+).

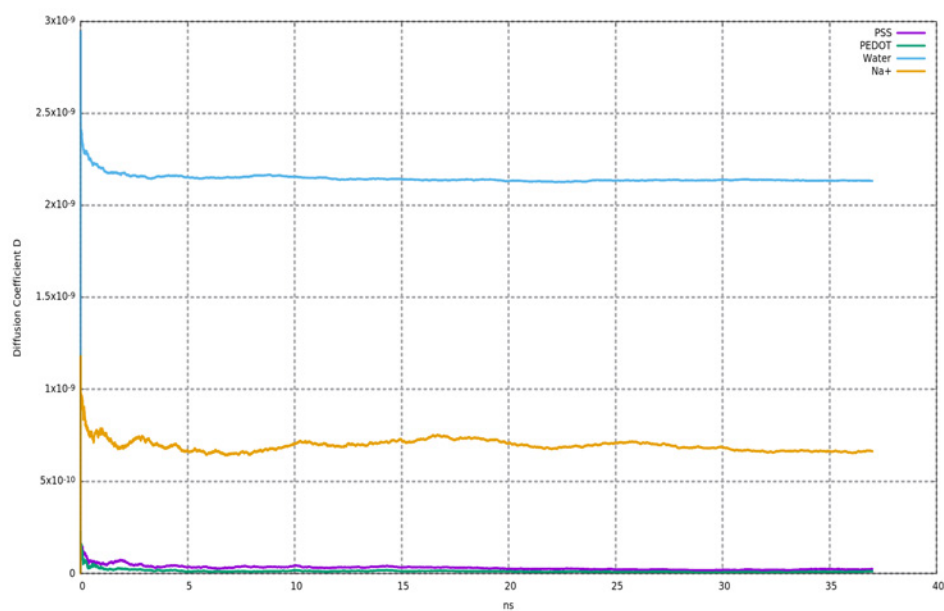


Figure 4.50: Diffusion Coefficients of the components of bulk system at $T = 25$ °C, with charged PEDOT.

4.3 PEDOT:PSS/SiO₂ interface

Once that we observed a good qualitative and quantitative agreement between our computational model for the bulk phase and experimental data, we went further simulating the polymer blend in presence of a rigid amorphous SiO₂ surface.

The interest about this configuration lies in the fact that several experiments have shown that layer thickness has a crucial impact on conducting polymer properties, indicating the differences between interfacial and bulk behavior.

Thereafter we worked with a non-cubic simulation box with a vacuum column of $\sim 20\text{-}25$ Å above the polymer blend in contact with the surface, to match with the Periodic Boundary Conditions.

180 PEDOT monomers and 360 PSS polymers are presents, together with 300 or 360 Na⁺ counterions whose number depends on the charge of PEDOT oligomers (to assure a globally electrically neutral system). This time, however, the number of water molecules is not constant as we considered (for the moment) the system at $T = 90$ °C and so the process of evaporation is involved.

At the beginning of the simulation the polymer blend was carefully brought closer to the surface, and then the target temperature of $T = 90$ °C was reached.

In the case of simulation with neutral PEDOT oligomers, that has been the first of the pair to be performed, the temperature has been increased gradually in order to find an optimal target temperature. In the case of simulation with charged PEDOT oligomers, the temperature has been set since the beginning at $T = 90$ °C and has not been changed anymore. This results in a bigger evaporation rate for the neutral system, compared with the charged one (Fig. 4.51).

An extra condition has been added to the AKMD program to simulate the evaporation process: namely, with an *if condition*, all the water molecules

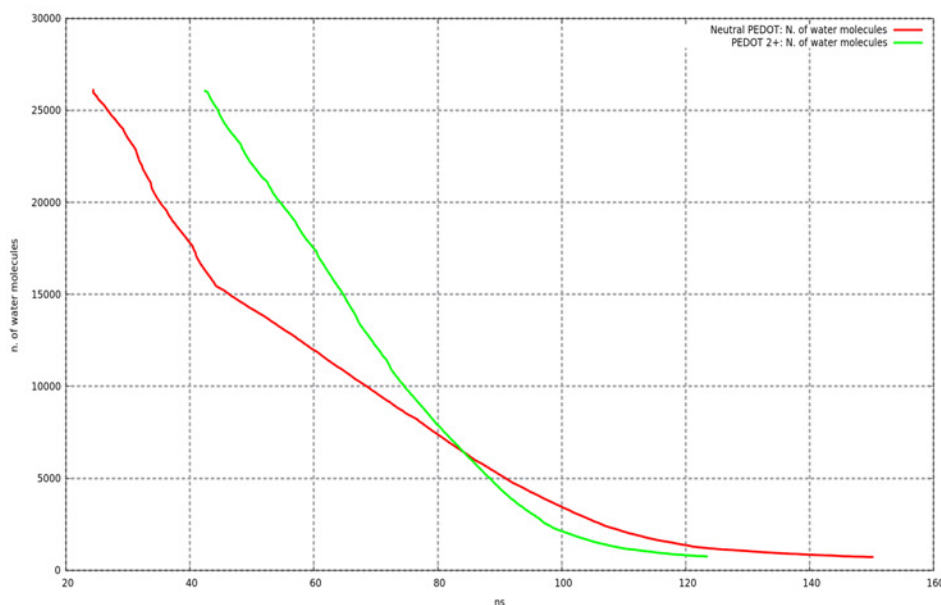


Figure 4.51: Time dependence of water molecules in both system at $T = 90$ °C.

whose z coordinate was bigger than a certain threshold have been deleted from the simulation every 50 fs (Fig. 4.52).

Simulations have been performed in a NVT ensemble with a time step of $\tau = 2$ fs: the equilibration of the systems required about 20 ns of simulation because of the heavy masses of the PEDOT oligomers and PSS polymers. The argumentation regarding the required time for the equilibration is the same done for the two systems in the bulk phase.

Water molecules have been modeled using the SPC/E model and the evolution of the whole system is determined by the bonded interactions (2-body harmonic interactions, 3-body angle bending and 4-body torsional interaction) and by the inter-molecular interactions, namely the electrostatic and van der Waals terms.

For this simulations the Diffusion Coefficients have not been analyzed. This

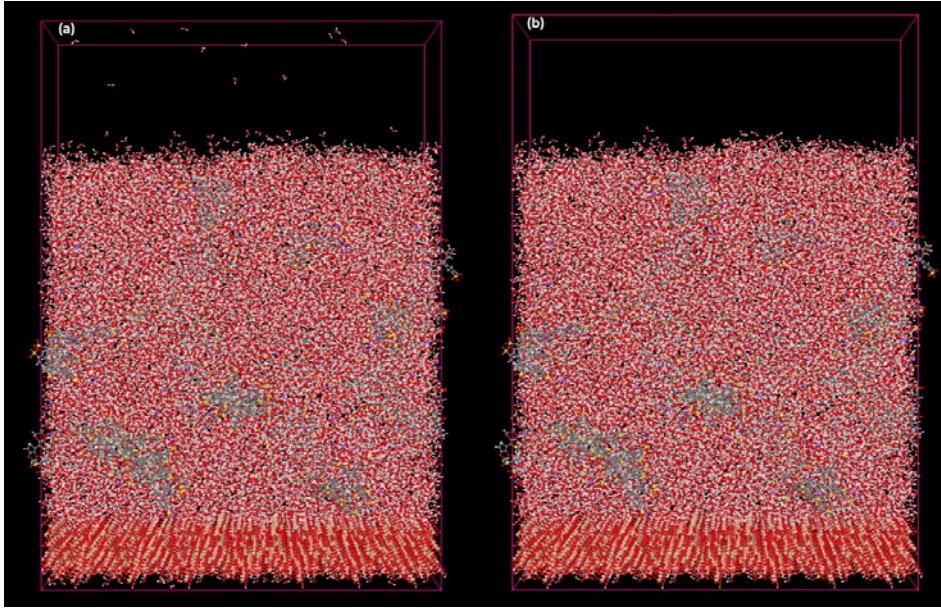


Figure 4.52: Evaporation process at $t = 42.433348$ ns (a) and $t = 42.433350$ ns (b). Note the disappearance of water molecules at the top of the simulation cell in Fig. b.

is because the system has a 2-dimensional “restricted” diffusion, due to the chosen configuration. Diffusion along z -axes is restricted by the glass surface and vacuum phase. So we have only diffusion in the $x - y$ plane.

Moreover, after the evaporation of water the system became too viscous and condensed on the glass.

Attention is hence focused on the analysis of the distribution of molecules of the 4 species during evaporation, as a function of z -coordinate and time.

Only heavy atoms have been considered during calculations, without taking into account Hydrogen atoms. The resulting graphs for the density probability are the normalized number of atoms of each species, as respect to the glass surface. Glass surface is placed at about 0, where the word “about” reflects the rough nature of this surface.

The initial height of the liquid, in both cases, was of about 106 Å; during evaporation of water, the height started to decrease.

4.3.1 System at $T = 90$ °C with neutral PEDOT

In the beginning of the evaporation for the neutral system, only water molecules are presents on the top of the liquid. With the continuation of the simulation, in particular at about 60-80 ns (Figg. 4.59, Figg. 4.60, Figg. 4.61), the number of water molecules decreases because of the high temperature, and two peaks of the density function appear due to this molecules; the peaks in particular are placed on the top of the layer and near the glass surface.

In the advanced stage of the evaporation, in the range of 100-150 ns, water molecules remains on the glass surface and so their density decrease on the top of the layer.

Finally, at around 140-150 ns (Figg. 4.66, 4.67), almost every molecule of water is evaporated (only ~ 700 are left). Between the glass surface and PEDOT oligomers, there are some water molecules and PSS polymers.

The conclusion is that, when the process of sediment is completed, neutral PEDOT has no direct contact with the glass surface (Fig. 4.67).

Hereafter are reported the results regarding the Density Probability of the components of the system, as a function of the distance respect to the glass surface.

The images are ordered following the evaporation process, and so they span from 20 ns to 150 ns of simulation. Each images is obtained by considering the mean value over a time interval of 9.99 ns (e.g. from 20.00 ns to 29.99 ns, from 30.00 ns to 39.99 ns etc.).

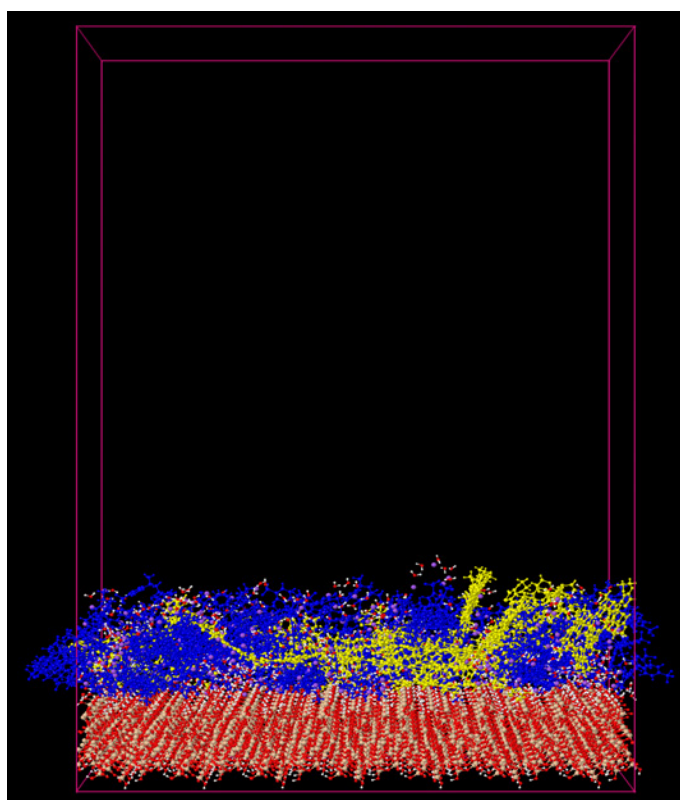


Figure 4.53: Front view of the PEDOT:PSS system in presence of a glass surface at $T = 90\text{ }^{\circ}\text{C}$, with neutral PEDOT, at the end of the water evaporation process. Yellows are PEDOT oligomers and blue are PSS polymers.

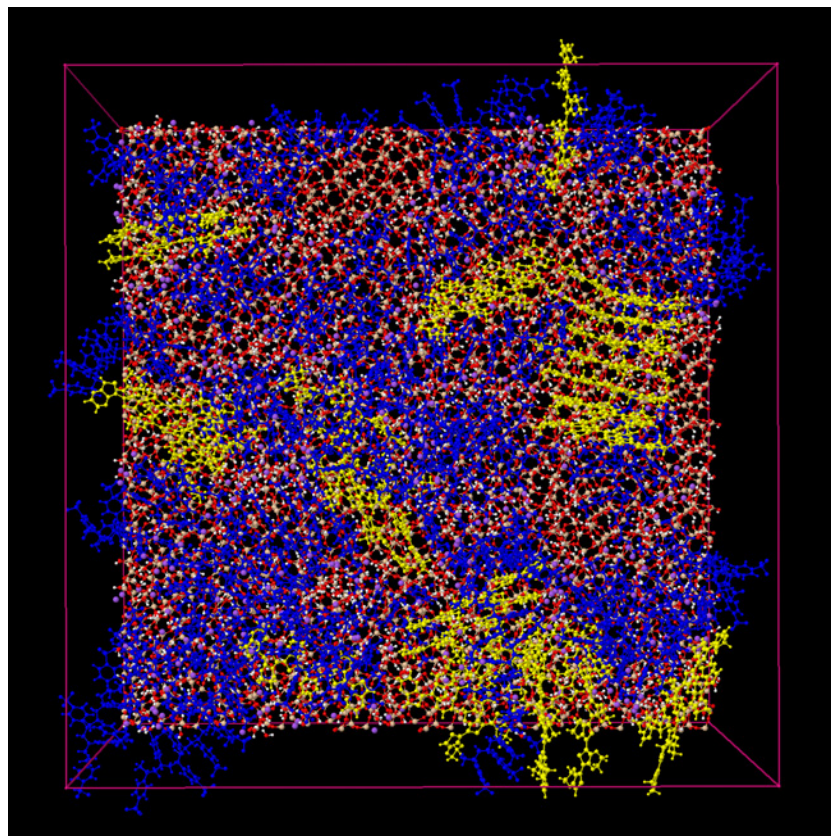


Figure 4.54: Top of view of the PEDOT:PSS system in presence of a glass surface at $T = 90$ °C, with neutral PEDOT, at the end of the water evaporation process. Yellow molecules are PEDOT oligomers and blue molecules are PSS polymers. Note also the stacking ordering of PEDOT.

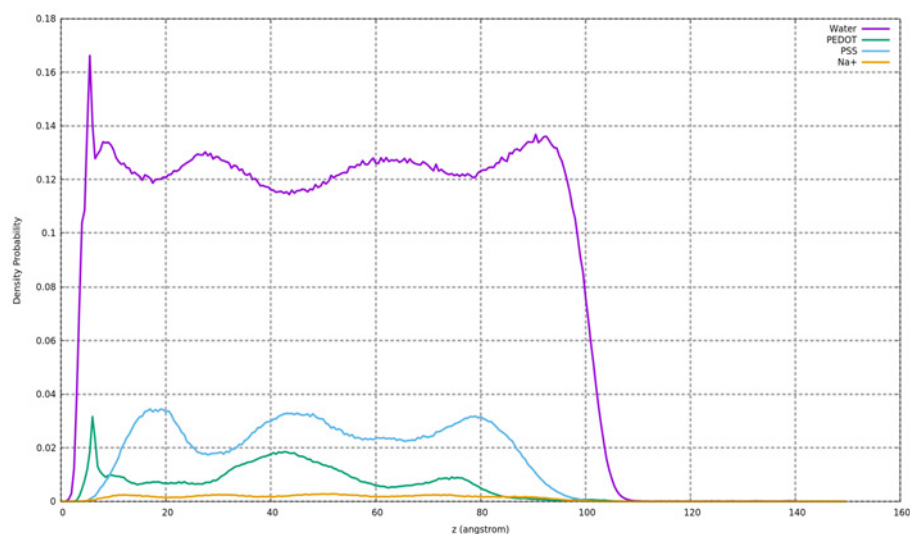


Figure 4.55: Distribution of components of the system, as a function of the z -coordinate. Data are obtained by considering the average values for the simulation time among 20.00 ns and 29.99 ns.

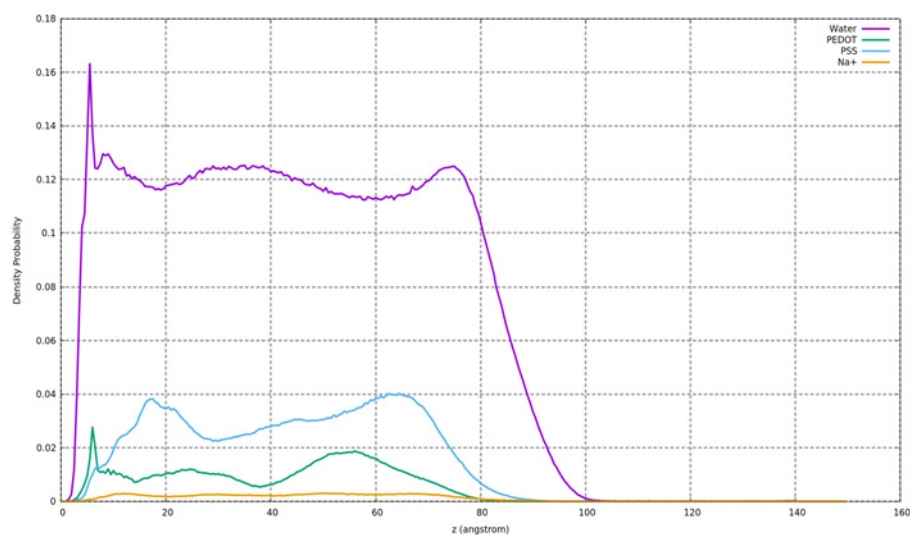


Figure 4.56: Distribution of components of the system, as a function of the z -coordinate. Data are obtained by considering the average values for the simulation time among 30.00 ns and 39.99 ns.

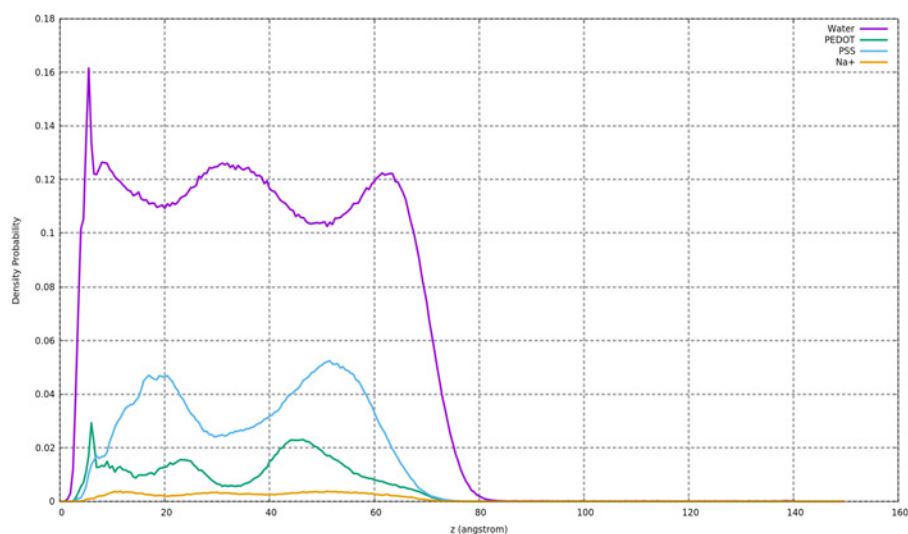


Figure 4.57: Distribution of components of the system, as a function of the z -coordinate. Data are obtained by considering the average values for the simulation time among 40.00 ns and 49.99 ns.

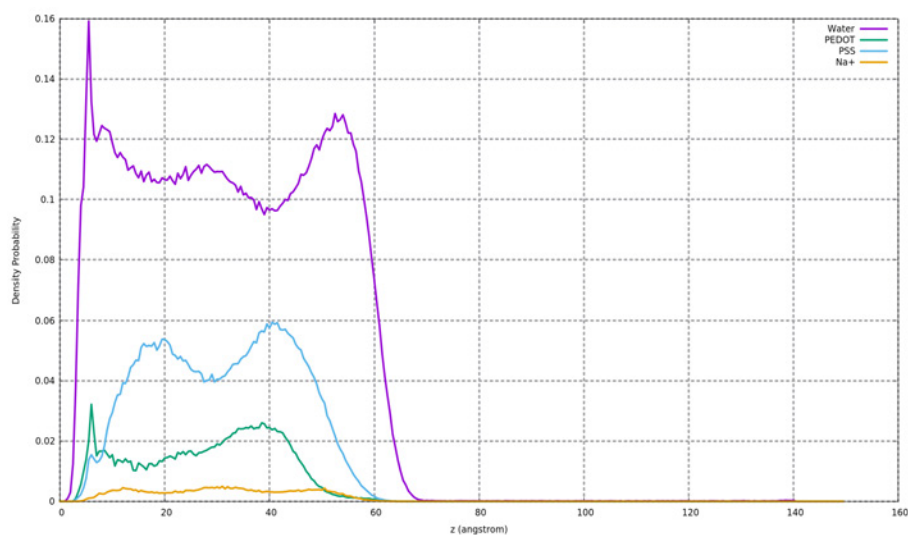


Figure 4.58: Distribution of components of the system, as a function of the z -coordinate. Data are obtained by considering the average values for the simulation time among 50.00 ns and 59.99 ns.

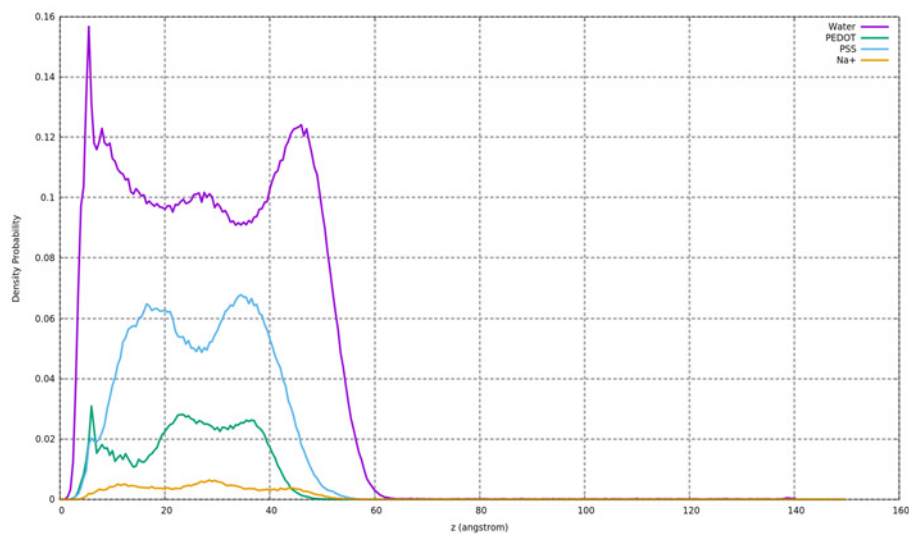


Figure 4.59: Distribution of components of the system, as a function of the z -coordinate. Data are obtained by considering the average values for the simulation time among 60.00 ns and 69.99 ns.

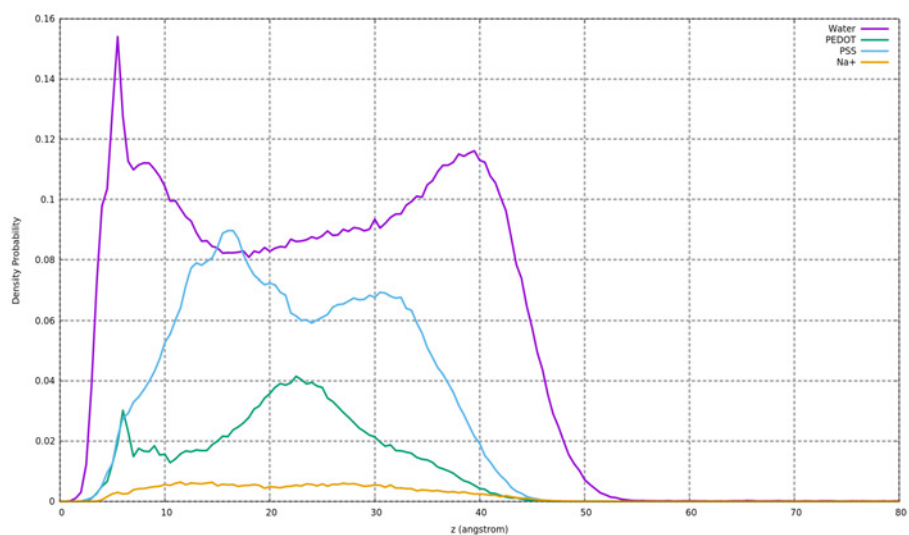


Figure 4.60: Distribution of components of the system, as a function of the z -coordinate. Data are obtained by considering the average values for the simulation time among 70.00 ns and 79.99 ns.

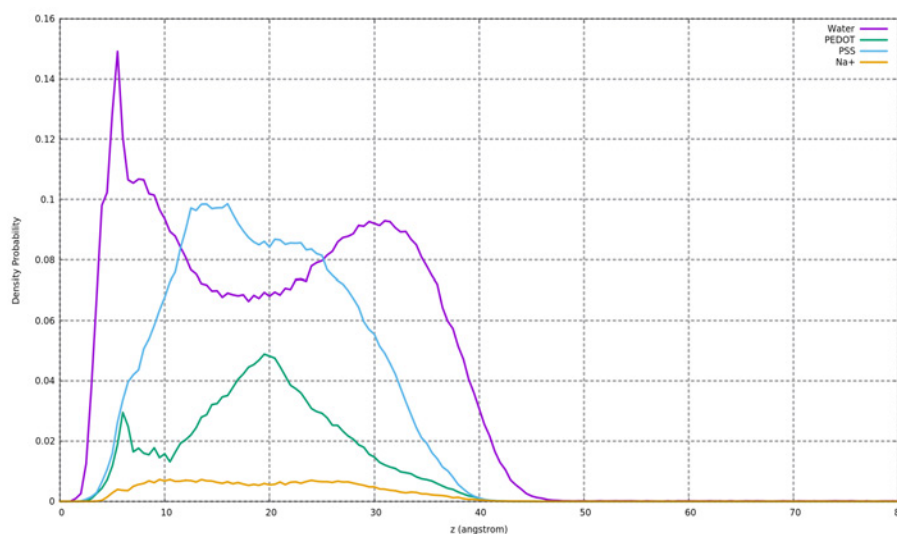


Figure 4.61: Distribution of components of the system, as a function of the z -coordinate. Data are obtained by considering the average values for the simulation time among 80.00 ns and 89.99 ns.

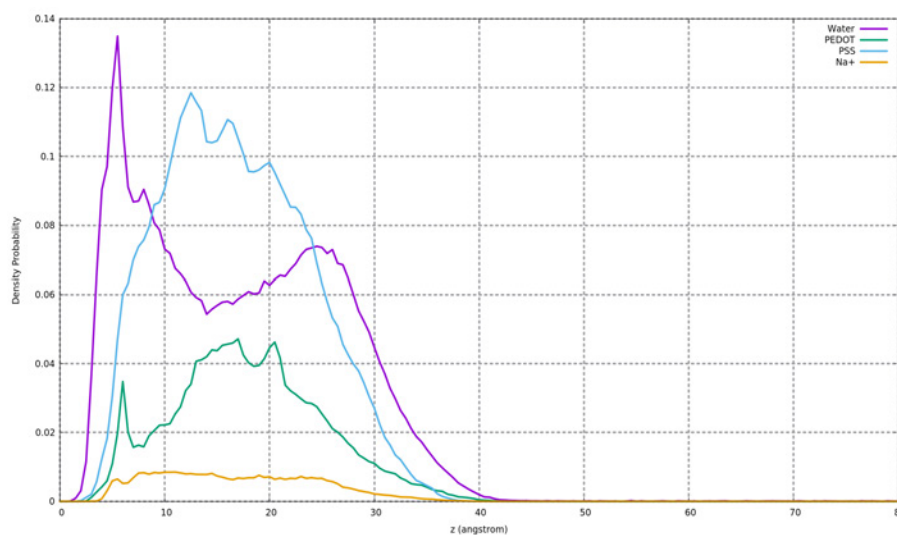


Figure 4.62: Distribution of components of the system, as a function of the z -coordinate. Data are obtained by considering the average values for the simulation time among 90.00 ns and 99.99 ns.

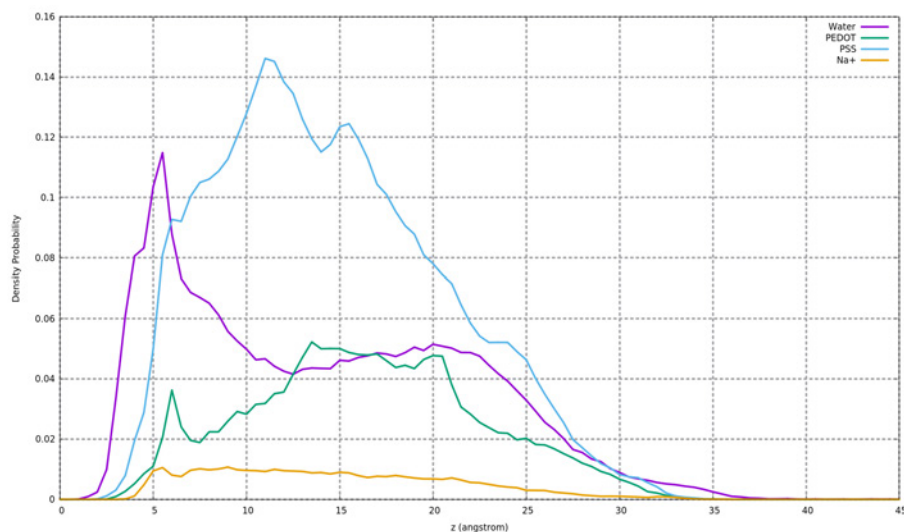


Figure 4.63: Distribution of components of the system, as a function of the z -coordinate. Data are obtained by considering the average values for the simulation time among 100.00 ns and 109.99 ns.

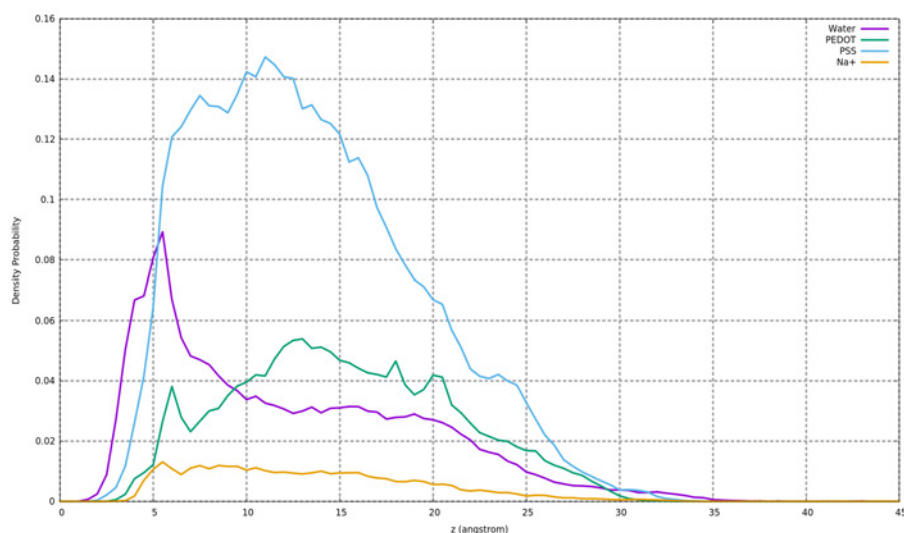


Figure 4.64: Distribution of components of the system, as a function of the z -coordinate. Data are obtained by considering the average values for the simulation time among 110.00 ns and 119.99 ns.

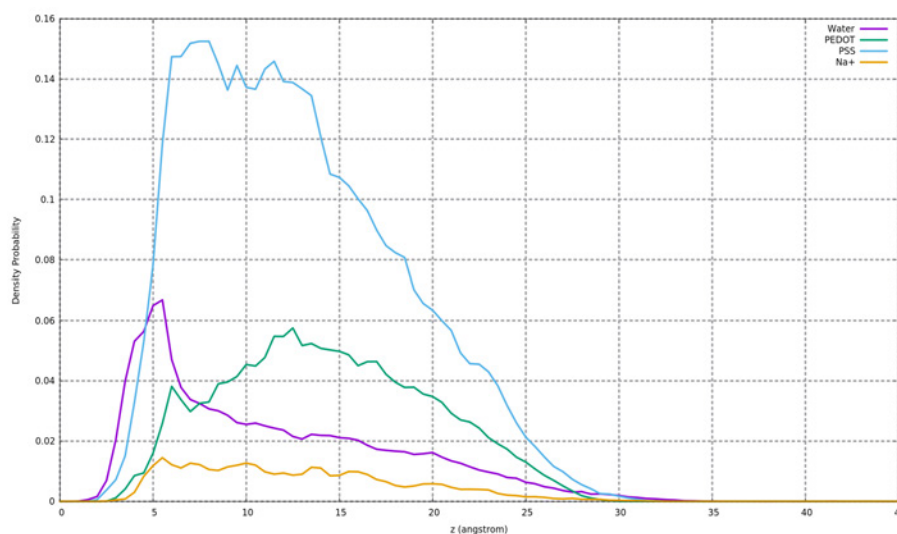


Figure 4.65: Distribution of components of the system, as a function of the z -coordinate. Data are obtained by considering the average values for the simulation time among 120.00 ns and 129.99 ns.

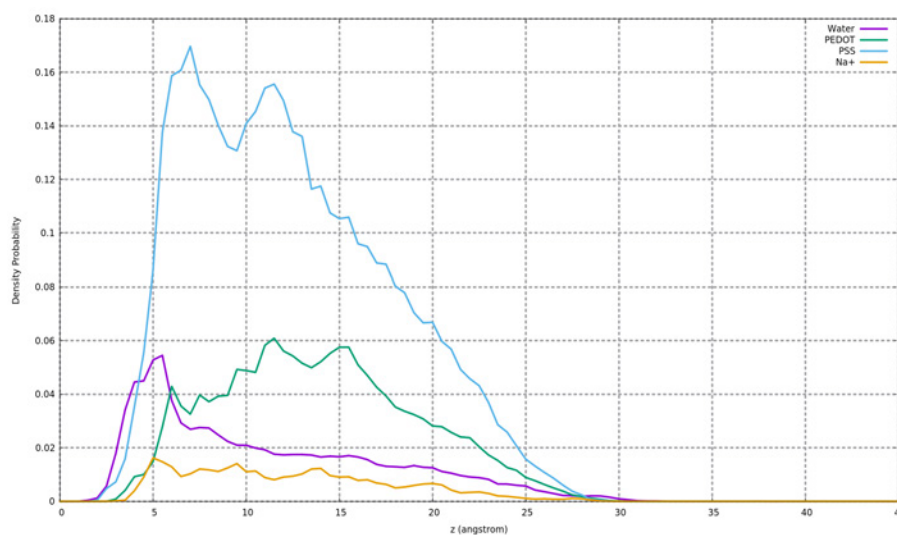


Figure 4.66: Distribution of components of the system, as a function of the z -coordinate. Data are obtained by considering the average values for the simulation time among 130.00 ns and 139.99 ns.

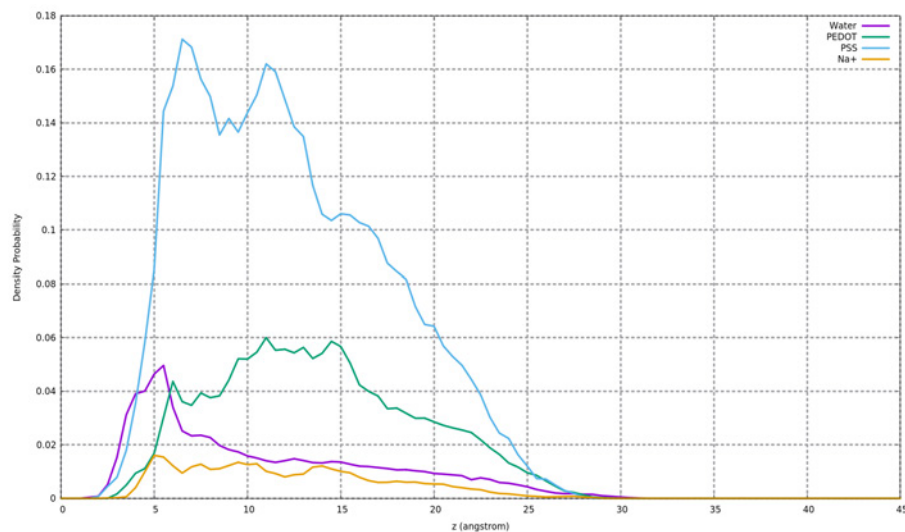


Figure 4.67: Distribution of components of the system, as a function of the z -coordinate. Data are obtained by considering the average values for the simulation time among 140.00 ns and 149.99 ns.

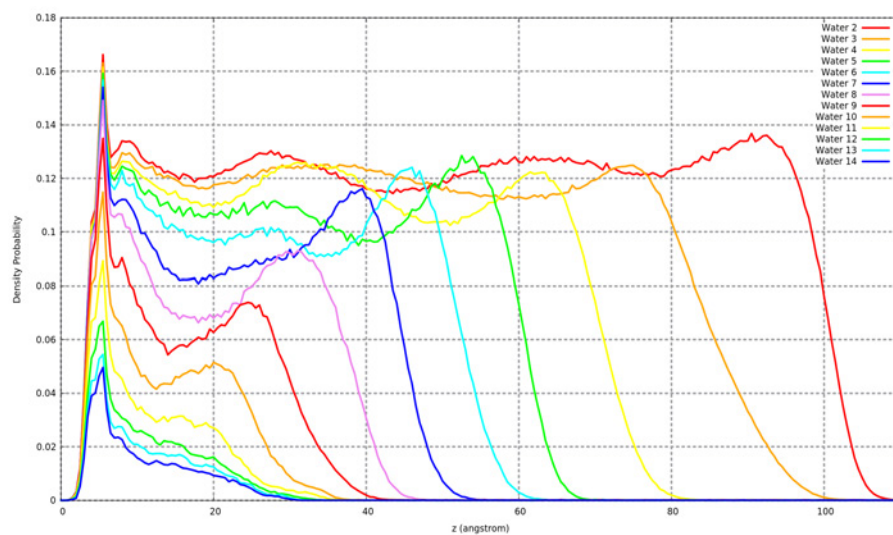


Figure 4.68: Water Density Probability during evaporation process, among 20.00 ns and 149.99 ns.

4.3.2 System at $T = 90$ °C with PEDOT 2+

Also in the case of PEDOT 2+ the whole evaporation process has been observed, starting from 40 ns until 123.413 ns, where only ~ 750 water molecules remained in the system (Fig. 4.69, 4.70). During this simulation, the rate of evaporation for water molecules was greater than that for system with neutral PEDOT oligomers (in presence of a surface, at $T = 90$ °C), as in this case we set since the beginning the target temperature of $T = 90$ °C.

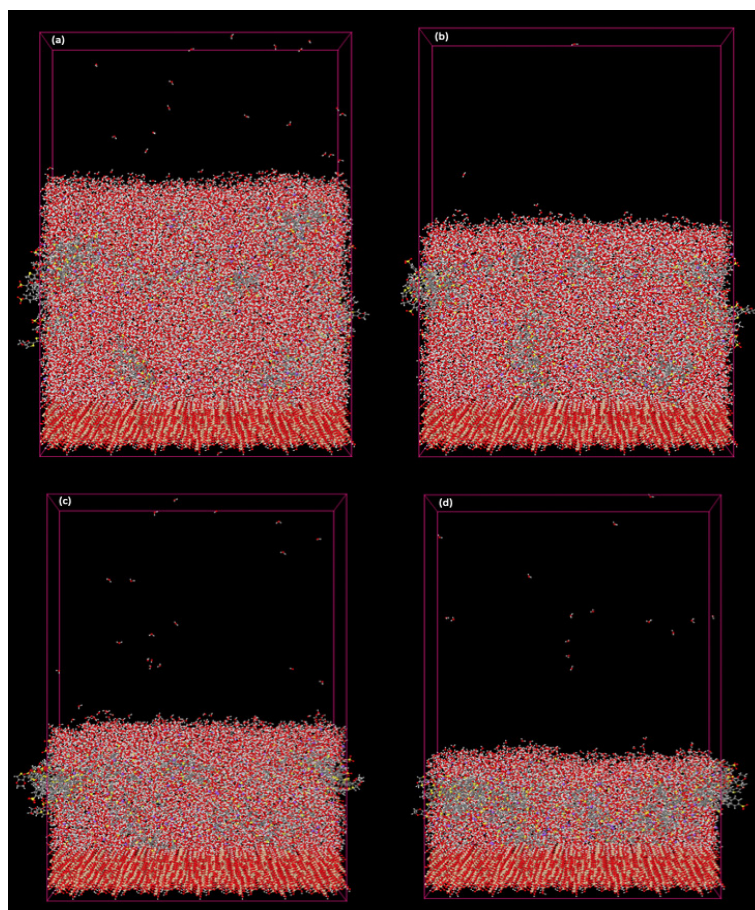


Figure 4.69: Evaporation of water in system with charged PEDOT 2+ at a) 53.4 ns b) 63.4 ns c) 73.4 ns d) 83.4 ns.

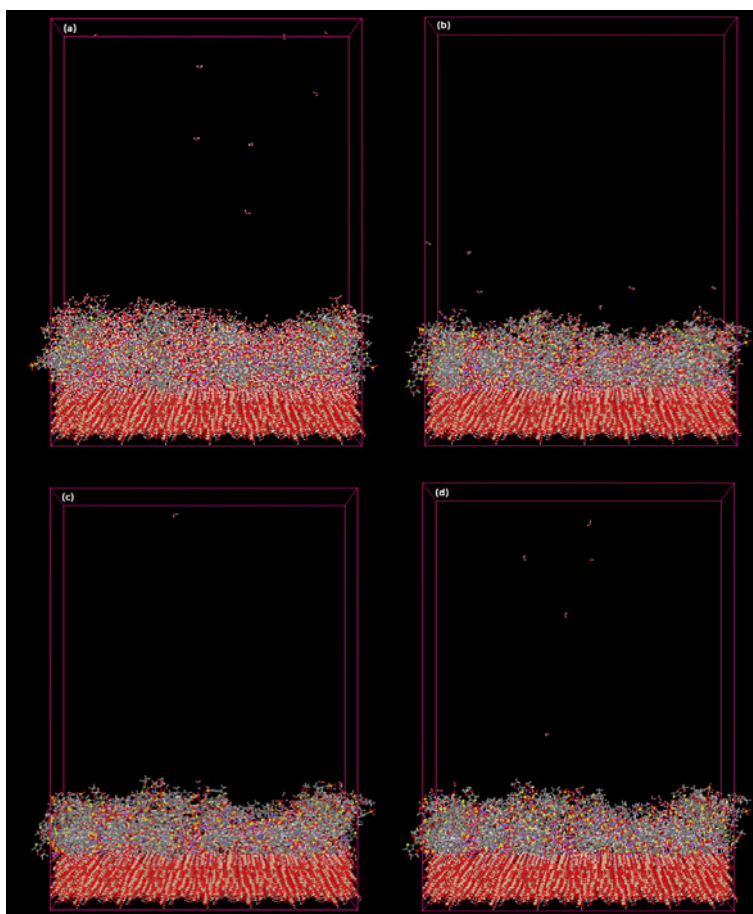


Figure 4.70: Evaporation of water in system with charged PEDOT 2+ at a) 93.4 ns b) 103.4 ns c) 113.4 ns d) 123.4 ns.

We can notice that at 70-79 ns both PEDOT and PSS float up, as can be seen from the peak between 20-40 Å. The distribution of PEDOT is shifted of $\sim 3-4$ Å for the 2+ charged one, respect to the distribution of neutral PEDOT.

This can be especially noted comparing Figg. 4.61 and 4.75, where the distributions of water are almost identical. A direct comparison is given in Fig. 4.81.

The next images are ordered following the evaporation process, and they

span from 40.00 ns to 123.413 ns of simulation. Each images is obtained by considering the mean value over a time interval of 9.99 ns (e.g. from 20.00 ns to 29.99 ns, from 30.00 ns to 39.99 ns etc.).

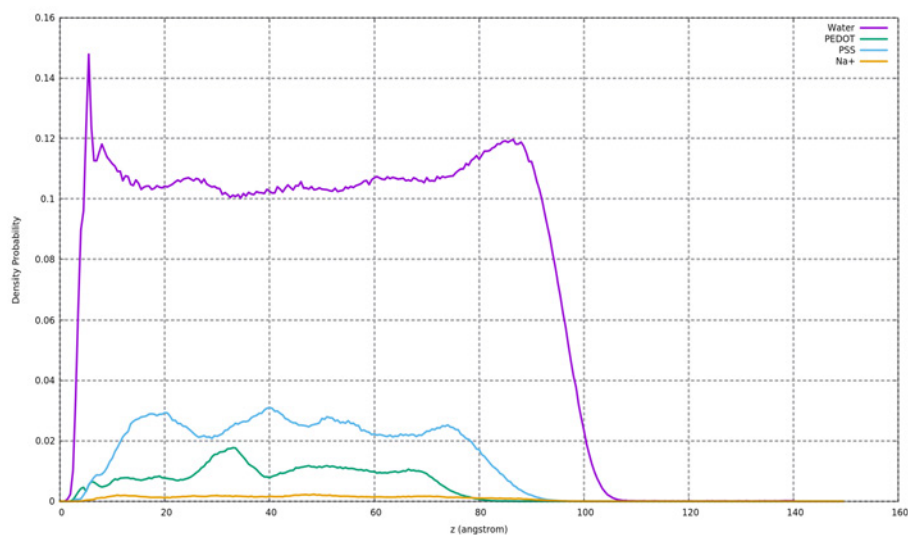


Figure 4.71: Distribution of components of the system, as a function of the z -coordinate. Data are obtained by considering the average values for the simulation time among 40.00 ns and 49.99 ns.

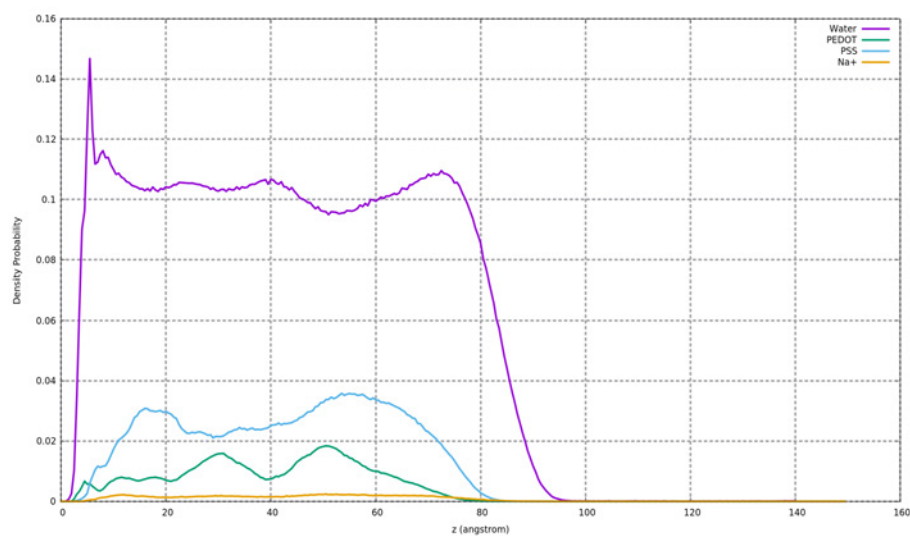


Figure 4.72: Distribution of components of the system, as a function of the z -coordinate. Data are obtained by considering the average values for the simulation time among 50.00 ns and 59.99 ns.

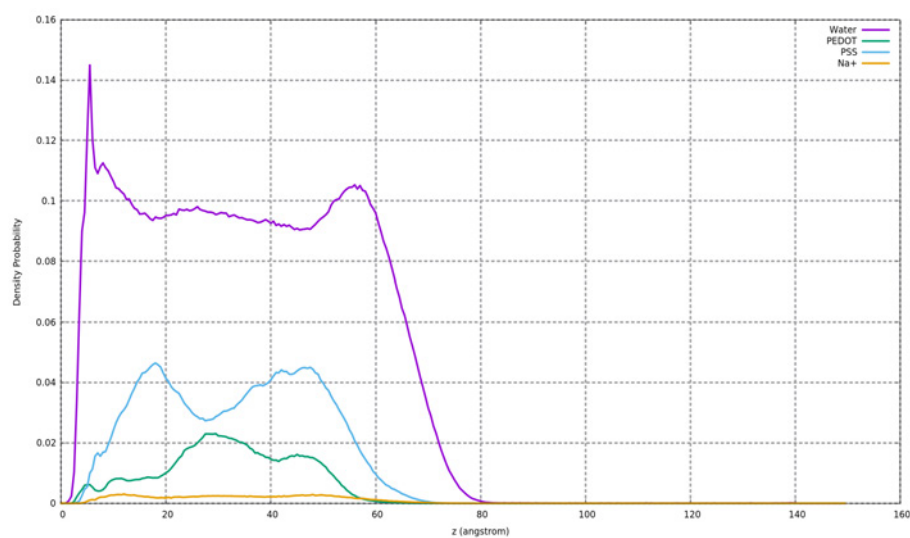


Figure 4.73: Distribution of components of the system, as a function of the z -coordinate. Data are obtained by considering the average values for the simulation time among 60.00 ns and 69.99 ns.

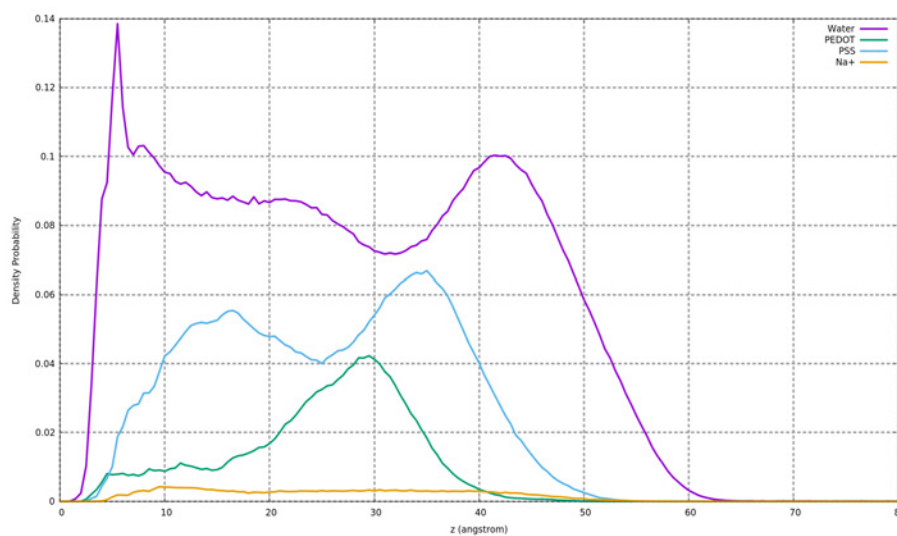


Figure 4.74: Distribution of components of the system, as a function of the z -coordinate. Data are obtained by considering the average values for the simulation time among 70.00 ns and 79.99 ns.

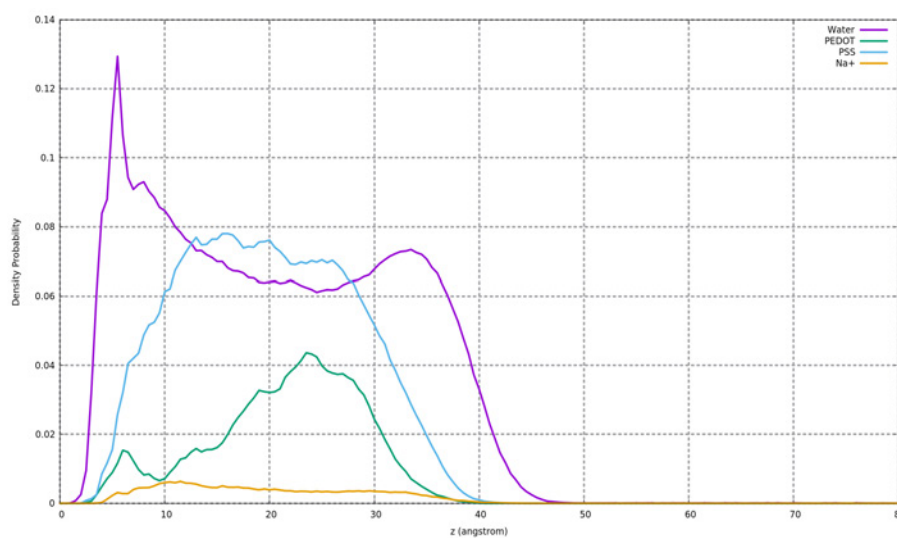


Figure 4.75: Distribution of components of the system, as a function of the z -coordinate. Data are obtained by considering the average values for the simulation time among 80.00 ns and 89.99 ns.

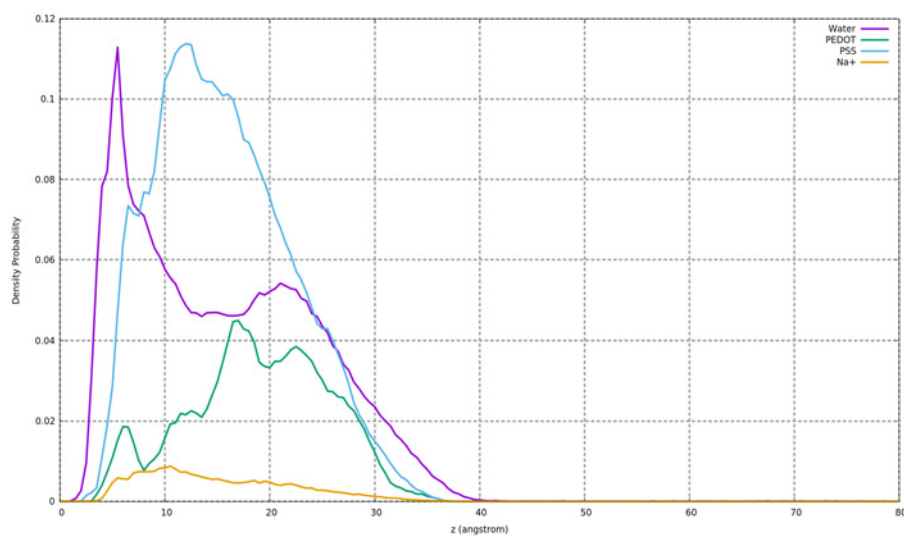


Figure 4.76: Distribution of components of the system, as a function of the z -coordinate. Data are obtained by considering the average values for the simulation time among 90.00 ns and 99.99 ns.

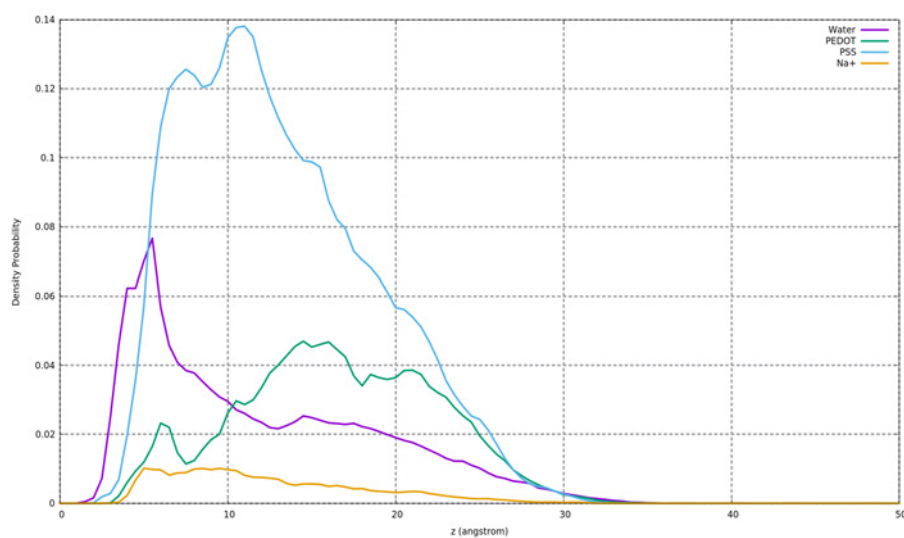


Figure 4.77: Distribution of components of the system, as a function of the z -coordinate. Data are obtained by considering the average values for the simulation time among 100.00 ns and 109.99 ns.

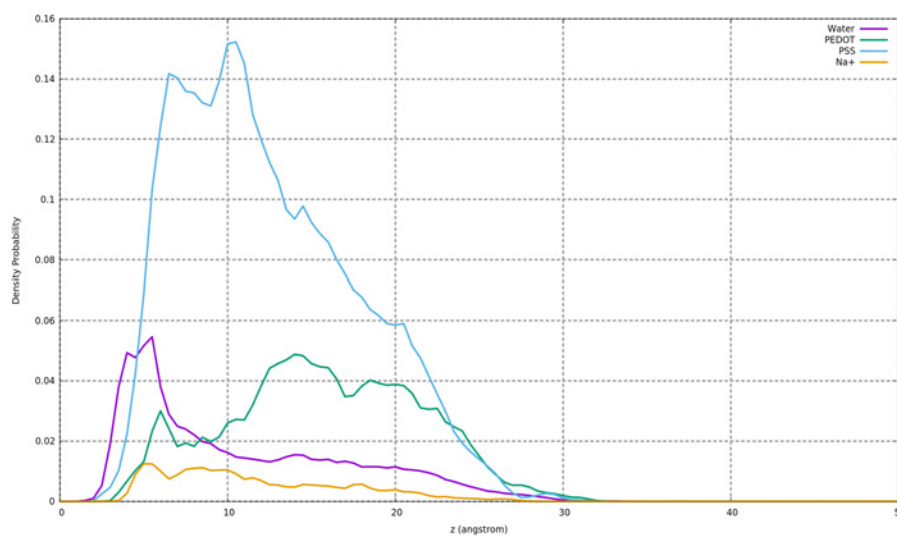


Figure 4.78: Distribution of components of the system, as a function of the z -coordinate. Data are obtained by considering the average values for the simulation time among 110.00 ns and 199.99 ns.

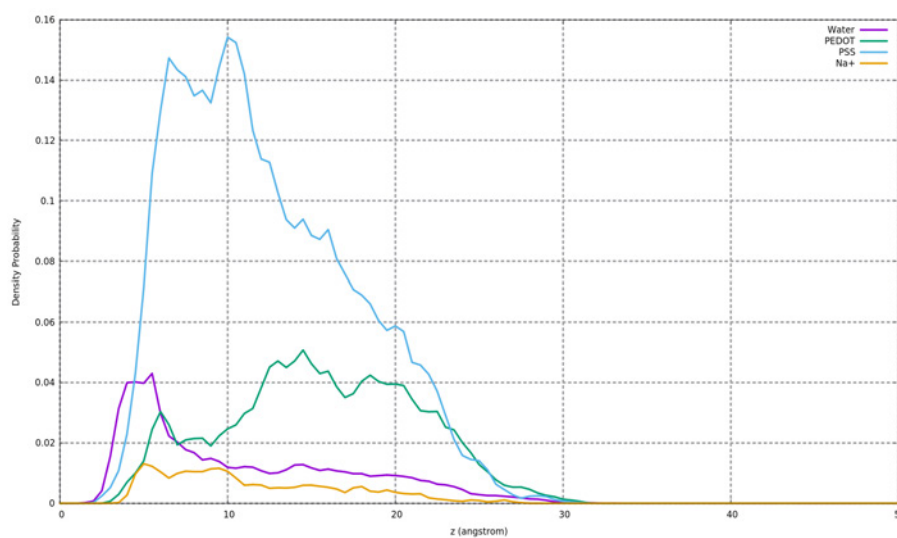


Figure 4.79: Distribution of components of the system, as a function of the z -coordinate. Data are obtained by considering the average values for the simulation time among 120.00 ns and 123.413 ns.

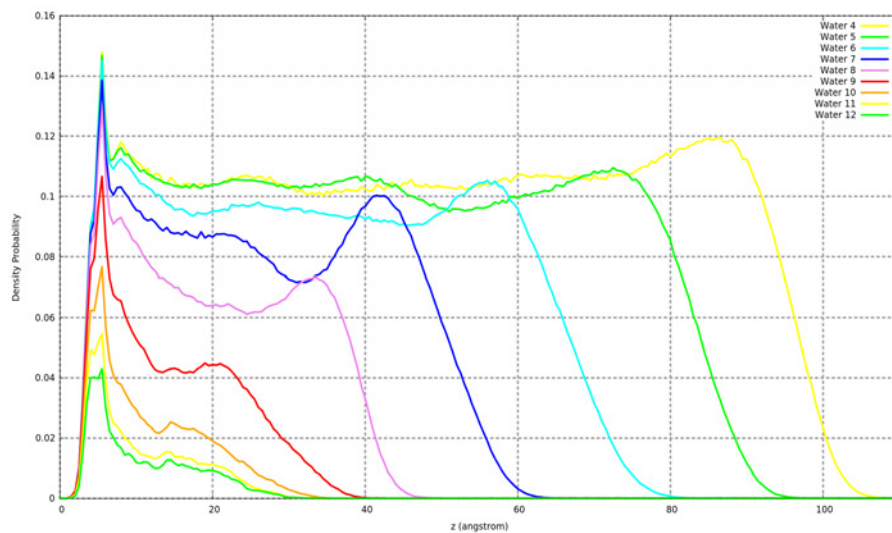


Figure 4.80: Water Density Probability during evaporation process, among 40.00 ns and 123.413 ns.

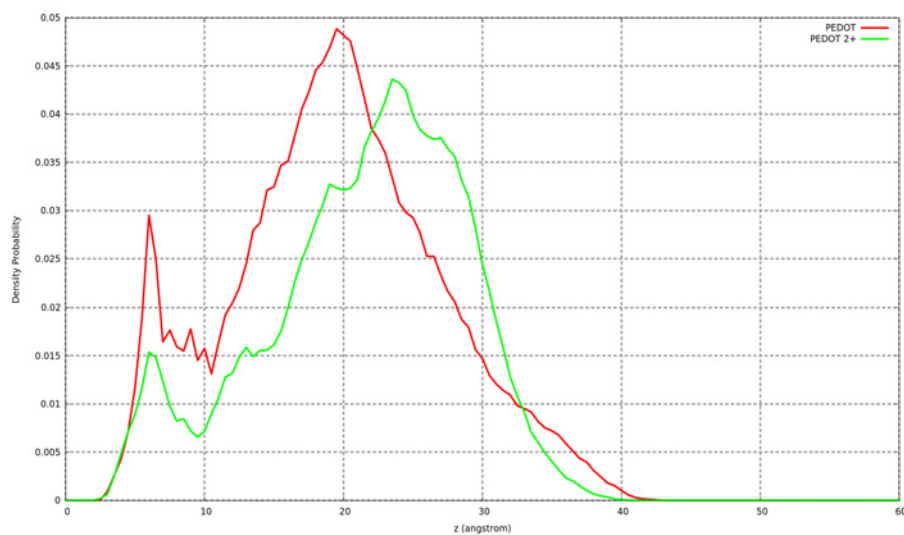


Figure 4.81: Comparison of Density Probability among PEDOT and PEDOT 2+ after ~ 80 ns of simulation.

Chapter 5

Conclusions

In this work we performed Molecular Dynamics Simulations to study, from a computational point of view, the behavior of an organic semiconductor based on a polymer blend, namely poly(3,4-ethylenedioxythiophene):poly(styrene sulfonate) (PEDOT:PSS). The interest of this work lies in the fundamental importance of this material in the field of organic conducting polymers, being the material of choice for many applications and being by far one of the most used in bioelectronics [34]. Several experimental investigations of its morphology and electronic properties have been reported in the literature [104][105][106][107][108][109]. However, these studies are limited due to difficulty to obtain atomistic information about the materials structure, due to its disordered and nano-crystalline character. A consistent theoretical description of the structure has not been presented yet, and the methods of Molecular Dynamics appeared to be suitable to provide atomistic structures of the polymer blend, giving access to structural models of such composite and overcoming the limitations.

In particular have been investigated the structural models of PEDOT:PSS in different physical conditions, and we analyzed the relationship between the structure and the properties of the system.

Several simulations have been considered to extend the comparison with ex-

perimental results and to understand the influence of certain parameters on the dynamics of the material.

Much attention has been paid in the choice of the initial configuration, as it strongly influence the evolution of the system.

The starting structure geometries have been generated by creating atactic PSS polymers and PEDOT oligomers, and choosing the most suitable Force Field. Also the optimized geometries and the charge distribution have been calculated.

After choosing the dimensions of the simulation box (i.e. the number of total atoms involved in the calculations) and the relative amount of the different components of the system, the initial configurations of the systems have been made to evolve, paying attention that the simulation time was long enough to ensure a proper equilibration of the system.

Finally data have been collected from the analysis of the trajectories, that are the output files of the simulations.

For simulations performed in bulk phase (Section 4.2) we calculated the Diffusion Coefficients for the different components of the system, the bending of PSS polymers through the pdf function of the distance between the Carbon atoms at the ends of the chain and equilibrium distances of the Na^+ cations from the SO_3 groups of PSS.

Through the use of MRI (Magnetic Resonance Imaging) software we visualized the local structures of the system; in particular we focused on the intra-molecular interactions of PEDOT oligomers and on their aggregation in lamellar structures. The interactions among PEDOT oligomers and PSS polymers have been studied as well, taking into account the 3-dimensional densities of Carbon atoms and Oxygen atoms of PSS (belonging to the backbone, to the phenyl rings and to the SO_3 group) around PEDOT.

From the analysis of the Diffusion Coefficients it turns out that the presence of a positive charge on PEDOT influences quite strongly the dynamics

of the system. The values of D for both PEDOT and PSS in the system with charged PEDOT are 3 times smaller than those in the system with neutral PEDOT (respectively 1×10^{-11} m²/s and 2×10^{-11} m²/s, compared with 3×10^{-11} m²/s and 6×10^{-11} m²/s). This is a consequence of the stronger electrostatic interaction among the two components.

The Diffusion Coefficient instead is only slightly influenced by the presence of this charge (6.6×10^{-10} m²/s, compared with 8×10^{-10} m²/s), while the Diffusion Coefficient for water molecules is not influenced at all.

The bending of PSS polymers shows two different behaviors, as some of them are in contact or at least relatively very near to the PEDOT lamellar structures, while others are not.

Those that are approaching the PEDOT stacks will inevitably be affected by a stronger and directional/non balanced interaction, resulting in an almost non bended shape. This can be seen from the peak on the right of Figg. 4.35, 4.48.

Those that are not approaching the PEDOT stacks will be influenced by random/non directional forces and they will be more free to bend (peaks on the left of Figg. 4.35, 4.48).

For a complete statistical analysis we would need a greater number of polymers, as we are far from the large N limit, but we can conclude that the freely jointed chain model cannot work in this framework, especially for those PSS that are approaching the PEDOT stacks.

The observed pdf results from the balancing of intra and inter-molecular interactions, which give rise to some equilibrium configurations, and with the charge upon PEDOT oligomers that induce a slightly more ordered configurations (see peaks on the left in Figg. 4.35 and 4.48).

Equilibrium distances of Na⁺ counterions from the SO₃ groups is not influenced by the presence of charges on PEDOT (Figg. 4.17, 4.18).

The only difference is given by the mean distance of the Na⁺ counterions

respect to the Oxygens and the Sulfur atoms of SO₃ groups: Oxygen atoms are more peripheral in this structure, hence they appear to be closer to the counterions.

From the visualization of the local structures we obtained further information about the influence of the charged PEDOT on the system.

Stacking of charged PEDOT is bigger in volume than the one of uncharged PEDOT, as bigger lamellar structures arise. The distance among the planes however remains the same, with a mean value of 3.5-3.6 Å. This is due to the relative big size of PEDOT oligomers.

The charge on the PEDOT oligomers influences quantitatively but not qualitatively the behavior of Oxygen and Carbon atoms of PSS around PEDOT. Oxygen atoms are essentially located at the edge of PEDOT oligomers, while Carbon atoms are essentially located under the oligomers.

Charged PEDOT results in a stronger interaction with PSS, and hence in a brighter signal, compared with the uncharged one.

Also the distributions of Carbon atoms of phenyl rings of PSS around PEDOT have been calculated. They show us that, in the system with charged PEDOT oligomers, the contact of phenyl rings with PEDOT in the plane of the oligomer is more emphasized.

For the simulations in presence of a glass surface we focused on the evaporation process of water, considering a temperature $T = 90$ °C, both for charged and uncharged PEDOT.

Diffusion Coefficients instead have not been considered, because of the 2-Dimensional final conformation (at the end of the evaporation process) of the system and because of the big viscosity due to the almost total lack of water molecules at the end.

The (almost) complete evaporation of water molecules has been reached after ~ 140 ns of simulation for the system with uncharged PEDOT.

System with charged PEDOT oligomers (in presence of the glass surface)

has been simulated up to ~ 123 ns, enough time to observe again a complete evaporation process, with just ~ 750 water molecules left in the system.

In both cases the initial height of the liquid column was of ~ 106 Å, with this value becoming smaller and smaller as the evaporation proceed. Moreover, after ~ 50 ns of simulation, the number of water molecules decrease enough and two peaks appears in the density function: one on the top of the layer and the other on the glass surface. Both PEDOT and PSS float up in this simulation interval, and in the charged system PEDOT oligomers appear to float higher than ones in uncharged system. This results in a shifted distribution of charged PEDOT, of about 3-4 Å to the right, with respect to the distribution of uncharged PEDOT (Fig. 4.81).

Again, for both systems at $T = 90$ °C, we can conclude that at the end of the evaporation processes there are some water molecules ($\sim 700/750$) and PSS polymers (Figg. 4.67, 4.79) between the glass surface and PEDOT oligomers. This means that neutral PEDOT has no direct contact with the glass surface.

Evaporation process appear to be faster in the case of system with charged PEDOT oligomers, but this is only because for this simulation we already knew the target temperature, so we set it already from the beginning of the simulation to a fixed value.

In all four simulations here proposed we also observe a phase separation in PEDOT-rich regions and PSS-rich regions, where we have many ~ 2 nm large lamellar structures of PEDOT oligomers, surrounded by PSS-rich phase. This is in accordance with experimental findings.

Drawing the conclusions, we have found that the use of Molecular Dynamics methods has allowed us to successfully access the structural models of this polymer blend. The obtained data can be used to be compared with experimental data or other computer simulations, but also can be used in view of subsequent calculations. Starting from this point other experimentally

accessible parameters can be obtained via Molecular Dynamics simulations, such as correlations functions, electronic properties, mechanical properties and swelling properties.

Because of the huge number of atoms/molecules involved in the simulations, calculations are quite heavy and require some time to create trajectories files (~ 0.75 ns/day) and, because of the big masses of the involved polymers, also the required time to equilibrate the systems is relatively big (more than 2 month of calculations).

Future work hence has already been planned to go further with the discussion and to gain a deeper understanding about the involved phenomena.

It will be interesting to exploit all the possible combinations among the parameters that we considered in this thesis (charges on PEDOT oligomers, different temperatures and presence of a surface) to continuing study the relationships that exist among them and the output results.

PEDOT:PSS is often found in presence of a surface, that is not only made by glass: this is why is of interest to study the system also in presence of other kinds of surfaces. In particular we started to create an ABA Carbon surface, with Bernal stacking order, for future calculations.

Finally, probably, considering a flexible surface rather than a rigid one will lead to slightly different quantitative results, and this will be part too of the planned future works.

Bibliography

- [1] Adamczyk Z., Jachimska B., Jasiński T., Warszyński P., Wasilewska M., *Structure of poly (sodium 4-styrenesulfonate) (PSS) in electrolyte solutions: Theoretical modeling and measurements*, Colloids and Surfaces A: Physicochemical and Engineering Aspects, Colloid and Surface Science for Nanotechnology, 2009.
- [2] Adams J. B., Rockett A., Kieffer J., Xu W., Nomura M., Kilian K. A., Richards D. F., Ramprasad R., *Atomic-Level Computer Simulation*, Journal of Nuclear Materials 216 265-274, 1994.
- [3] Alemán Carlos, Armelin Elaine, Iribarren José Ignacio, Liesa Francisco, Laso Manuel, Casanovas Jordi *Structural and electronic properties of 3,4-ethylenedioxythiophene, 3,4-ethylenedisulfanylfurane and thiophene oligomers: A theoretical investigation*, Synthetic Metals, 2005.
- [4] Allen Michael P., Tildesley Dominic J. *Computer simulation of liquids.*, Oxford university press, 2017.
- [5] Ampaiwan Marutaphan, Yotsarayuth Seekaew, Chatchawal Wongchoosuk *Self-Consistent Charge Density Functional Tight-Binding Study of Poly(3,4-ethylenedioxythiophene): Poly(styrenesulfonate) Ammonia Gas Sensor*, Nanoscale research letters, 2017.
- [6] Anderson R. Luke, Yang Quan, Ediger M. Andrew, *Comparing gas transport in three polymers: Via molecular dynamics simulation*, Physical Chemistry Chemical Physics, 2018.

-
- [7] Barisik Murat, Beskok Ali, *Wetting characterisation of silicon (1,0,0) surface*, Molecular Simulation, doi:10.1080/08927022.2012.758854, 2013.
- [8] Baschnagel Jörg , Wittmer Joachim P., Meyer Hendrik, Attig Norbert, Binder Kurt, Grubmüller Helmut, Kremer Kurt (eds , Baschnagel J., Wittmer J. P., Meyer H., *Monte Carlo Simulation of Polymers: Coarse-Grained Models*, 2004.
- [9] Ben-Nun Michal, Martínez Todd. J., *Ab Initio Quantum Molecular Dynamics*, Advances in Chemical Physics, 2002.
- [10] Bergdorf, Michael and Peter, Christine and Hünenberger, Philippe H. *Influence of cut-off truncation and artificial periodicity of electrostatic interactions in molecular simulations of solvated ions : A continuum electrostatics study*, The Journal of Chemical Physics, 2003.
- [11] Bisquert, J., *Nanostructured Energy Devices: Equilibrium Concepts and Kinetics*, 2014.
- [12] Brütting, W., *Physics of Organic Semiconductors*, Wiley, 2006.
- [13] Cabaj Joanna, Soloduchko Jadwiga, *Conducting Polymers as Elements of Miniature Biocompatible Sensor*, 2018.
- [14] Carrillo Jan-Michael Y., Dobrynin Andrey V., *Detailed Molecular Dynamics Simulations of a Model NaPSS in Water*, The Journal of Physical Chemistry B, 2010.
- [15] Chipot Chris, *Numerical methods for molecular dynamics simulations of biological systems*, 2019.
- [16] Cho Soowon, Jeong Sohdam, Kim Jun Mo, Baig Chunggi, *Molecular dynamics for linear polymer melts in bulk and confined systems under shear flow*, 2017.

- [17] Christmann, K., *Introduction to Surface Physical Chemistry - Topics in Physical Chemistry*, Springer, 1991.
- [18] Cooke, B., Schmidler, S. C., *Statistical prediction and molecular dynamics simulation*, Biophysical journal, 95(10), 4497-4511. doi:10.1529/biophysj.108.131623, 2008.
- [19] Crain Jason, Komolkin Andrei, *Simulating Molecular Properties of Liquid Crystal*, Advances in Chemical Physics, 2007.
- [20] Cramer T., Zerbetto F., García R., *Molecular Mechanism of Water Bridge Buildup: Field-Induced Formation of Nanoscale Menisci*, Langmuir, doi:10.1021/la800220r, 2008.
- [21] Cramer Tobias, Steinbrecher Thomas, Koslowski Thorsten, Case David A., Biscarini Fabio, Zerbetto Francesco, *Water-induced polaron formation at the pentacene surface: Quantum mechanical molecular mechanics simulations*, Phys. Rev. B, American Physical Society, doi:10.1103/PhysRevB.79.155316, 2009.
- [22] Cygan Randall T., Greathouse Jeffery A, Heinz Hendrik, Kalinichev Andrey G. *Molecular models and simulations of layered materials*, J. Mater. Chem., The Royal Society of Chemistry, 2009.
- [23] Desai Tapan, Keblinski Pawel, Kumar Sanat K., *Molecular dynamics simulations of polymer transport in nanocomposites*, The Journal of Chemical Physics, 2005.
- [24] Dkhissi Ahmed, Beljonne David, Lazzaroni Roberto *Atomic scale modeling of interfacial structure of PEDOT/PSS*, Synthetic Metals, doi:10.1016/j.synthmet.2008.11.022, 2009.
- [25] Dkhissi A., Beljonne D., Lazzaroni R., Louwet F., Groenendaal L., Brédas J. L., *Density functional theory and Hartree-Fock studies of*

- the geometric and electronic structure of neutral and doped ethylenedioxythiophene (EDOT) oligomers*, International Journal of Quantum Chemistry, 2003.
- [26] Dkhissi A., Louwet F., Groenendaal L., Beljonne D., Lazzaroni R. Brédas J.L., *Theoretical investigation of the nature of the ground state in the low-bandgap conjugated polymer, poly(3,4-ethylenedioxythiophene)*, Chemical Physics Letters, 2002.
- [27] Dobrynin Andrey, *Theory and simulations of charged polymers: From solution properties to polymeric nanomaterials*, Current Opinion in Colloid & Interface Science, 2008.
- [28] Doniach Sebastian, Eastman Peter *Protein dynamics simulations from nanoseconds to microseconds*, Current opinion in structural biology, 1999.
- [29] Douglas Tobias J., Glenn Martyna J., Klein Michael L. *Molecular dynamics simulations of a protein in the canonical ensemble*, The Journal of Physical Chemistry, 1993.
- [30] Egorov A.V., Komolkin Andrei, Chizhik Vladimir, Padro Kh.A., Gvardia E., *Molecular dynamics simulation of the structure of water in a wide temperature range*, Zhurnal Fizicheskoi Khimii, 2000.
- [31] Elmahmoudy, Mohammed *Micro- and nano-patterning of conducting polymers for biomedical applications*, 2017.
- [32] Elschner A. , Kirchmeyer S., Lövenich W., Merker U., Reuter K., *PE-DOT - Principles and Applications of an Intrinsically Conductive Polymer*, CRC Press, 2011.
- [33] Fermeglia Maurizio, Pricl Sabrina, *Multiscale modeling for polymer system of industrial interest*, Progress in Organic Coatings, 2007.

- [34] Franco-Gonzalez Juan Felipe, Zozoulenko V. Igor *Molecular Dynamics Study of Morphology of Doped PEDOT: From Solution to Dry Phase*, The journal of physical chemistry. B, 2017.
- [35] Gangopadhyay Rupali, Das Bidisa, Molla Mijanur Rahaman, *How does PEDOT combine with PSS? Insights from structural studies*, RSC Adv., The Royal Society of Chemistry, doi:10.1039/C4RA08666J, 2014.
- [36] Glotzer Sharon C., Paul Wolfgang, *Molecular and Mesoscale Simulation Methods for Polymer Materials*, Annual Review of Materials Research, 2002.
- [37] González Manuel Víctor Albi, *Force fields and molecular dynamics simulations*, 2011.
- [38] Han Yue, Elliott James *Molecular dynamics simulations of the elastic properties of polymer/carbon nanotube composites*, 2007.
- [39] Harmandaris Vagelis A., Daoulas Kostas Ch., Mavrantzas Vlasis G., *Molecular Dynamics Simulation of a Polymer Melt/Solid Interface: Local Dynamics and Chain Mobility in a Thin Film of Polyethylene Melt Adsorbed on Graphite*, Macromolecules, 2005.
- [40] Hautman Joseph, Klein L. Michael *An Ewald summation method for planar surfaces and interfaces*, Molecular Physics, Taylor & Francis, 1992.
- [41] Heermann, D.W., *Computer simulation methods in theoretical physics*, Springer-Verlag, 1986.
- [42] Holland Dominic, Marder, M. *Ideal Brittle Fracture of Silicon Studied with Molecular Dynamics*, Phys. Rev. Lett., American Physical Society, 1998.
- [43] Hospital, A., Goñi, J. R., Orozco, M., Gelpí, J. L. . *Molecular dynamics simulations: advances and applications*, Advances and

- applications in bioinformatics and chemistry : AABC, 8, 37?47, doi:10.2147/AABC.S70333, 2015.
- [44] Hura Greg, Russo Daniela, Glaeser Robert M., Head-Gordon Teresa, Krack Matthias, Parrinello Michele, *Water structure as a function of temperature from X-ray scattering experiments and ab initio molecular dynamics*, Phys. Chem. Chem. Phys., The Royal Society of Chemistry, 2003.
- [45] Jensen Frank, *Introduction to Computational Chemistry*, Wiley, 2017.
- [46] Jimison L. H. et al., *Applications of Conducting Polymer Devices in Life Sciences*, Retrieved June 26, 2019, from <https://www.sigmaaldrich.com/technical-documents/articles/materials-science/applications-of-conducting-polymer-devices-in-life-sciences.html>
- [47] Jorgensen William L., Tirado-Rives Julian, *Potential energy functions for atomic-level simulations of water and organic and biomolecular systems*, National Academy of Sciences, 2005.
- [48] Kaiser. A. B., *Systematic conductivity behavior in conducting polymers: Effects of heterogeneous disorder*. Adv. Mater., 13(12-13):927?941, 2001.
- [49] Karplus M., McCammon J. A., *Molecular dynamics simulations of biomolecules*, Nature Structural Biology, 2002.
- [50] Kergoat, L. , Herlogsson, L. , Braga, D. , Piro, B. , Pham, M. , Crispin, X. , Berggren, M. and Horowitz, G., *A Water-Gate Organic Field-Effect Transistor*. Adv. Mater., 22: 2565-2569, 2010.
- [51] Khodagholy D., Doublet T., Gurfinkel M., Quilichini P., Ismailova E., Leleux P., Herve T., Sanaur S., Bernard C., Malliaras, G. G., *Highly Conformable Conducting Polymer Electrodes for In Vivo Recordings*. Adv. Mater., 23: H268-H272. doi:10.1002/adma.201102378, 2011.

- [52] Komolkin Andrei, *Equilibration of Liquid Crystals for Simulation of Molecular Dynamics*, 1997.
- [53] Komolkin Andrei, V. Molchanov Yu, Yakutseni Pavel, Computer simulation of a real liquid crystal, *Liquid Crystals*, 1989.
- [54] Köhler Anna, Bässler H, *Electronic processes in organic semiconductors: An introduction*, 2015.
- [55] Lang U., Naujoks N., Dual J, *Mechanical characterization of PEDOT:PSS thin films*, *Synth. Met.*, 159(5-6):473-479, 2009.
- [56] Laplace, Pierre-Simon, *Théorie Analytique des Probabilités*, 1812.
- [57] Lemak, A. S. and Balabaev, N. K. *Molecular dynamics simulation of a polymer chain in solution by collisional dynamics method*, *Journal of Computational Chemistry*, 1996.
- [58] Lenz Annika, Kariis Hans, Pohl Anna, Persson Petter, Ojamäe Lars, *The electronic structure and reflectivity of PEDOT:PSS from density functional theory*, *Chemical Physics*, 2011.
- [59] Liu Chuan, Huang Kairong, Park Won-Tae, Li Minmin, Yang Tengzhou, Liu Xuying, Liang Lijuan, Minari Takeo, Noh Yong-Young, *A unified understanding of charge transport in organic semiconductors: the importance of attenuated delocalization for the carriers*, *Mater. Horiz.*, The Royal Society of Chemistry, 10.1039/C7MH00091J, 2017.
- [60] Lopez Carlos G., Richtering Walter, *Conformation and dynamics of flexible polyelectrolytes in semidilute salt-free solutions*, *The Journal of Chemical Physics*, 2018.
- [61] Löffler Susanne, Libberton Ben, Richter-Dahlfors Agneta, *Organic Bio-electronic Tools for Biomedical Applications*, *Electronics*, 2015.
- [62] Lubianez R.P., Kirchmeyer S.S., Gaiser D., Starck H., *Advances in PEDOT : PSS Conductive Polymer Dispersions*, 2008.

- [63] Marzocchi Marco, *Conducting Polymers as Novel Tools for Biosensing and Tissue Engineering*, PhD dissertation, Bologna, 2016.
- [64] Metzger, R., *Unimolecular and Supramolecular Electronics I Chemistry and Physics Meet at Metal-Molecule Interfaces Preface*, Topics in current chemistry, 2012.
- [65] Michaud-Agrawal N., Denning E.J., Woolf T.B., Beckstein O., *MD-Analysis: A toolkit for the analysis of molecular dynamics simulations*, Journal of Computational Chemistry, vol. 32, no. 10, pp. 2319-2327. <https://doi.org/10.1002/jcc.21787>, 2011.
- [66] Monard, G., Merz, K. M., *Combined Quantum Mechanical/Molecular Mechanical Methodologies Applied to Biomolecular Systems*, Accounts of Chemical Research, 1999.
- [67] Neverov Vladimir, Komolkin Andrei, *A study of the structural and thermodynamic properties of water by the molecular dynamics method*, Russian Journal of Physical Chemistry B, 2010.
- [68] Nosé S., *A molecular dynamics method for simulations in the canonical ensemble*, Molecular Physics, Taylor & Francis, 1984.
- [69] Nosé S., *Constant-temperature molecular dynamics*, Journal of Physics: Condensed Matter, IOP Publishing, 1990.
- [70] Odegard G.M., Clancy T.C., Gates T.S., *Modeling of the mechanical properties of nanoparticle/polymer composites*, Polymer, 2005.
- [71] Pasini P., Zannoni C., *Advances in the Computer Simulations of liquid crystals*, Springer Science & Business Media, 2013.
- [72] Pereira Simao, Scocchi Giulio, Toth Radovan, Posocco Paola, Nieto Daniel, Priel Sabrina, Fermeglia Maurizio, *Multiscale modelling of polymer/clay nanocomposites*, Journal of Multiscale Modelling, 2011.

- [73] Petrenko, R., Meller, J., *Molecular dynamics*, Wiley Online Library, 2001.
- [74] Rivnay, Jonathan and Owens, Róisín M and Malliaras, George G *The rise of organic bioelectronics*. Chemistry of Materials, ACS Publications, 2013.
- [75] Roberts, N., Anderson, D., Deal, R., Garet, M., Shaffer, W., *Introduction to Computer Simulation-A System Dynamics Modeling Approach*, Journal of the Operational Research Society, 1997.
- [76] Römer Frank, Lervik Anders, Bresme Fernando *Nonequilibrium molecular dynamics simulations of the thermal conductivity of water: A systematic investigation of the SPC/E and TIP4P/2005 models*, The Journal of Chemical Physics, 2012.
- [77] Samanta Tanusree, Mukherjee M., *Swelling Dynamics of Ultrathin Films of Strong Polyelectrolytes*, Macromolecules, 2011.
- [78] Sandström Dick, Komolkin Andrei, Maliniak Arnold, *Molecular dynamics simulation of a liquid crystalline mixture*, The Journal of Chemical Physics, 1997.
- [79] Shaw D.E., Dror R.O., Salmon J.K., Grossman J.P., Mackenzie K.M., Bank J.A. et al. *Millisecond-scale molecular dynamics simulations on Anton*, in Proceedings of the Conference on High Performance Computing Networking, Storage and Analysis. Association for Computing Machinery. 2009 <https://doi.org/10.1145/1654059.1654126>.
- [80] Shinar, J., *Organic Light-Emitting Devices: A Survey*, 10.1007/978-0-387-21720-8, 2004.
- [81] Sun Kuan, Zhang Shupeng, Li Pengcheng, Xia Yijie, Zhang Xiang, Du Donghe, Isikgor Furkan, Ouyang Jianyong *Review on application of PEDOTs and PEDOT:PSS in energy conversion and storage devices*, J Mater Sci: Mater Electron, 2015.

- [82] Takemura Kazuhiro, Kitao Akio, *Effects of Water Model and Simulation Box Size on Protein Diffusional Motions*, The Journal of Physical Chemistry B, 2007.
- [83] Tasaki K., McDonald, S., Brady, J.W. *Observations concerning the treatment of long-range interactions in molecular dynamics simulations*, Journal of Computational Chemistry, 1993.
- [84] Thijssen, J., *Computational Physics*, Cambridge University Press. doi:10.1017/CBO9781139171397, 2007.
- [85] Torres J., Nealey F. P., de Pablo Juan *Molecular Simulation of Ultrathin Polymeric Films Near the Glass Transition*, Physical review letters, 2000.
- [86] Toukmaji A.Y., Board J.A. *Ewald summation techniques in perspective: a survey*, 1996.
- [87] Ugliengo Piero, Sodupe Mariona, Musso F., Bush Ian, Orlando R., Dovesi Roberto, *Coordinates of the optimum amorphous silica structures*, 2013.
- [88] Van Bruijnsvoort M., Tijssen Robert, Kok Wim, *Assessment of the Diffusional Behavior of Polystyrene Sulfonates in the Dilute Regime by Hollow-Fiber Flow Field Flow Fractionation*, Journal of Polymer Science Part B: Polymer Physics, doi:10.1002/polb.1149, 2001.
- [89] van der Spoel David, van Maaren Paul J., Berendsen Herman J. C., *A systematic study of water models for molecular simulation: Derivation of water models optimized for use with a reaction field*, The Journal of Chemical Physics, 1998.
- [90] Vega Carlos, Abascal Jose L. F. *Simulating water with rigid non-polarizable models: a general perspective*, Phys. Chem. Chem. Phys., The Royal Society of Chemistry, 2011.

- [91] Volpi R., *Modelling Charge Transport for Organic Solar Cells within Marcus Theory*, PhD dissertation, Linköping, 2017.
- [92] Xu Guofeng, Luo Shuangjiang, Yang Qingbo, Yang Jingfa, Zhao Jiang, *Single chains of strong polyelectrolytes in aqueous solutions at extreme dilution: Conformation and counterion distribution*, The Journal of Chemical Physics, 2016.
- [93] Yeh In-Chul, Hummer Gerhard, *System-Size Dependence of Diffusion Coefficients and Viscosities from Molecular Dynamics Simulations with Periodic Boundary Conditions*, The Journal of Physical Chemistry B, 2004.
- [94] Yuan, Yongbo and Giri, Gaurav and Ayzner, Alexander and P Zoombelt, Arjan and C B Mannsfeld, Stefan and Chen, Jihua and Nordlund, Dennis and F Toney, Michael and Huang, Jinsong and Bao, Zhenan *Ultra-High Mobility Transparent Organic Thin Film Transistors Grown by an off-Centre Spin-Coating Method*. Nature communications, 10.1038/ncomms4005, 2014.
- [95] Wenping Hu, Fenglian Bay, Xiong Gong, Xiaowei Zhan, Hongbing Fu, Thomas Bjornholm, *Organic Optoelectronics*, Wiley, 2012.
- [96] Widmer, J., *Charge Transport and Energy Levels in Organic Semiconductors*, PhD dissertation, 2014
- [97] Zakharov Alex, Komolkin Andrei, Maliniak A., *Rotational Viscosity in a Nematic Liquid Crystal: A Theoretical Treatment and Molecular Dynamics Simulation*, Physical review. E, Statistical physics, plasmas, fluids, and related interdisciplinary topics, 1999.
- [98] Zaki, T., *Short-Channel Organic Thin-Film Transistors Fabrication, Characterization, Modeling and Circuit Demonstration*, Springer, 2015.
- [99] Zhu Sheng-Bai, Philpott R. Michael: *Interaction of water with metal surfaces*, J. Chem. Phys. 100, 6961, 1994.

- [100] Inzelt G., *Conducting Polymers - A New Era in Electrochemistry*, Springer, 2012.
- [101] Conwell E. M., *Handbook of Organic Conductive Molecules and Polymers*, volume 4. John Wiley & Sons, 2000.
- [102] Kiebooms R., Aleshin A., Hutchison K., Wudl F., *Thermal and electromagnetic behavior of doped poly(3,4-ethylenedioxythiophene) films*, J. Phys. Chem. B, 101(51):11037, 1997.
- [103] Heywang G., Jonas F., *Poly(alkylenedioxythiophene)s new, very stable conducting polymers*, Adv. Mater., 4(2):116?118, 1992.
- [104] Volkov Anton V., Wijeratne Kosala, Mitraka Evangelia, Ail Ujwala, Zhao Dan, Tybrandt Klas, Andreasen Jens Wenzel, Berggren Magnus, Crispin Xavier, Zozoulenko Igor V., *Understanding the Capacitance of PEDOT:PSS*, Advanced Functional Materials, 2017.
- [105] Wang Yue, Zhu Chenxin, Pfattner Raphael, Yan Hongping, Jin Lihua, Chen Shucheng, Molina-Lopez Francisco, Lissel Franziska, Liu Jia, Rabbiah Noelle I., Chen Zheng, Chung Jong Won, Linder Christian, Toney Michael F., Murmann Boris, Bao Zhenan, *A highly stretchable, transparent, and conductive polymer*, American Association for the Advancement of Science, 2017.
- [106] Stavrinidou Eleni, Leleux Pierre, Rajaona Harizo, Khodagholy Dion, Rivnay Jonathan, Lindau Manfred, Sanaur Sébastien, Malliaras George G., *Direct Measurement of Ion Mobility in a Conducting Polymer*, Advanced Materials, 2013.
- [107] Proctor C. M., Rivnay J., Malliaras G. G., *Understanding volumetric capacitance in conducting polymers*, Journal of Polymer Science, Part B: Polymer Physics, 54(15), 1433-1436. <https://doi.org/10.1002/polb.24038>, 2016.

-
- [108] Rudd Sam, Franco-Gonzalez Juan F., Kumar Singh Sandeep, Ullah Khan Zia, Crispin Xavier, Andreasen Jens W., Zozoulenko Igor, Evans Drew, *Charge transport and structure in semimetallic polymers*, Journal of Polymer Science Part B: Polymer Physics, 2018.
- [109] Amorini Fabrizio, Zironi Isabella, Marzocchi Marco, Gualandi Isacco, Calienni Maria, Cramer Tobias, Fraboni Beatrice, Castellani Gastone, *Electrically Controlled “Sponge Effect” of PEDOT:PSS Governs Membrane Potential and Cellular Growth*, ACS Applied Materials & Interfaces, 2017.